



저작자표시-비영리-변경금지 2.0 대한민국

이용자는 아래의 조건을 따르는 경우에 한하여 자유롭게

- 이 저작물을 복제, 배포, 전송, 전시, 공연 및 방송할 수 있습니다.

다음과 같은 조건을 따라야 합니다:



저작자표시. 귀하는 원저작자를 표시하여야 합니다.



비영리. 귀하는 이 저작물을 영리 목적으로 이용할 수 없습니다.



변경금지. 귀하는 이 저작물을 개작, 변형 또는 가공할 수 없습니다.

- 귀하는, 이 저작물의 재이용이나 배포의 경우, 이 저작물에 적용된 이용허락조건을 명확하게 나타내어야 합니다.
- 저작권자로부터 별도의 허가를 받으면 이러한 조건들은 적용되지 않습니다.

저작권법에 따른 이용자의 권리는 위의 내용에 의하여 영향을 받지 않습니다.

이것은 [이용허락규약\(Legal Code\)](#)을 이해하기 쉽게 요약한 것입니다.

[Disclaimer](#)

이학박사 학위논문

Interplay between topological phase
transition and the long-range Coulomb
interaction

원거리 쿨롱 상호작용과 위상 상전이의 상호 작용

2020년 2월

서울대학교 대학원
물리천문학부
이 창 희

이학박사 학위논문

Interplay between topological phase
transition and the long-range Coulomb
interaction

원거리 쿨롱 상호작용과 위상 상전이의 상호 작용

2020년 2월

서울대학교 대학원
물리천문학부
이창희

Interplay between topological phase transition and the long-range Coulomb interaction

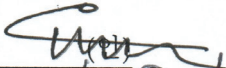

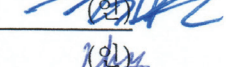
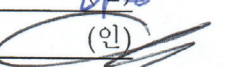

원거리 쿨롱 상호작용과 위상 상전이의 상호 작용

지도교수 민 홍 기

이 논문을 이학박사 학위논문으로 제출함
2020년 2월

서울대학교 대학원
물리천문학부
이 창 희

이창희의 이학박사 학위 논문을 인준함
2020년 2월

위원장	유재준	
부위원장	민홍기	
위원	김기훈	
위원	양범정	
위원	정석민	(인) 

Abstract

In the study of a variety of materials and the phase of them, classifying and dividing them in a consistent and useful way essentially requires some insight of the materials and eventually helps deepening our understanding of the materials and the phase. The conventional way of the classification of the phase of a material is developed based on Landau's theory of the phase transition, and use the broken symmetry of the phase of a material.

However, in the mid of 2000, it is suggested that there is another way of classifying the phase of a material with respect to the topology of the electronic structure of the material, which is overlooked in the conventional way. The discovery of the topological phase of materials stimulates the researches on seeking for what is new in the topologically non-trivial phase of material. Motivated by this new discovery of the topological phase, we focus on the study of the effect of the long-range Coulomb interaction in electronic systems whose band structure is a topologically non-trivial.

The first subject of this thesis is devoted to a study of the exciton-polariton condensate in the microcavity of a monolayer transition metal dichalcogenides. Exciton-polariton is a state in which an exciton and a photon are coherently combined. As it is composed of a photon by part, the mass of the exciton-polariton is very small which makes it a good candidate for the room-temperature Bose-Einstein condensation. In this thesis, we take the Diracness of the low-energy electronic degree of freedom into account in a monolayer transition metal dichalcogenides. By Diracness, we mean that there is a non-vanishing Berry curvature around the extremum of the conduction and valence band. The result of our study shows that topological and first-order phase transitions in the exciton-polariton condensate can be achieved by increasing the excitation

density. It contrasts to the previous researches employing the effective mass approximations on similar systems. In those researches, a continuous BEC-BCS crossover is expected to occur rather than a first-order, thus discontinuous, topological phase transition. Furthermore, we find that various types of topological phase can appear in the exciton-polariton system in a microcavity with a monolayer transition dichalcogenides.

The second subject is related to the double-Weyl semimetal which hosts double-Weyl nodes near the Fermi level. A double-Weyl node is an extension of a Weyl node. A Weyl node can appear anywhere in the Brillouin zone, does not require any symmetry, and has ± 1 topological charge. On the other hand, a double-Weyl node is only protected by C_4 or C_6 rotation symmetries and can appear on the axis invariant under the rotation. The magnitude of the topological charge it can possess is 2. When it comes to the energy dispersion, the energy dispersion of a Weyl node depends on momentum linearly in any direction, while that of a double-Weyl node is linear along only the rotationally invariant axis and quadratic along the direction perpendicular to the rotationally invariant axis.

It has been proposed that a double-Weyl semimetal can undergo a topological phase transition between the semi-metallic phase and insulating phases by applying the physical or chemical pressure. At the point of the topological phase transition, called a critical point, the energy dispersion of the electronic degree of freedom is quadratic in momentum in all directions in the low-energy limit. As a system with a quadratic dispersion can be a non-Fermi liquid in the presence of the long-range interaction, we study the critical point of a double-Weyl semimetal using two standard renormalization group methods, the large N_f method and the $\epsilon = 4 - d$ expansion method. The result of both methods implies consistently that the double-Weyl semimetal at the critical point

is in an anisotropic non-Fermi liquid phase in the presence of the long-range Coulomb interaction between electrons. We also provide the correction of the power-law of several physical observables as an experimental guide in sought.

keywords: excition, exciton-polariton, topological phase transition, double-Weyl semimetal, long-range Coulomb interaction.

student number: 2013-22992

Contents

Abstract	i
Contents	iv
List of Tables	viii
List of Figures	ix
1 Introduction	1
2 Low energy theory and the topological characterization of 2D TMD and multi-Weyl semimetals	4
2.1 Chern number	4
2.1.1 General formula for the abelian Berry curvature and Chern number	4
2.1.2 Two-band model	5
2.1.3 Massive Dirac fermion in the two-dimensional free space .	7
2.1.4 Fermi surface of a Weyl fermion system	7
2.1.5 Constraints by symmetry	9
2.1.5.1 Time-reversal symmetry	9
2.1.5.2 Inversion symmetry	11
2.2 Low-energy effective theory of electronic structure	12

2.2.1	Representation of a symmetry group and invariance of Hamiltonian	13
2.2.2	Monolayer transition metal dichalcogenides	14
2.2.3	Multi-Weyl node	17
2.2.3.1	Multi-Weyl nodes protected by a n -fold rotational symmetry	19
2.2.3.2	Other symmetries \mathcal{IT} , $\sigma_h\mathcal{T}$, and σ_v	20
3	Self-consistent method in the mean-field level	22
3.1	Derivation of the self-consistent equation using the Hartree-Fock factorization	22
3.2	Derivation of the self-consistent equation using the variational principle	24
3.3	The self-energies in a multi-orbital system	29
3.4	The Hartree-Fock description of the homogeneous electron gas	30
4	Exciton-Polariton condensate in two-dimensional TMDC	33
4.1	Introduction	33
4.2	Model	35
4.3	Self-consistent mean-field equation	36
4.3.1	Details of the optical-valley selection rule	37
4.4	Competition between s- and p- wave order parameter	40
4.5	Topological phase transition of a single photon-coupled massive Dirac particle system and its Phase diagram	42
4.6	Topological phase transition of 2D TMD cavity and its Phase diagram	47
4.7	Conclusion	49
5	Emergent anisotropic non-Fermi liquid at a topological phase transition in three dimensions	50

5.1	Introduction	50
5.2	Model	52
5.3	Large N_f calculation	54
5.4	$\epsilon = 4 - d$ calculatioin	56
5.5	Physical observables	59
5.6	Short-range interaction and the stability of anisotropic non-Fermi liquid fixed point	61
5.7	Discussion	67
5.8	Conclusion	68
6	Conclusion	69
	Bibliography	70
	Appendix A Coulomb interaction in the band basis	79
	Appendix B Relation between the Chern number in the normal phase and the Skyrmion number of Hartree-Fock quasiparticle bands	84
	Appendix C Details of calculation of the renormalization group calculation	87
C.1	Details of the $\epsilon = 4 - d$ method	87
C.1.1	Proof of the emergent rotational symmetry along the k_z -axis	88
C.1.1.1	Proof of $a_x = a_y$	88
C.1.1.2	Proof of $t_x = t_y$	89
C.1.2	Renormalization group equations in the $\epsilon = 4 - d$ expansion	92
C.1.3	Effects of the symmetry-allowed parabolic term	95
C.1.3.1	Boson self-energy	96
C.1.3.2	Fermion self-energy	96

C.1.3.3	RG flow equation	99
C.2	Details of the large N_f calculation	100
C.2.1	Boson self-energy	100
C.2.1.1	q_\perp dependence	100
C.2.1.2	q_z dependence	101
C.2.1.3	Arbitrary q dependence	102
C.2.2	Fermion self-energy	103
C.2.2.1	ω correction δ_ω	103
C.2.2.2	t_\perp correction δ_{t_\perp}	104
C.2.2.3	t_z correction δ_{t_z}	105
C.2.3	Vertex correction	106
C.3	Consistency between the large N_f calculation and ϵ expansion	106
C.4	Physical observables in the non-interacting limit	107
C.4.1	Density of states	108
C.4.2	Free energy	108
C.4.2.1	Specific heat	110
C.4.2.2	Compressibility	110
C.4.3	Diamagnetic susceptibility	110
C.4.4	Optical conductivity	113
C.5	Effect of extra relevant perturbations	114
C.6	Sanity check of the power-law correction	115

List of Tables

2.1	Fitting parameters a , t , Δ , and λ . [1]	17
2.2	Effective Hamiltonians on the rotationally invariant line.	21
4.1	Phase classification in the two valleys coupled to the photons of both circular polarizations. The alphabet letters in the left-most column refer to each phase mentioned in Fig. 4.3. $\mathcal{C}_S \equiv \sum_{\tau,\sigma} \sigma \mathcal{C}_{\tau,\sigma}/2$ and $\mathcal{C}_V \equiv \sum_{\tau,\sigma} \tau \mathcal{C}_{\tau,\sigma}/2$ are the spin and the valley Chern numbers respectively. Refer the main text for further details.	48

List of Figures

3.1	The Fock term, or the exchange self energy, and the energy dispersion of the homogeneous two- and three- dimensional electron gases. (a) and (c) : The exchange self-energy in two- and three-dimension divided by the Fermi energy. (b) and (d): Comparison between the non-interacting energy dispersion and the self-energy corrected energy dispersion of the two- and three-dimensional electron gases.	31
4.1	(a) Photon fraction and mean-field band exciton gap parameters $\Delta^{s,p}$ averaged over the momentum space as the functions of R_s for the photon frequency $\hbar\omega_c = 2.1\text{eV}\text{\AA}$, the dielectric constant $\epsilon = 10$, the Dirac velocity $\hbar v = 3.7\text{eV}\text{\AA}$, and the band gap of $E_{\text{gap}} = 2.0\text{eV}\text{\AA}$. (b)-(e) Pseudo-spin textures at the R_s values indicated in (a). Arrow represents $\hat{\eta}_{\parallel}$ and false color represents $\eta_z(\mathbf{k})$; for convenience, we have plotted the $\tau = -$ valley coupled to $I = -$ photons.	42

4.2	(a) The dependence of photon fraction for the single-valley TMDC polariton system on δ and R_s shown with $\hbar v = 3.7\text{eV}\text{\AA}$, $\epsilon = 10$ and $E_{\text{gap}} = 2.0$ eV; the green solid, the green dashed and the black dotted curves represent the first-order transitions, the second-order transitions, and the crossovers, respectively. (b) Phase boundaries for the first-order (solid) and second-order (dashed) transitions for $\epsilon=10$ and $E_{\text{gap}}=2$ eV (green), $\epsilon=15$ and $E_{\text{gap}}=2$ eV (red), and $\epsilon=10$ and $E_{\text{gap}}=2.5$ eV (blue).	46
4.3	Photon fraction (above) and mean-field band exciton gap parameters $\Delta^{s,p}$ (below) for two valleys ($\tau = \pm 1$) as the functions of R_s for the photon frequency $\hbar\omega_c = 2.1\text{eV}$ and other physical parameters following those of Fig. 4.2 (a).	47
5.1	Phase diagram for the TQPT between the DWSM and insulator phases with the tuning parameter m . The insets show the energy dispersions for the (a) DWSM, (b) insulator and (c) TQPT. . . .	52
5.2	Feynman diagrams at one-loop order for the (a) fermion self-energy, (b) boson self-energy, and (c) vertex correction. A straight line with an arrowhead and a wavy line represent the fermion and boson propagators, respectively.	56
5.3	RG flows of α and γ for (a) $N_f = 1$ and (b) $N_f = 10$ at $\epsilon = 1$. The red dots represent the fixed points (α^*, γ^*) . For $N_f = 1$, $(\alpha^*, \gamma^*) = (0.671, 0.748)$ and for $N_f = 10$, $(\alpha^*, \gamma^*) = (0.096, 0.966)$ obtained from Eq. (5.19).	58
5.4	Feynman diagrams generated by the short-range interaction and long-range Coulomb interactions. The dashed and wavy lines stand for the short-range interaction and long-range Coulomb interaction, respectively. The solid line with arrow tip stands for the fermion.	62

5.5	RG flow diagrams in terms of N_f when s_\perp is ignored.	66
5.6	RG flow diagrams in terms of N_f when s_\perp is allowed.	66
A.1	Paring terms with various m integrated along the radial direction with the condition in Fig. 1 of the main text. The rotational symmetry preserving solution appears in $R_{c2} < R_s < R_{c3}$	82
C.1	Plots of $F_\perp(x)$ and $F_z(x)$. The blue solid line and red dashed line represent $F_\perp(x)$ and $F_z(x)$, respectively.	94

Chapter 1

Introduction

When it comes to the condensed matter physics, the past decade is arguably an era of the introduction and the development of the symmetry protected topological phase of materials[2, 3, 4, 5, 6], such as the quantum-spin Hall phase of the two-dimensional and the three-dimensional system with the time-reversal symmetry, and the synthesis of materials with the unprecedented properties, for example, the two-dimensional materials like a graphene[7], a monolayer transition dichalcogenide [1, 8, 9] as well as the topological insulators like the HgTe quantum well and Bi₂Se₃[10, 11], etc.

The topological phase of a material completely originates from the quantum nature of the electrons in the material. For example, Zak's phase[12] determining the topological phase of a one-dimensional system with both of chiral symmetry and inversion symmetry is a total sum of the phase of the wave function acquired by an electron during a travel over the whole one-dimensional Brillouin zone[12, 2]. As the phase with the trivial Zak's phase and the phase with a non-trivial Zak's phase are subject to the same symmetry group, the subtle distinction between those two phases is not captured in the conventional classification of the phase of materials based on broken symmetries. Also, the phase of the wave function is understood as a purely quantum mechanical quantity,

which implies that the phase with the non-trivial Zak's phase emerges due to a purely quantum mechanical origin.

The topological non-trivial phases are accompanied by interesting properties such as the existence of the symmetry-protected boundary modes on the boundaries of the system [2, 13]. For instance, a two-dimensional topological insulator hosts at least one helical edge mode on each edge. A sort of the three-dimensional topological semimetals, called Weyl semimetal[14], hosts a nodal point in the Brillouin zone which is very stable against any perturbation as long as it is not strong enough that two Weyl-node come into the pair annihilation.

However, the classification of the topological phase is complete only in the non-interacting limit. When the interactions are taken into account, the topological phase of a material can change regardless of the occurrence of the symmetry-breaking due to the interaction. Therefore, the interplay between interactions and the topological structures of electronic bands are needed to be considered in the study of the topological characterization of a system.

Especially, in a set of newly synthesized materials like graphene and monolayer transition dichalcogenide, which are featured by their quasi two-dimensional geometry, electric fields are not screened well as much as it is in the three dimensional insulators or metals due to the lower dimension of the materials. Hence, we can expect a strong influence of the long-range Coulomb interaction between electrons in this system. Also, materials in a topological semimetallic phase or at the phase transition between the topological semimetallic phase and the insulating phase have gapless nodes. Such a gapless node can induce quantum critical phenomena which result in singular behaviours of physical observables when there are suitable interactions.

Motivated by the anticipation that the topological structure of the electronic system in concert with the long-range Coulomb interaction between electrons may yield astonishing outcomes, we explore the interplay between them in a

microcavity with a monolayer transition metal dichalcogenide and in a double-Weyl semimetal at the topological phase transition point.

This thesis is outlined as follows.

In chapter 2, a brief introduction to the topological Chern number is introduced. Also, the low-energy model of the monolayer transition metal dichalcogenide and the multi-Weyl semimetals are introduced in the group representation theoretical point of view.

In chapter 3, the self-consistent mean-field method is exposed in detail. Two approaches are used to derive the self-consistent equations. One is called the Hartree-Fock factorization and the other derivation originates from the variational principle.

In chapter 4, the excitation-polaritonic system in a microcavity with a monolayer transition metal dichalcogenide is studied in the self-consistent Hartree-Fock method. We show two excitonic order parameters with different symmetry characters appear because of the diracness of the electronic band structure of a monolayer transition metal dichalcogenide in the low-energy limit. It turns out that the resultant phase diagram shows interesting topological first order phase transitions which are not seen in the previous researches.

In chapter 5, we investigate the effect of the long-range Coulomb interaction in a double-Weyl semimetal at its topological quantum phase transition. Two standard renormalization group methods, the large N_f expansion and the $\epsilon = 4 - d$ expansion are used and both two methods yield a consistent result that a double-Weyl semimetal at the topological phase transition between the double-Weyl semimetallic phase and insulating phases will exhibit an anisotropic non-Fermi liquid behavior. As a guideline for experimental confirmation of the anisotropic non-Fermi phase, we provide the power-laws of physical observables.

In chapter 6, this thesis concludes with a summary.

Chapter 2

Low energy theory and the topological characterization of 2D TMD and multi-Weyl semimetals

2.1 Chern number

2.1.1 General formula for the abelian Berry curvature and Chern number

Let us start with a general way of calculating the Chern number. Assuming that the energy structure of a Hamiltonian $H(\mathbf{k})$ is gapped at an energy E_F , not necessarily to be the Fermi energy. The energy levels are denoted by $E_n(\mathbf{k})$ and the eigenstate of it are $|\psi_{n,\mathbf{k}}\rangle$, and the (abelian) Berry phase acquired by the n -th band through a trip around a closed path P is

$$\gamma_n = \oint_P \mathcal{A}_n(\mathbf{k}) \cdot d\mathbf{k}$$

where $\mathcal{A}_n(\mathbf{k}) = i \langle \psi_{n,\mathbf{k}} | \nabla_{\mathbf{k}} | \psi_{n,\mathbf{k}} \rangle$ is the Berry connection of the n -th band. Note that a physical quantity is expressed through a line integral over a closed path, which can be re-expressed using the Stoke's theorem.

$$\oint_P \mathcal{A}_n(\mathbf{k}) \cdot d\mathbf{k} = \int_S \mathcal{F}_n(\mathbf{k}) \cdot d^2\mathbf{k}$$

where $P = \partial S$. $\mathcal{F}_n(\mathbf{k}) \equiv \nabla_{\mathbf{k}} \times \mathcal{A}_n(\mathbf{k})$ is known as the Berry curvature. A gauge-invariant expression for the Berry curvature is known

$$\begin{aligned}
[\mathcal{F}_n(\mathbf{k})]_r &= i\varepsilon_{pqr} \sum_m \left\langle \partial_p \psi_n \middle| \psi_m \right\rangle \left\langle \psi_m \middle| \partial_q \psi_n \right\rangle \\
&= i\varepsilon_{pqr} \sum_{m \neq 0} \frac{\langle \psi_n | \partial_p H | \psi_m \rangle \langle \psi_m | \partial_q H | \psi_n \rangle}{(E_{n,\mathbf{k}} - E_{m,\mathbf{k}})^2} \\
&= -\varepsilon_{pqr} \sum_{m \neq 0} \frac{2\text{Im} [\langle \psi_n | \partial_p H | \psi_m \rangle \langle \psi_m | \partial_q H | \psi_n \rangle]}{(E_{n,\mathbf{k}} - E_{m,\mathbf{k}})^2}, \quad (2.1)
\end{aligned}$$

which is very useful in the numerical calculation. As long as $E_{n,\mathbf{k}} \neq E_{m,\mathbf{k}}$ for all m, n , the Berry curvature is not singular. Also, the Berry curvature from all bands sums up to zero: $\sum_n \mathcal{F}_n(\mathbf{k}) = 0$.

It is interesting to find the close analogy between the Berry curvature $\mathcal{F}_n(\mathbf{k})$ and the magnetic field, and between the Berry connection $\mathcal{A}_n(\mathbf{k})$ and the vector potential in the classical theory of electromagnetism. In the same line of thought of the classical theory of electromagnetism, we can obtain the net charge of a "magnetic" monopole, which is quantized, by integrating the "magnetic" *fields* $\mathcal{F}_n(\mathbf{k})$ over a closed surface S . This is the Chern number of the n -th band.

$$C_n = \frac{1}{2\pi} \oint_S \mathcal{F}_n(\mathbf{k}) \cdot d\mathbf{S}. \quad (2.2)$$

In the two-dimensional free space, \mathbf{S} is taken to be the whole (k_x, k_y) plane. If there is a periodic potential in the two-dimensional space, as it is in a the two-dimensional lattice system, \mathbf{S} can be taken as the first Brillouin zone of the lattice. If the system is three-dimensional metallic system, we can think of S as the Fermi surface. In the following sections, several examples relevant to what will follow are going to be exposed.

2.1.2 Two-band model

It is heuristic to apply something new to a two-band model since two-band model is able to be treated completely analytically and provides good intuition.

A general two-band model Hamiltonian is reads as

$$H(\mathbf{k}) = a_0(\mathbf{k})\sigma_0 + \mathbf{a}(\mathbf{k}) \cdot \boldsymbol{\sigma},$$

whose eigen energies are $E_{\pm} = a_0(\mathbf{k}) \pm |\mathbf{a}(\mathbf{k})|$ and the eigenstates are

$$\begin{aligned} |+\rangle &= \frac{1}{\sqrt{2}|\mathbf{a}|\sqrt{|\mathbf{a}|+a_3}} \begin{pmatrix} a_3 + |\mathbf{a}| \\ a_1 + ia_2 \end{pmatrix}, \\ |-\rangle &= \frac{1}{\sqrt{2}|\mathbf{a}|\sqrt{|\mathbf{a}|-a_3}} \begin{pmatrix} a_3 - |\mathbf{a}| \\ a_1 + ia_2 \end{pmatrix}. \end{aligned}$$

Evaluation of Eq. (2.1) with these eigen states turns out to be

$$\begin{aligned} [\mathcal{F}_+(\mathbf{k})]_r &= i\varepsilon_{pqr} \frac{\partial_p a_i(\mathbf{k}) \cdot \langle +|\sigma_i|-\rangle \partial_q a_j(\mathbf{k}) \cdot \langle -|\sigma_j|+\rangle}{8|\mathbf{a}|^2} \\ &\quad - i\varepsilon_{pqr} \frac{\partial_q a_i(\mathbf{k}) \cdot \langle +|\sigma_i|-\rangle \partial_p a_j(\mathbf{k}) \cdot \langle -|\sigma_j|+\rangle}{8|\mathbf{a}|^2} \\ &= i\varepsilon_{pqr} \frac{\partial_p a_i(\mathbf{k}) \partial_q a_j(\mathbf{k}) \{ \langle +|\sigma_i|-\rangle \langle -|\sigma_j|+\rangle - \langle +|\sigma_j|-\rangle \langle -|\sigma_i|+\rangle \}}{8|\mathbf{a}|^2} \\ &= i\varepsilon_{pqr} \frac{\partial_p a_i(\mathbf{k}) \partial_q a_j(\mathbf{k}) \{ \langle +|\sigma_i \sigma_j|+\rangle - \langle +|\sigma_j \sigma_i|+\rangle \}}{8|\mathbf{a}|^2} \\ &= -\varepsilon_{pqr} \varepsilon_{ijk} \frac{\partial_p a_i(\mathbf{k}) \partial_q a_j(\mathbf{k}) \langle +|\sigma_k|+\rangle}{4|\mathbf{a}|^2} \\ &= -\frac{\varepsilon_{pqr}}{4|\mathbf{a}|^3} (\partial_p \mathbf{a} \times \partial_q \mathbf{a}) \cdot \mathbf{a}. \end{aligned} \tag{2.3}$$

When it comes to a constant unitary transformation $a_i(\mathbf{k}) = B_{ij}b_j(\mathbf{k})$, the Berry curvatures expressed with \mathbf{a} or \mathbf{b} are related by

$$\begin{aligned} -\varepsilon_{pqr} \varepsilon_{ijk} \partial_p a_i(\mathbf{k}) \partial_q a_j(\mathbf{k}) \langle +|\sigma_k|+\rangle &= -\varepsilon_{pqr} \varepsilon_{ijk} B_{ia} B_{jb} B_{kc} \partial_p b_a(\mathbf{k}) \partial_q b_b(\mathbf{k}) b_c \\ &= -\det B [\varepsilon_{pqr} \varepsilon_{abc} \partial_p b_a(\mathbf{k}) \partial_q b_b(\mathbf{k}) b_c]. \end{aligned}$$

Hence a transformation B with $\det B < 0$ changes the direction of the Berry curvature, and thus the sign of Chern number.

2.1.3 Massive Dirac fermion in the two-dimensional free space

Let us assume that a system described by a Hamiltonian of the two-dimensional massive Dirac fermion:

$$H = \begin{pmatrix} m & k_x - ik_y \\ k_x + ik_y & -m \end{pmatrix} = (k_x, k_y, m) \cdot \boldsymbol{\sigma}.$$

The eigen energies are $E_{\pm} = \pm\sqrt{k^2 + m^2}$, which shows that the system is gapped as long as $m \neq 0$, and the eigenstates of the Hamiltonian are

$$\begin{aligned} |+\rangle &= \frac{1}{\sqrt{2E_+}\sqrt{E_+ + m}} \begin{pmatrix} m + \sqrt{k^2 + m^2} \\ ke^{i\phi} \end{pmatrix}, \\ |-\rangle &= \frac{1}{\sqrt{2E_+}\sqrt{E_+ - m}} \begin{pmatrix} m - \sqrt{k^2 + m^2} \\ ke^{i\phi} \end{pmatrix}. \end{aligned}$$

Putting these into Eq 2.1 and 2.2, we get

$$\begin{aligned} [\mathcal{F}_+(\mathbf{k})]_3 &= -\frac{2\text{Im}[\langle\psi_+|\partial_1 H|\psi_-\rangle\langle\psi_+|\partial_2 H|\psi_-\rangle]}{(E_{+, \mathbf{k}} - E_{-, \mathbf{k}})^2} \\ &= -\frac{mk}{m^2 + k^2}, \end{aligned}$$

and thus

$$C = -\frac{1}{2\pi} \int_{\mathbb{R}^2} \frac{1}{2} \frac{m k}{(m^2 + k^2)^{3/2}} dk d\phi = -\frac{\text{sign}(m)}{2}.$$

Hence, the electronic structure of a massive Dirac fermion bears a Chern number $\pm\frac{1}{2}$ whose sign is determined by the opposite of the sign of the mass m .

2.1.4 Fermi surface of a Weyl fermion system

In the three-dimensional case, the most famous system possessing Chern number is the metallic Weyl node system. The electronic structure around a Weyl node is described by a Hamiltonian of the massless Weyl fermion. In the most

general form, the Hamiltonian of the Weyl node is written as

$$H = \sum_{i,j=1,2,3} c_{ij} k_i \sigma_j,$$

with $\det(c_{ij}) \neq 0$. Using Eq 2.3, we get the Berry curvature

$$[\mathcal{F}_+(\mathbf{k})]_r = - \frac{k_r \det c}{2 \left| \sum_j (\sum_i c_{ij} k_i)^2 \right|^{3/2}},$$

and the Chern number over a closed two-dimensional surface in the three-dimensional space

$$\begin{aligned} C_+ &= -\frac{\det c}{4\pi} \oint_{\text{FS}} \frac{dS_{\mathbf{k}} \cdot \mathbf{k}}{\left(\left| \sum_j (\sum_i c_{ij} k_i)^2 \right| \right)^{3/2}} \\ &= -\frac{\text{sign}[\det c]}{4\pi} \oint_{\text{FS}} dS_{\mathbf{p}} \cdot \frac{\mathbf{p}}{|\mathbf{p}|^3} \\ &= -\text{sign}[\det c]. \end{aligned}$$

where a substitution $p_j = c_{ij} k_i$ is used in the last line. In conclusion, what we learn is that the Fermi surface around a Weyl node has a non-zero Chern number which originates at a singular point $\mathbf{k} = 0$, where the energy gap closes. Sometimes, we call the Chern number, $-\text{sign}[\det c]$, the topological charge of a Weyl node.

From the point of view that a topological number only changes by an interger number, the topological number of a Weyl node implies the stability of the Weyl node. Let us imagine an arbitrary perturbation $V = -\mathbf{a} \cdot \boldsymbol{\sigma}$ applied to a Weyl node described by a Hamiltonian $H_0 = v_F \mathbf{k} \cdot \boldsymbol{\sigma}$. Considering the perturbed Hamiltonian $H = H_0 + V$, the role of the perturbation is a mere displacement of the Weyl node from $\mathbf{k} = (0, 0, 0)$ to $\mathbf{k} = v_F^{-1} \mathbf{a}$, and thus the Weyl node does robustly survive against any type of small perturbation.

2.1.5 Constraints by symmetry

2.1.5.1 Time-reversal symmetry

When the system is invariant under the time-reversal symmetry represented by a $\mathcal{P}_{\mathcal{T}} = \epsilon K$ with a matrix $\epsilon = -is_y$ acting on the spin space and the complex conjugation K , we can find a matrix, so called the sewing matrix, $\Gamma(\mathcal{T})$, which relates the eigenstates at \mathbf{k} and $-\mathbf{k}$ sharing the same eigenenergy.

$$\begin{aligned}\mathcal{P}_{\mathcal{T}}\psi_n(\mathbf{k}) &\equiv \epsilon\psi_n^*(\mathbf{k}) \\ &= [\Gamma(\mathcal{T})]_{\bar{n}n} \psi_{\bar{n}}(-\mathbf{k}).\end{aligned}\tag{2.4}$$

Antisymmetric matrix $[\Gamma(\mathcal{T})]_{\bar{n}n}$ is non-zero only when \bar{n} -th band at $-\mathbf{k}$ is the Krammer partner of n -th band at \mathbf{k} . Let us denote the Krammer partner of $\psi_n(\mathbf{k})$ by $\psi_{\mathcal{T}n}(-\mathbf{k})$. Transformation rules of physical observables are derived from Eq 2.4, and that of $[A^{(p)}(\mathbf{k})]_{nm} = \partial_p \psi_n^\dagger(\mathbf{k}) \cdot \psi_m(\mathbf{k})$ is our interest. For example, using Eq 2.4 and $[A^{(p)}(\mathbf{k})]_{nm} = -[A^{(p)*}(\mathbf{k})]_{mn} = -\partial_p \psi_m^T(\mathbf{k}) \cdot \psi_n^*(\mathbf{k})$, or $A^{(p)}(\mathbf{k}) = -A^{(p)\dagger}(\mathbf{k})$, we get

$$\begin{aligned}[A^{(p)}(\mathbf{k})]_{nm} &= -\partial_p (\epsilon\psi_m^*(\mathbf{k}))^\dagger \cdot \epsilon\psi_n^*(\mathbf{k}) \\ &= -\Gamma_{\bar{m}m}^*(\mathcal{T}) \partial_p \psi_{\bar{m}}^\dagger(-\mathbf{k}) \cdot \psi_{\bar{n}}(-\mathbf{k}) \Gamma_{\bar{n}n}(\mathcal{T}) \\ &= \left[\Gamma^\dagger(\mathcal{T}) A^{(p)}(-\mathbf{k}) \Gamma(\mathcal{T}) \right]_{mn}, \\ \therefore A^{(p)}(\mathbf{k}) &= \left[\Gamma^\dagger(\mathcal{T}) A^{(p)}(-\mathbf{k}) \Gamma(\mathcal{T}) \right]^T,\end{aligned}\tag{2.5}$$

Using Eq 2.1 and Eq 2.5, we have

$$\begin{aligned}
[\mathcal{F}_n(\mathbf{k})]_r &= i\varepsilon_{pqr} \sum_m [A^{(p)}(\mathbf{k})]_{nm} [A^{(q)}(\mathbf{k})]_{mn} \\
&= i\varepsilon_{pqr} \sum_m [\Gamma^\dagger(\mathcal{T})A^{(p)}(-\mathbf{k})\Gamma(\mathcal{T})]_{mn} [\Gamma^\dagger(\mathcal{T})A^{(q)}(-\mathbf{k})\Gamma(\mathcal{T})]_{nm} \\
&= i\varepsilon_{pqr} [\Gamma^\dagger(\mathcal{T})A^{(q)}(-\mathbf{k})A^{(p)}(-\mathbf{k})\Gamma(\mathcal{T})]_{nn} \\
&= i\varepsilon_{pqr} [\Gamma^\dagger(\mathcal{T})]_{n,\mathcal{T}n} \sum_m [A^{(q)}(-\mathbf{k})]_{\mathcal{T}n,m} [A^{(p)}(-\mathbf{k})]_{m,\mathcal{T}n} [\Gamma(\mathcal{T})]_{\mathcal{T}n,n} \\
&= -i\varepsilon_{pqr} \sum_m [A^{(p)}(-\mathbf{k})]_{\mathcal{T}n,m} [A^{(q)}(-\mathbf{k})]_{m,\mathcal{T}n},
\end{aligned}$$

$$\therefore [\mathcal{F}_n(\mathbf{k})]_r = -[\mathcal{F}_{\mathcal{T}n}(-\mathbf{k})]_r, \quad (2.6)$$

where we have used $[\Gamma^\dagger(\mathcal{T})]_{n,\mathcal{T}n} [\Gamma(\mathcal{T})]_{\mathcal{T}n,n} = 1$ since n -th band at \mathbf{k} and $\mathcal{T}n$ -th band at $-\mathbf{k}$ are Kramer partners.

As an application of Eq 2.6, let us imagine a system with Weyl nodes. If there is a Weyl node at \mathbf{k}_0 and a Fermi pocket is formed by the upper band stemming from the Weyl node, there should be another Weyl node at $-\mathbf{k}_0$ whose upper band also crosses the Fermi energy. Two upper bands of Weyl nodes are related by the time-reversal symmetry. Supposing that the Fermi pockets are disjoint, then it is the topological charge $C(\mathbf{k}_0)$ of a Weyl node that the integral of Berry curvature of the upper band of the Weyl node at \mathbf{k} over the Fermi pocket around the Weyl node.

$$C(\mathbf{k}_0) = \frac{1}{2\pi} \oint \mathcal{F}_{\text{upper}}(\mathbf{k}_0 + \mathbf{q}) \cdot d\mathbf{S}_{\mathbf{q}}.$$

The topological charge $C(-\mathbf{k}_0)$ of the Weyl node at $-\mathbf{k}_0$ is obtainable using Eq

2.6.

$$\begin{aligned}
C(-\mathbf{k}_0) &= \frac{1}{2\pi} \oint \mathcal{F}_{\mathcal{T}n}(-\mathbf{k}_0 + \mathbf{q}) \cdot d\mathbf{S}_{\mathbf{q}} \\
&= \frac{1}{2\pi} \oint \mathcal{F}_{\mathcal{T}n}(-\mathbf{k}_0 - \mathbf{q}) \cdot d\mathbf{S}_{-\mathbf{q}} \\
&= \frac{(-1)^2}{2\pi} \oint \mathcal{F}_n(\mathbf{k} + \mathbf{q}) \cdot d\mathbf{S}_{\mathbf{q}}, \\
&= C(\mathbf{k}_0)
\end{aligned}$$

where we have used $d\mathbf{S}_{-\mathbf{q}} = -d\mathbf{S}_{\mathbf{q}}$. Therefore, any pair of Weyl nodes related by the time-reversal symmetry shares a common topological charge.

Another example is

2.1.5.2 Inversion symmetry

When the system is invariant under a spatial inversion, represented by a unitary matrix $\mathcal{P}_{\mathcal{I}}$, we can relate two states at \mathbf{k} and $-\mathbf{k}$ by a matrix $\Gamma(\mathcal{I})$.

$$\mathcal{P}_{\mathcal{I}}\psi_n(\mathbf{k}) = [\Gamma(\mathcal{I})]_{\bar{n}n} \psi_{\bar{n}}(-\mathbf{k}). \quad (2.7)$$

Here, $[\Gamma(\mathcal{I})]_{\bar{n}n}$ is non-zero only when $\bar{n} = \mathcal{I}n$.

$$\begin{aligned}
\left[A^{(p)}(\mathbf{k})\right]_{nm} &= \partial_p \psi_n^\dagger(\mathbf{k}) \cdot \psi_m(\mathbf{k}) \\
&= \partial_p \psi_n^\dagger(\mathbf{k}) \mathcal{P}_{\mathcal{I}}^\dagger \cdot \mathcal{P}_{\mathcal{I}} \psi_m(\mathbf{k}) \\
&= - \left[\Gamma^\dagger(\mathcal{I}) A^{(p)}(-\mathbf{k}) \Gamma(\mathcal{I}) \right]_{nm}, \\
\therefore A^{(p)}(\mathbf{k}) &= - \left[\Gamma^\dagger(\mathcal{I}) A^{(p)}(-\mathbf{k}) \Gamma(\mathcal{I}) \right], \quad (2.8)
\end{aligned}$$

which is slightly different from Eq 2.5. In the same way with the derivation of Eq 2.6, we can derive the constraints forced by \mathcal{I} .

$$\begin{aligned}
[\mathcal{F}_n(\mathbf{k})]_r &= i\varepsilon_{pqr} \sum_m [A^{(p)}(\mathbf{k})]_{nm} [A^{(q)}(\mathbf{k})]_{mn} \\
&= i\varepsilon_{pqr} \sum_m \left[\Gamma^\dagger(\mathcal{I}) A^{(p)}(-\mathbf{k}) \Gamma(\mathcal{I}) \right]_{nm} \left[\Gamma^\dagger(\mathcal{I}) A^{(q)}(-\mathbf{k}) \Gamma(\mathcal{I}) \right]_{mn} \\
&= i\varepsilon_{pqr} \left[\Gamma^\dagger(\mathcal{I}) A^{(p)}(-\mathbf{k}) A^{(q)}(-\mathbf{k}) \Gamma(\mathcal{I}) \right]_{nn} \\
&= i\varepsilon_{pqr} \left[\Gamma^\dagger(\mathcal{I}) \right]_{n,\mathcal{I}n} \sum_m \left[A^{(p)}(-\mathbf{k}) \right]_{\mathcal{I}n,m} \left[A^{(q)}(-\mathbf{k}) \right]_{m,\mathcal{I}n} \left[\Gamma(\mathcal{I}) \right]_{\mathcal{I}n,n} \\
&= i\varepsilon_{pqr} \sum_m \left[A^{(p)}(-\mathbf{k}) \right]_{\mathcal{I}n,m} \left[A^{(q)}(-\mathbf{k}) \right]_{m,\mathcal{I}n}, \\
\therefore [\mathcal{F}_n(\mathbf{k})]_r &= [\mathcal{F}_{\mathcal{I}n}(-\mathbf{k})]_r. \tag{2.9}
\end{aligned}$$

Applying 2.8 to the pair of Weyl nodes related by the inversion symmetry \mathcal{I} , we can show

$$\begin{aligned}
C(-\mathbf{k}_0) &= \frac{1}{2\pi} \oint \mathcal{F}_{\mathcal{I}n}(-\mathbf{k}_0 + \mathbf{q}) \cdot d\mathbf{S}_q \\
&= \frac{1}{2\pi} \oint \mathcal{F}_{\mathcal{I}n}(-\mathbf{k}_0 - \mathbf{q}) \cdot d\mathbf{S}_{-\mathbf{q}} \\
&= \frac{(-1)^1}{2\pi} \oint \mathcal{F}_n(\mathbf{k}_0 + \mathbf{q}) \cdot d\mathbf{S}_q, \\
&= -C(\mathbf{k}_0),
\end{aligned}$$

thus the inversion transformation flips the sign of topological charge of a Weyl node.

2.2 Low-energy effective theory of electronic structure

In the following subsections, the low-energy effective theories of a single layer transition metal dichalcogenides and a multi-Weyl node are going to be exposed.

As the group representation theory would play a central role in the determination of the possible structure of the electronic structure, it comes first and the application of it to the case of a single layer transition metal dichalcogenides and a multi-Weyl node system will follow.

2.2.1 Representation of a symmetry group and invariance of Hamiltonian

Let a system subject to a symmetry group G and be described by wave functions spanned by a set of functions, $\{\psi_i(\mathbf{r})|i = 1, \dots, n\}$, called the basis functions. For convenience, $\{\psi_i\}$ are assumed to be orthonormal. Applying a transformation $P(g)$ corresponding to an element $g \in G$ to ψ_i , we can obtain the representation matrix $\Gamma(g)$ of g from the following relation.

$$P(g)\psi_j(\mathbf{r}) \equiv \psi_j(\hat{g}^{-1}\mathbf{r}) = \Gamma(g)_{ij}\psi_i(\mathbf{r})$$

yielding $[\Gamma(g)]_{ij} = \int d^d\mathbf{r}\psi_i^*(\mathbf{r})\psi_j(\hat{g}^{-1}\mathbf{r})$. Here, \hat{g} is the faithful representation of $O(d)$ in the d -dimensional real space. For example, when g means a counter-clockwise rotation of a point, or a vector, along the z -axis, then the 3×3 matrix \hat{g} is

$$\hat{g} = \begin{pmatrix} \cos \alpha & -\sin \alpha & 0 \\ \sin \alpha & \cos \alpha & 0 \\ 0 & 0 & 1 \end{pmatrix}.$$

The Hamiltonian restricted to the space spanned by the basis functions is defined by

$$h_{ij} \equiv \int d^d\mathbf{r}\psi_i^*(\mathbf{r})H(\hat{\mathbf{r}}, \hat{\mathbf{p}})\psi_j(\mathbf{r}).$$

The invariance of $H(\hat{\mathbf{r}}, \hat{\mathbf{p}})$ under $g \in G$ implies $h = \Gamma(g)^\dagger h \Gamma(g)$ stating the invariance of h .

In a periodic system, each basis functions are labelled by the crystal momentum \mathbf{k} , thus $\{\psi_{\mathbf{k},i}(\mathbf{r})|\mathbf{k} \in \text{FBZ}, i = 1, \dots, n\}$ is the set of basis functions.

The restricted Hamiltonian h is also labelled by \mathbf{k} :

$$[h(\mathbf{k})]_{ij} \equiv \int d^d \mathbf{r} \psi_{\mathbf{k},i}^*(\mathbf{r}) H(\hat{\mathbf{r}}, \hat{\mathbf{p}}) \psi_{\mathbf{k},j}(\mathbf{r}),$$

whose invariance under g is represented by

$$\Gamma(g) h(\hat{g}^{-1} \mathbf{k}) \Gamma(g)^\dagger = h(\mathbf{k}). \quad (2.10)$$

2.2.2 Monolayer transition metal dichalcogenides

As an insulator, the electronic band structure of a single layer transition metal dichalcogenides is gapped. The minimum(maximum) of the conduction band(valence band) is located around the corners K and $K' \equiv -K$ of the first Brillouin zone, whose group of the wave vector is C_{3h} while the lattice is invariant under D_{3h} . It is known that the edges of the conduction and the valence bands at τK consist of $\{d_{z^2}, d_{x^2-y^2}, d_{xy}\}$ orbitals of Mo atoms[15]. Hence, we can construct an effective Hamiltonian near \mathbf{K} using the Bloch basis functions:

$$\psi_1(\mathbf{r}) = \frac{1}{\sqrt{N}} \sum_{\mathbf{R}} e^{-i\mathbf{K} \cdot \mathbf{R}} d_{z^2}(\mathbf{r} - \mathbf{R}), \quad (2.11)$$

$$\psi_2(\mathbf{r}) = \frac{1}{\sqrt{N}} \sum_{\mathbf{R}} e^{-i\mathbf{K} \cdot \mathbf{R}} \left(\frac{d_{x^2-y^2}(\mathbf{r} - \mathbf{R}) + i d_{xy}(\mathbf{r} - \mathbf{R})}{\sqrt{2}} \right), \quad (2.12)$$

$$\psi_3(\mathbf{r}) = \frac{1}{\sqrt{N}} \sum_{\mathbf{R}} e^{-i\mathbf{K} \cdot \mathbf{R}} \left(\frac{d_{x^2-y^2}(\mathbf{r} - \mathbf{R}) - i d_{xy}(\mathbf{r} - \mathbf{R})}{\sqrt{2}} \right), \quad (2.13)$$

where \mathbf{R} denotes the lattice sites of Mo atoms. The representation matrices of C_3 and σ_h on these basis functions are

$$\Gamma(C_3) = \begin{pmatrix} 1 & 0 & 0 \\ 0 & e^{-\frac{4\pi i}{3}} & 0 \\ 0 & 0 & e^{\frac{4\pi i}{3}} \end{pmatrix}, \quad \Gamma(\sigma_h) = \begin{pmatrix} 1 & 0 & 0 \\ 0 & 1 & 0 \\ 0 & 0 & 1 \end{pmatrix}.$$

Only C_3 among C_{3h} effectively constraints the possible form of $h(\mathbf{K} + \mathbf{q})$. Application of Eq 2.10 with $g = C_3$ yields

$$h(K + q) = \begin{pmatrix} h_{11} & h_{12}(q_x - iq_y) & h_{13}(q_x + iq_y) \\ h_{12}^*(q_x + iq_y) & h_{22} & h_{23}(q_x - iq_y) \\ h_{13}^*(q_x - iq_y) & h_{23}^*(q_x + iq_y) & h_{33} \end{pmatrix} + O(q^2).$$

Turning the spin degree of freedom on, the basis functions are

$$\begin{aligned} \phi_1(\mathbf{r}) &= \psi_1(\mathbf{r}) |\uparrow\rangle, & \phi_2(\mathbf{r}) &= \psi_2(\mathbf{r}) |\uparrow\rangle, & \phi_3(\mathbf{r}) &= \psi_3(\mathbf{r}) |\uparrow\rangle, \\ \phi_4(\mathbf{r}) &= \psi_1(\mathbf{r}) |\downarrow\rangle, & \phi_5(\mathbf{r}) &= \psi_2(\mathbf{r}) |\downarrow\rangle, & \phi_6(\mathbf{r}) &= \psi_3(\mathbf{r}) |\downarrow\rangle, \end{aligned}$$

and the representation matrices of C_3 and σ_h on these basis functions are

$$\Gamma(C_3) = e^{-\frac{\pi i}{3}} \begin{pmatrix} 1 & & & & & \\ & e^{\frac{2\pi i}{3}} & & & & \\ & & e^{-\frac{2\pi i}{3}} & & & \\ & & & e^{\frac{2\pi i}{3}} & & \\ & & & & e^{-\frac{2\pi i}{3}} & \\ & & & & & 1 \end{pmatrix},$$

$$\Gamma(\sigma_h) = \begin{pmatrix} -i & & & & & \\ & -i & & & & \\ & & -i & & & \\ & & & i & & \\ & & & & i & \\ & & & & & i \end{pmatrix}.$$

Using $\Gamma(\sigma_h)h(K + \mathbf{q})\Gamma(\sigma_h)^\dagger = h(K + \mathbf{q})$, we know that $h(\mathbf{K} + \mathbf{q})$ takes a block diagonalized form

$$h(\mathbf{K} + \mathbf{q}) = \begin{pmatrix} h_\uparrow(\mathbf{K} + \mathbf{q}) & 0 \\ 0 & h_\downarrow(\mathbf{K} + \mathbf{q}) \end{pmatrix}.$$

Note that the spin-up and spin-down are completely decoupled due to σ_h . Making use of $\Gamma(C_3)$, what we obtain is

$$h_s(\mathbf{K} + \mathbf{q}) = \begin{pmatrix} h_{11,s} & h_{12,s}(q_x - iq_y) & h_{13,s}(q_x + iq_y) \\ h_{12,s}^*(q_x + iq_y) & h_{22,s} & h_{23,s}(q_x - iq_y) \\ h_{13,s}^*(q_x - iq_y) & h_{23,s}^*(q_x + iq_y) & h_{33,s} \end{pmatrix} + O(q^2).$$

Also, $h(\mathbf{K} + \mathbf{q}) = (\Gamma(\sigma_v)\epsilon) h^*(\mathbf{K} + (q_x, -q_y)) (\Gamma(\sigma_v)\epsilon)^\dagger$ shows that all $h_{ij,s}$ are real, where $\mathcal{T} = \epsilon K$ is the time-reversal symmetry with

$$\epsilon = \begin{pmatrix} 0 & -X \\ X & 0 \end{pmatrix} = \begin{pmatrix} 0 & 0 & 0 & -1 & 0 & 0 \\ 0 & 0 & 0 & 0 & 0 & -1 \\ 0 & 0 & 0 & 0 & -1 & 0 \\ 1 & 0 & 0 & 0 & 0 & 0 \\ 0 & 0 & 1 & 0 & 0 & 0 \\ 0 & 1 & 0 & 0 & 0 & 0 \end{pmatrix},$$

and

$$\Gamma(\sigma_v) = \begin{pmatrix} 0 & -iX \\ -iX & 0 \end{pmatrix}$$

is the representation matrix of a reflection $\sigma_v : (x, y, z) \rightarrow (-x, y, z)$.

The difference between $h_{ij,\uparrow}$ and $h_{ij,\downarrow}$ mainly comes from the spin-orbit coupling. Without it, $h_{ij,\uparrow} = h_{ij,\downarrow} \equiv h_{ij}$. Assuming the on-site $\mathbf{L} \cdot \mathbf{S}$ coupling,

$$h(\mathbf{K} + \mathbf{q}) = \begin{pmatrix} h_0 + \frac{\lambda}{2}L_z & 0 \\ 0 & h_0 - \frac{\lambda}{2}L_z \end{pmatrix},$$

with $L_z = \text{diag}(0, 2, -2)$. Note that the on-site spin-orbit coupling does not split the bands of $\psi_1 = d_{z^2}$. The splitting by the $\mathbf{L} \cdot \mathbf{S}$ spin-orbit is 2λ . First principle calculations have report that $h_{33} > h_{11} > h_{22} \gg |2\lambda|$ and the Fermi energy lies between the bands from ψ_1 and $\psi_{2(3)}$ at $K(-K)$. Using this knowledge, we can obtain the 4×4 low-energy effective model Hamiltonian[Di Xiao

	a	t	Δ	2λ
MoS ₂	3.193	1.66	1.66	0.15
WS ₂	3.197	1.79	1.79	0.43
MoSe ₂	3.313	1.47	1.47	0.18
WSe ₂	3.310	1.60	1.60	0.46

Table 2.1: Fitting parameters a , t , Δ , and λ . [1]

2012] for a single layer transition metal dichalcogenides

$$h_{\text{eff}}(\tau\mathbf{K} + \mathbf{q}) = at\mathbf{q} \cdot \boldsymbol{\sigma} + \frac{\Delta}{2}\sigma_z - \lambda\tau\frac{\sigma_z - 1}{2}s_z, \quad (2.14)$$

with the lattice constant a , $t = h_{12}/a$, and $\Delta = h_{11} - h_{22}$. Here, σ_i acts on the orbital space spanned by $\{\psi_1, \psi_2\}$ and s_z acts on the spin space. Note that t is the spin-up band among the two spin-split valence bands which is placed above if $\tau\lambda > 0$. The fitting parameters a , t , Δ , and λ are shown in Table (..)[Di Xiao 2012]. In all listed materials, $\lambda > 0$ which means the upper band of the two spin-split valence bands consists of $\psi_{2\uparrow}(\mathbf{r})$ and $\psi_{3\downarrow}(\mathbf{r})$ at \mathbf{K} and $-\mathbf{K}$, respectively.

2.2.3 Multi-Weyl node

A Weyl node does not require any symmetry. It can exist at any point in the Brillouin zone. The stability of a Weyl node also reflects the fact that a Weyl node does not require any special symmetry. However, its extension for a higher topological charge is not stable. For example, a version of extension of a Weyl node described by the following Hamiltonians

$$H_{2\text{-Weyl}}(\mathbf{k}) = \begin{pmatrix} k_z & k_-^2 \\ k_+^2 & -k_z \end{pmatrix},$$

$$H_{3\text{-Weyl}}(\mathbf{k}) = \begin{pmatrix} k_z & k_-^3 \\ k_+^3 & -k_z \end{pmatrix},$$

which will turn out to be Hamiltonians for a double- and a triple-Weyl node, have topological charges of magnitude 2 or 3. However, they are not stable. They are gapped if a perturbation $a_x\sigma_x + a_y\sigma_y$ is added to $H_{2(3)\text{-Weyl}}$. To have such nodal points stable, we need some special symmetries. In the remaining part of this section, we will show that some rotational symmetries make the nodes stable.

Let us begin with a general implication of a n -fold rotational symmetry. When a lattice is invariant under a n -fold rotational symmetry along an axis, the Hamiltonian should satisfy

$$H(\mathbf{k}) = \Gamma[C_n]H(\hat{C}_n^{-1}\mathbf{k})\Gamma[C_n]^\dagger. \quad (2.15)$$

If the wave vector \mathbf{k} is a point on the line called the rotationally invariant line, then the Hamiltonian at that \mathbf{k} is invariant under C_n , $[\Gamma[C_n], H(\mathbf{k})] = 0$, and the states on this line can be labeled with the eigenvalues of C_n . At a general point of the rotationally invariant line only four types of transformation can be included in the group of the wave vector. One is the rotation, another is the space-time inversion \mathcal{IT} , and the third is a combination of mirror reflection and time-reversal $\sigma_h\mathcal{T}$, and the other is a mirror reflection σ_v . Here, σ_h is the mirror reflection against the plane perpendicular to the rotationally invariant line, while σ_v is a mirror reflection against a plane on which the rotationally invariant line lies. Combinations of C_2 rotation along an axis perpendicular to the rotationally invariant line and either of the time-reversal, spatial inversion, or a mirror reflection, such as $C_2\mathcal{T}$ or $C_2\mathcal{I}$, can be made by the combination of those four. For example, $C_2\mathcal{T} = \sigma_v\mathcal{IT}$. We first consider the case in which only the rotations are the symmetry of the wave vector of the general points on the rotationally invariant line.

2.2.3.1 Multi-Weyl nodes protected by a n -fold rotational symmetry

When only the n -fold rotation and its powers C_n^m are the symmetries of the wave vector, no degeneracy in the electronic band structures is protected by the symmetries because all irreducible representation of the group of the wave vector is one-dimensional. However, accidental degeneracies can happen and these are what is of our interest. To investigate the electronic structure around the accidental degeneracy, let us begin with a 2×2 Hamiltonian of the form

$$H(\mathbf{K} + \mathbf{q}) = f(\mathbf{K}, \mathbf{q})\sigma_+ + f^*(\mathbf{K}, \mathbf{q})\sigma_- + g(\mathbf{K}, \mathbf{q})\sigma_z,$$

where $\sigma_{\pm} = \sigma_x \pm i\sigma_y$. Here, \mathbf{K} does denote a general point in the rotationally invariant line, not the corners of the hexagonal Brillouin zone. Also, \mathbf{q} is an deviation of a wave vector from the rotationally invariant line, and thus \mathbf{q} is perpendicular to the line. The Hamiltonian describes two bands near the rotationally invariant line. In general, $f(\mathbf{K}, \mathbf{0}) = 0$ and $g(\mathbf{K}, \mathbf{0}) \neq 0$ if the eigenvalues of C_n of two bands are different. However, if there is a point $\mathbf{K} = \mathbf{K}_0$ such that $g(\mathbf{K}_0, \mathbf{0}) = 0$, an accidental degeneracy happens and we are going to find the possible symmetry allowed forms of $f(\mathbf{K}, \mathbf{q})$. Taking the spin degree of freedom into account, the eigenvalue of C_n is $e^{-i\frac{2\pi p}{n}} e^{-i\frac{F\pi p}{n}}$ with $p = 0, 1, 2, \dots, n-1$ and $F = \pm 1$. However, we can set $F = 1$ because $2p + 1 = 2(p + 1) - 1$. Hence, The representation matrix of C_n would be

$$\Gamma[C_n] = \begin{pmatrix} e^{-i\frac{(2p+1)\pi}{n}} & 0 \\ 0 & e^{-i\frac{(2q+1)\pi}{n}} \end{pmatrix} = e^{-i\frac{(p+q+1)\pi}{n}} \begin{pmatrix} e^{-i\frac{(p-q)\pi}{n}} & 0 \\ 0 & e^{i\frac{(p-q)\pi}{n}} \end{pmatrix},$$

with which we can get the constraints of f and g

$$\begin{aligned} f(\mathbf{K}, \mathbf{q}) &= e^{-\frac{2(p-q)\pi i}{n}} f(\mathbf{K}, \hat{C}_n^{-1}\mathbf{q}), \\ g(\mathbf{K}, \mathbf{q}) &= g(\mathbf{K}, \hat{C}_n^{-1}\mathbf{q}), \end{aligned} \tag{2.16}$$

from Eq. (2.15). Making the z -axis coincide with the rotationally invariant line, Eq. (2.16) reads as

$$\begin{aligned} f(K_z, q_+, q_-) &= e^{-\frac{2(p-q)\pi i}{n}} f(K_z, e^{-\frac{2\pi i}{n}} q_+, e^{\frac{2\pi i}{n}} q_-), \\ g(K_z, q_+, q_-) &= g(K_z, e^{-\frac{2\pi i}{n}} q_+, e^{\frac{2\pi i}{n}} q_-), \end{aligned}$$

which lead

$$\begin{aligned} f(K_z, q_+, q_-) &= \sum_{(\alpha-\beta+p-q)\bmod n=0} F_{\alpha\beta}^{(p,q)}(K_z) q_+^\alpha q_-^\beta, \\ g(K_z, q_+, q_-, q_z) &= \sum_{\alpha \geq 0} G_\alpha(K_z) q_\perp^{2\alpha}, \end{aligned}$$

with $q_\perp = \sqrt{q_x^2 + q_y^2}$. The possible forms of f for all possible n and $p - q$ are listed in Table 2.2. One can easily find the cases in which we can get a stable double- or triple-Weyl node when only the rotational symmetries are considered. (Actually, because of the required cancellation of the topological charge in the whole Brillouin zone, there must be another Weyl, or a double-Weyl, or a triple-Weyl nodes in the other site of the Brillouin zone to cancel the topological change of the double- or triple-Weyl node we have found.)

2.2.3.2 Other symmetries \mathcal{IT} , $\sigma_h\mathcal{T}$, and σ_v

If other symmetries such as \mathcal{IT} , $\sigma_h\mathcal{T}$, and σ_v are present, parts of the Table 2.2 change. With \mathcal{IT} , every bands are doubly degenerate and a node is essentially a composition of two node of opposite topological charge leaving net topological charge zero. When it comes to $\sigma_h\mathcal{T}$, the commutation relations of $[C_n, \sigma_h] = 0$ and $[C_n, \mathcal{T}] = 0$ play an important role. Let $\phi_p(\mathbf{r})$ be an eigenstate of C_n with the eigenvalue $\exp\left[-\frac{2\pi pi}{n}\right]$. Then,

$$C_n [\sigma_h\mathcal{T}\phi_p(\mathbf{r})] = \sigma_h\mathcal{T} [C_n\phi_p(\mathbf{r})] = e^{i\frac{2\pi p}{n}} [\sigma_h\mathcal{T}\phi_p(\mathbf{r})]$$

shows that $\sigma_h\mathcal{T}\phi_p(\mathbf{r})$ is an eigenstate of C_n with eigenvalue $\exp\left[\frac{2\pi pi}{n}\right]$, which means that $\sigma_h\mathcal{T}$ enforces all bands doubly degenerate on the rotationally in-

n	$p - q \bmod n$	$H(\mathbf{K} + \mathbf{q})$
2	1	$m(K_z)\sigma_z + (aq_- + bq_+)\sigma_+ + \text{h.c}$
3	2	$m(K_z)\sigma_z + aq_+\sigma_+ + \text{h.c}$
	1	$m(K_z)\sigma_z + aq_-\sigma_+ + \text{h.c}$
4	3	$m(K_z)\sigma_z + aq_+\sigma_+ + \text{h.c}$
	2	$m(K_z)\sigma_z + (aq_+^2 + bq_-^2)\sigma_+ + \text{h.c}$
	1	$m(K_z)\sigma_z + aq_-\sigma_+ + \text{h.c}$
6	5	$m(K_z)\sigma_z + aq_+\sigma_+ + \text{h.c}$
	4	$m(K_z)\sigma_z + aq_+^2\sigma_+ + \text{h.c}$
	3	$m(K_z)\sigma_z + (aq_+^3 + bq_-^3)\sigma_+ + \text{h.c}$
	2	$m(K_z)\sigma_z + aq_-^2\sigma_+ + \text{h.c}$
	1	$m(K_z)\sigma_z + aq_-\sigma_+ + \text{h.c}$

Table 2.2: Effective Hamiltonians on the rotationally invariant line.

variant line. As it is with \mathcal{IT} , no node with non-zero net topological charge is possible.

The last remaining case is a system with σ_v . Let the mirror plane of σ_v be yz , and thus $\sigma_v : (x, y, z) \rightarrow (-x, y, z)$. It is easy to see that

$$\sigma_v C_n \sigma_v = C_n^{-1}$$

for any n . Therefore, we again get a two-fold degenerate bands on the rotationally invariant line of C_n .

In conclusion, multi-Weyl nodes are stable only when one of the following conditions is satisfied.

- No time-reversal symmetry and no vertical mirror reflection $\sigma_v \Rightarrow C_{4h}$ and C_{6h}
- No mirror reflection $\Rightarrow C_4$ and C_6 (Note that inversion symmetry is absent when C_4 or C_6 symmetries are present with all mirror reflections broken.)

Chapter 3

Self-consistent method in the mean-field level

This chapter is prepared to provide a short course about the self consistent method, especially focusing on the Hartree-Fock method. The Hartree-Fock method is arguably one of the most famous way used in the condensed matter theory taking the self-consistency of a many-body problem, together with the density functional theory. We derive the self-consistent equations using the Hartree-Fock factorization [16], and then we show that the same equation can be obtained in the more elegant method of variation from which we also derive the self-consistent equation in a multi-orbital system. After the derivation, the homogeneous electron gas is studied in detail for a heuristic purpose

3.1 Derivation of the self-consistent equation using the Hartree-Fock factorization

The homogeneous electron gas is a system of electrons invariaiant under any translation and rotation. This assumption is simply encoded into the following Hamiltonian:

$$\hat{H} = \sum_{\mathbf{k},\sigma} \varepsilon_{\mathbf{k},\sigma} \hat{c}_{\mathbf{k},\sigma}^\dagger \hat{c}_{\mathbf{k},\sigma} + \frac{1}{2V} \sum_{\mathbf{k},\mathbf{p},\mathbf{q}} \sum_{\sigma,s} V(\mathbf{q}) \hat{c}_{\mathbf{k}+\mathbf{q},\sigma}^\dagger \hat{c}_{\mathbf{p}-\mathbf{q},s}^\dagger \hat{c}_{\mathbf{p},s} \hat{c}_{\mathbf{k},\sigma}, \quad (3.1)$$

where s and σ denote the spin indices and V is the total volume of the system.

When

$$V(\mathbf{q}) = \begin{cases} \frac{4\pi e^2}{q^2} & d = 3, \\ \frac{2\pi e^2}{q} & d = 2, \end{cases}$$

the interaction corresponds to the long-range Culomb interaction. Assuming that the fluctation of the expectation value of $\hat{c}_{\mathbf{k},s}^\dagger \hat{c}_{\mathbf{p},\sigma}$ is quite small, we can substitute $\hat{c}_{\mathbf{k},\sigma}^\dagger \hat{c}_{\mathbf{p},s}$ by

$$\hat{c}_{\mathbf{k},\sigma}^\dagger \hat{c}_{\mathbf{p},s} \rightarrow \langle \hat{c}_{\mathbf{p},s}^\dagger \hat{c}_{\mathbf{p},s} \rangle \delta_{\mathbf{k},\mathbf{p}} \delta_{s,\sigma} + \delta \left(\hat{c}_{\mathbf{k},\sigma}^\dagger \hat{c}_{\mathbf{p},s} \right)$$

where $\delta \left(\hat{c}_{\mathbf{k},\sigma}^\dagger \hat{c}_{\mathbf{p},s} \right) \equiv \hat{c}_{\mathbf{k},\sigma}^\dagger \hat{c}_{\mathbf{p},s} - \langle \hat{c}_{\mathbf{p},s}^\dagger \hat{c}_{\mathbf{p},s} \rangle \delta_{s,\sigma} \delta_{\mathbf{k},\mathbf{p}}$ is the fluctuation of $\hat{c}_{\mathbf{k},\sigma}^\dagger \hat{c}_{\mathbf{p},s}$ assumed to be very small. After substitution and dropping terms involving the small fluctuations , we get

$$\begin{aligned} \hat{H}_{\text{MF}} &= \sum_{\mathbf{k},\sigma} \varepsilon_{\mathbf{k},s} \hat{c}_{\mathbf{k},s}^\dagger \hat{c}_{\mathbf{k},s} \\ &\quad - \frac{1}{2V} \sum_{\mathbf{k},\mathbf{p},\mathbf{q}} \sum_{\sigma,s} V(\mathbf{q}) \delta_{\mathbf{q},\mathbf{p}-\mathbf{k}} \left\{ \langle \hat{c}_{\mathbf{k}+\mathbf{q},\sigma}^\dagger \hat{c}_{\mathbf{p},s} \rangle \hat{c}_{\mathbf{p}-\mathbf{q},s}^\dagger \hat{c}_{\mathbf{k},\sigma} + \langle \hat{c}_{\mathbf{p}-\mathbf{q},s}^\dagger \hat{c}_{\mathbf{k},\sigma} \rangle \hat{c}_{\mathbf{k}+\mathbf{q},\sigma}^\dagger \hat{c}_{\mathbf{p},s} \right\} \\ &\quad + \frac{1}{2V} \sum_{\mathbf{k},\mathbf{p},\mathbf{q}} V(\mathbf{q}) \delta_{\mathbf{q},0} \left\{ \langle \hat{c}_{\mathbf{k}+\mathbf{q}}^\dagger \hat{c}_{\mathbf{k}} \rangle \hat{c}_{\mathbf{p}-\mathbf{q}}^\dagger \hat{c}_{\mathbf{p}} + \langle \hat{c}_{\mathbf{p}-\mathbf{q}}^\dagger \hat{c}_{\mathbf{p}} \rangle \hat{c}_{\mathbf{k}+\mathbf{q}}^\dagger \hat{c}_{\mathbf{k}} \right\} \\ &= \sum_{\mathbf{k}} \varepsilon_{\mathbf{k}} \hat{c}_{\mathbf{k}}^\dagger \hat{c}_{\mathbf{k}} - \frac{1}{V} \sum_{\mathbf{k}} \left[\sum_{\mathbf{p}} V(\mathbf{p}-\mathbf{k}) \langle \hat{c}_{\mathbf{p}}^\dagger \hat{c}_{\mathbf{p}} \rangle \right] \hat{c}_{\mathbf{k}}^\dagger \hat{c}_{\mathbf{k}} \\ &\quad + \frac{1}{V} \sum_{\mathbf{k}} \left[\sum_{\mathbf{p}} V(\mathbf{0}) \langle \hat{c}_{\mathbf{p}}^\dagger \hat{c}_{\mathbf{p}} \rangle \right] \hat{c}_{\mathbf{k}}^\dagger \hat{c}_{\mathbf{k}}. \end{aligned} \tag{3.2}$$

The last term is called the Hartree term

$$\Sigma_H(\mathbf{k}) = \frac{1}{V} \sum_{\mathbf{p}} V(\mathbf{0}) \langle \hat{c}_{\mathbf{p}}^\dagger \hat{c}_{\mathbf{p}} \rangle, \tag{3.3}$$

and the second term is called the Fock term, or the exchange self-energy,

$$\Sigma_F(\mathbf{k}) = -\frac{1}{V} \sum_{\mathbf{p}} V(\mathbf{p}-\mathbf{k}) \langle \hat{c}_{\mathbf{p}}^\dagger \hat{c}_{\mathbf{p}} \rangle. \tag{3.4}$$

The role of the Hartree term Σ_H is to provide an additional chemical potential to all electrons. However, the electrostatic potential from the background positive ions is almost exactly the same and cancels the Hartree term, and thus we usually ignore it and focus on the Fock term $\Sigma_F(\mathbf{k})$ which renormalizes the electronic band dispersion $\varepsilon_{\mathbf{k}}$.

The definition of $\Sigma_F(\mathbf{k})$ requires us to calculate the electron density $n(\mathbf{k}) = \langle \hat{c}_{\mathbf{k}}^\dagger \hat{c}_{\mathbf{k}} \rangle$ whose sum over the whole momentum space must be the number of whole electrons N_{el} , typically an order of 10^{23} . In the single band model, the electron density can be calculated simply as

$$n(\mathbf{k}) = \Theta(\varepsilon_F - \varepsilon_{\mathbf{k}} - \Sigma_F(\mathbf{k})),$$

where ε_F is the Fermi level to be determined too, from which we get the self-consistent equation for $\Sigma_F(\mathbf{k})$:

$$\Sigma_F(\mathbf{k}) = \frac{1}{V} \sum_{\mathbf{p}} V(\mathbf{p} - \mathbf{k}) \Theta(\varepsilon_F - \varepsilon_{\mathbf{p}} - \Sigma_F(\mathbf{p})), \quad (3.5)$$

with a constraint on ε_F

$$N_{\text{el}} = \sum_{\mathbf{k}} \Theta(\varepsilon_F - \varepsilon_{\mathbf{k}} - \Sigma_F(\mathbf{k})). \quad (3.6)$$

3.2 Derivation of the self-consistent equation using the variational principle

As aforementioned, Sec 3.1 is revisited with the variation principle. The identical result can be obtained by minimizing the following functional of Φ

$$E[\Phi] = \frac{\langle \Phi | \hat{H} | \Phi \rangle}{\langle \Phi | \Phi \rangle}, \quad (3.7)$$

with

$$\hat{H} = \sum_{i,j \in I} h_{ij} \hat{c}_i^\dagger \hat{c}_j + \frac{1}{2} \sum_{i,j,k,l \in I} V_{ijkl} \hat{c}_i^\dagger \hat{c}_j^\dagger \hat{c}_k \hat{c}_l,$$

where $V_{ijkl} = -V_{jikl} = -V_{ijlk}$ is required due to the fermionic anticommutation relation.

To take the variation of E with respect to Φ , we assume that $|\Phi\rangle$ is well approximated by the Slater determinant composed of the eigenfunctions of the non-interacting part of \hat{H} .

$$|\Phi_N\rangle = \prod_{\mathbf{k},\sigma} \hat{c}_{\mathbf{k},\sigma}^\dagger |0\rangle \equiv \frac{1}{\sqrt{N!}} \sum_P \text{sgn}(P) |P(\mathbf{k}_1, \uparrow)\rangle |P(\mathbf{k}_1, \downarrow)\rangle \cdots |P(\mathbf{k}_{\frac{N}{2}}, \downarrow)\rangle, \quad (3.8)$$

where N is the number of electrons. To evaluate $\langle \Phi | \hat{H} | \Phi \rangle$, we need to know what we get by operating \hat{c} and \hat{c}^\dagger on $|\Phi\rangle$. For this purpose, we introduce two notations for states.

$$|\mathbf{r}_1, \mathbf{r}_2, \cdots, \mathbf{r}_N\rangle = |r_1\rangle |r_2\rangle \cdots |r_N\rangle, \quad (3.9)$$

$$\begin{aligned} |\mathbf{r}_1, \mathbf{r}_2, \cdots, \mathbf{r}_N\rangle &\equiv \frac{1}{\sqrt{N!}} \sum_P |r_{P(1)}, r_{P(2)}, r_{P(3)}, \cdots, r_{P(N)}\rangle & (3.10) \\ &= \frac{1}{\sqrt{N!}} \sum_P \text{sgn}(P) |r_{P(1)}\rangle |r_{P(2)}\rangle |r_{P(3)}\rangle \cdots |r_{P(N)}\rangle. \end{aligned}$$

The completeness of the vector space is expressed as

$$1 = \int_{\mathbf{r}_1} \int_{\mathbf{r}_2} \cdots \int_{\mathbf{r}_N} |\mathbf{r}_1, \mathbf{r}_2, \cdots, \mathbf{r}_N\rangle \langle \mathbf{r}_1, \mathbf{r}_2, \cdots, \mathbf{r}_N|, \quad (3.11)$$

$$1 = \frac{1}{N!} \int_{\mathbf{r}_1} \int_{\mathbf{r}_2} \cdots \int_{\mathbf{r}_N} |\mathbf{r}_1, \mathbf{r}_2, \cdots, \mathbf{r}_N\rangle \langle \mathbf{r}_1, \mathbf{r}_2, \cdots, \mathbf{r}_N|, \quad (3.12)$$

where the first relation is valid for both of Fock spaces of bosons and fermions while the second one is only valid for the Fock space of fermions. Provided with these notations, the normalized Slater determinant of a N -electron state

is represented as

$$\begin{aligned}
\langle \mathbf{r}_1, \mathbf{r}_2, \dots, \mathbf{r}_N | \Phi_N \rangle &= \frac{1}{\sqrt{N!}} \langle \mathbf{r}_1, \mathbf{r}_2, \dots, \mathbf{r}_N | \Phi_N \rangle \\
&= \frac{1}{\sqrt{N!}} \begin{vmatrix} \phi_{\alpha_1}(\mathbf{r}_1) & \phi_{\alpha_2}(\mathbf{r}_1) & \cdots & \phi_{\alpha_N}(\mathbf{r}_1) \\ \phi_{\alpha_1}(\mathbf{r}_2) & \phi_{\alpha_2}(\mathbf{r}_2) & \cdots & \phi_{\alpha_N}(\mathbf{r}_2) \\ \vdots & \vdots & \vdots & \vdots \\ \phi_{\alpha_1}(\mathbf{r}_N) & \phi_{\alpha_2}(\mathbf{r}_N) & \cdots & \phi_{\alpha_N}(\mathbf{r}_N) \end{vmatrix}, \quad (3.13)
\end{aligned}$$

where $\phi_{\alpha_n}(\mathbf{r})$ is an orthonormal basis function of the non-interaction systems labelled as α_i . Let us expand the field operator $\hat{\Psi}(\mathbf{x})$, annihilating an electron at a site \mathbf{x} , with another normalized basis $I = \{\chi_i | i = 1, 2, \dots, M\}$, not necessarily orthogonal,

$$\hat{\Psi}(\mathbf{r}) = \sum_{i \in I} \chi_i(\mathbf{r}) \hat{c}_i, \quad (3.14)$$

$$\hat{c}_i = [S^{-1}]_{ij} \int d^d r \chi_j^*(\mathbf{r}) \hat{\Psi}(\mathbf{r}), \quad (3.15)$$

with $S_{ij} = \int d^d r \chi_i^*(\mathbf{r}) \chi_j(\mathbf{r})$. Given the basis χ_i of the single particle Hilbert space, the eigenstates ϕ'_{α_n} s are expressed by a linear combination of the basis:

$$\phi_{\alpha_n} = \sum_i C_{in} \chi_i,$$

$$\langle i | n \rangle = \sum_i C_{jn} S_{ij}$$

which enables us to calculate $\langle r_1, r_2, \dots, r_{N-1} | \hat{c}_j | \Phi \rangle$:

$$\begin{aligned}
\langle r_1, r_2, \dots, r_{N-1} | \hat{c}_j | \Phi \rangle &= \sum_s [S^{-1}]_{js} \int d^d \mathbf{x} \chi_s^*(\mathbf{x}) \begin{vmatrix} \phi_{\alpha_1}(\mathbf{x}) & \phi_{\alpha_2}(\mathbf{x}) & \cdots & \phi_{\alpha_N}(\mathbf{x}) \\ \phi_{\alpha_1}(\mathbf{r}_1) & \phi_{\alpha_2}(\mathbf{r}_1) & \cdots & \phi_{\alpha_N}(\mathbf{r}_1) \\ \vdots & \vdots & \vdots & \vdots \\ \phi_{\alpha_1}(\mathbf{r}_{N-1}) & \phi_{\alpha_2}(\mathbf{r}_{N-1}) & \cdots & \phi_{\alpha_N}(\mathbf{r}_{N-1}) \end{vmatrix} \\
&= \sum_n (-1)^{n-1} C_{jn} \langle \mathbf{r}_1, \mathbf{r}_2, \dots, \mathbf{r}_{N-1} | \alpha_1, \dots, \alpha_{n-1}, \alpha_{n+1}, \dots \rangle, \quad (3.16)
\end{aligned}$$

and $\langle r_1, r_2, \dots, r_{N-2} | \hat{c}_k \hat{c}_l | \Phi \rangle$:

$$\begin{aligned}
\langle r_1, r_2, \dots, r_{N-2} | \hat{c}_k \hat{c}_l | \Phi \rangle &= \int_{\mathbf{x}_1, \dots, \mathbf{x}_{N-1}} \langle r_1, r_2, \dots, r_{N-2} | \hat{c}_k | x_1, x_2, \dots, x_{N-1} \rangle \\
&\quad \times \langle x_1, x_2, \dots, x_{N-1} | \hat{c}_l | \Phi \rangle \\
&= \sum_{\alpha_i} \eta_{mn} C_{km} C_{ln} \times t \tag{3.17} \\
&\quad \langle r_1, r_2, \dots, r_{N-2} | \alpha_1, \dots, \alpha_{m-1}, \alpha_{m+1}, \dots, \alpha_{n-1}, \alpha_{n+1} \dots \rangle,
\end{aligned}$$

with $\eta_{mn} = (-1)^{m+n}$. Also, the norm of $|\Phi\rangle$ is

$$\langle \Phi | \Phi \rangle = \left[\sum_{i,j \in I} C_{i,1}^* S_{ij} C_{j,1} \right] \left[\sum_{i,j \in I} C_{i,2}^* S_{ij} C_{j,2} \right] \left[\sum_{i,j \in I} C_{i,2}^* S_{ij} C_{j,2} \right] \tag{3.18}$$

Armed with Eq (3.16) and Eq (3.17), we can evaluate $\langle \Phi | H | \Phi \rangle$:

$$\langle \Phi | H | \Phi \rangle = \sum_{ij} h_{ij} \langle \Phi | \hat{c}_i^\dagger \hat{c}_j | \Phi \rangle + \frac{1}{2} \sum_{ijkl} V_{ijkl} \langle \Phi | \hat{c}_i^\dagger \hat{c}_j^\dagger \hat{c}_k \hat{c}_l | \Phi \rangle,$$

where the first quadratic term is rewritten as

$$\begin{aligned}
\sum_{ij} h_{ij} \langle \Phi | \hat{c}_i^\dagger \hat{c}_j | \Phi \rangle &= \frac{1}{(N-1)!} \sum_{ij} h_{ij} \int_{r_1, \dots, r_{N-1}} \langle \Phi | \hat{c}_i^\dagger | r_1, r_2, \dots, r_{N-1} \rangle \\
&\quad \times \langle r_1, r_2, \dots, r_{N-1} | \hat{c}_j | \Phi \rangle \\
&= \sum_{m,n} \sum_{ij} h_{ij} (-1)^{m+n} C_{im}^* C_{jn} M_{mn} \\
&= \sum_n \sum_{ij} C_{in}^* h_{ij} C_{jn}, \tag{3.19}
\end{aligned}$$

where $M_{mn} \equiv \langle \alpha_1, \dots, \alpha_{m-1}, \alpha_{m+1}, \dots, \alpha_N | \alpha_1, \dots, \alpha_{n-1}, \alpha_{n+1}, \dots, \alpha_N \rangle$, while

the second quadratic term turns out

$$\begin{aligned}
\frac{1}{2} \sum_{ijkl} V_{ijkl} \left\langle \Phi \left| \hat{c}_i^\dagger \hat{c}_j^\dagger \hat{c}_k \hat{c}_l \right| \Phi \right\rangle &= \frac{1}{2(N-2)!} \sum_{ijkl} V_{ijkl} \int_{\mathbf{r}_1, \dots, \mathbf{r}_{N-2}} \left\langle \Phi \left| \hat{c}_i^\dagger \hat{c}_j^\dagger \right| \mathbf{r}_1, \mathbf{r}_2, \dots, \mathbf{r}_{N-2} \right\rangle \\
&\quad \times \left\langle \mathbf{r}_1, \mathbf{r}_2, \dots, \mathbf{r}_{N-2} \left| \hat{c}_k \hat{c}_l \right| \Phi \right\rangle \\
&= \frac{1}{2} \sum_{ijkl} V_{ijkl} \sum_{m,n} \eta_{mn} C_{im}^* C_{jn}^* \times \sum_{p,q} \eta_{pq} C_{kp} C_{lq} M_{nm;pq} \\
&= \frac{1}{2} \sum_{ijkl} V_{ijkl} \sum_{m,n} \eta_{mn} C_{im}^* C_{jn}^* \times \sum_{p,q} \eta_{pq} C_{kp} C_{lq} (\delta_{mq} \delta_{np} - \delta_{mp} \delta_{nq}) \\
&= \frac{1}{2} \sum_{ijkl} V_{ijkl} \sum_{m,n} C_{im}^* C_{jn}^* (C_{kn} C_{lm} - C_{km} C_{ln}),
\end{aligned} \tag{3.20}$$

with $M_{nm;pq} = \langle \dots \alpha_{n-1}, \alpha_{n+1}, \dots, \alpha_{m-1}, \alpha_{m+1} \dots | \dots \alpha_{p-1}, \alpha_{p+1}, \dots, \alpha_{q-1}, \alpha_{q+1} \dots \rangle$.

Here, the last equality of Eq (3.19) and (3.20) are valid when the eigenfunctions $\phi_\alpha(\mathbf{x})$ are normalized. Applying the variational principle with respect to C_{in}^* , we get

$$0 = \frac{\partial E[\Phi]}{\partial C_{in}^*} = \frac{1}{\langle \Phi | \Phi \rangle} \left[\frac{\partial}{\partial C_{in}^*} \langle \Phi | H | \Phi \rangle - E[\Phi] \frac{\partial}{\partial C_{in}^*} \langle \Phi | \Phi \rangle \right], \tag{3.21}$$

giving us an equation of C'_{in} s:

$$ES_{il} C_{ln} = \sum_l h_{il} C_{ln} + \sum_{jkl} \sum_m (C_{jm}^* V_{ijkl} C_{km} - C_{jm}^* V_{ijkl} C_{lm}) C_{kn}, \tag{3.22}$$

where the $\int d^d \mathbf{x} \phi_{\alpha_m}^*(\mathbf{x}) \phi_{\alpha_n}(\mathbf{x}) = C_{im}^* S_{ij} C_{jn} = \delta_{mn}$ is assumed. The second term and the third term in the right-hand side of Eq (3.22) are actually the Hartree self-energy term and the Fock self energy term:

$$[\Sigma_H]_{il} = \sum_m \sum_{j,k} C_{jm}^* V_{ijkl} C_{km}, \tag{3.23}$$

$$[\Sigma_F]_{ik} = - \sum_m \sum_{j,l} C_{jm}^* V_{ijkl} C_{lm}, \tag{3.24}$$

and then Eq (3.22) is written as

$$ESC_n = (h + \Sigma_H + \Sigma_F) C_n$$

with $\mathbf{C}_n = (C_{1,n}, C_{2,n}, \dots, C_{M,n})^T$.

Applying to the translationally system in which the momentum is a good quantum number, i, j, k , and l in the summation $\sum_{ijkl} V_{ijkl} \hat{c}_i^\dagger \hat{c}_j^\dagger \hat{c}_k \hat{c}_l$ correspond to the momentum $\mathbf{k} + \mathbf{q}$, $\mathbf{p} - \mathbf{q}$, \mathbf{p} and \mathbf{k} . Eq (3.23) and (3.24) become

$$[\Sigma_H(\mathbf{p})]_{il} = \sum_m \sum_{\mathbf{k}, \mathbf{q}} C_m^*(\mathbf{k}) V(\mathbf{0}) C_m(\mathbf{k}), \quad (3.25)$$

$$[\Sigma_F(\mathbf{p})]_{il} = \sum_m \sum_{j, l} C_m^*(\mathbf{k}) V(\mathbf{k} - \mathbf{p}) C_m(\mathbf{k}), \quad (3.26)$$

which is identical to Eq (3.3) and (3.4) when M is 1.

3.3 The self-energies in a multi-orbital system

From Eq (3.25) and (3.26), the mean-field expression for the self-energies can be obtained. Here we use $M = N \times M_o$ functions to expand the single particle Hilbert space, where M_o is the number of Wannier orbitals in a unit cell and N is the number of unit cells in the system which will be sent to infinity. In this setting, the second quantized form of interaction is replaced by

$$\hat{V} = \frac{1}{2} \sum_{i,j,k,l \in I} V_{ijkl} \hat{c}_i^\dagger \hat{c}_j^\dagger \hat{c}_k \hat{c}_l \rightarrow \hat{V} = \frac{1}{2} \sum_{a,b,c,d=1}^{M_o} V_{abcd}(\mathbf{q}) \hat{c}_{\mathbf{k}+\mathbf{q},a}^\dagger \hat{c}_{\mathbf{p}-\mathbf{q},b}^\dagger \hat{c}_{\mathbf{p},c} \hat{c}_{\mathbf{k},d},$$

and the consequential expressions of self-energies are given as

$$[\Sigma_H(\mathbf{p})]_{ad} = \sum_m \sum_{\mathbf{k}, \mathbf{q}} C_{b,m}^*(\mathbf{k}) V_{abcd}(\mathbf{0}) C_{c,m}(\mathbf{k}), \quad (3.27)$$

$$[\Sigma_F(\mathbf{p})]_{ac} = \sum_m \sum_{\mathbf{k}, \mathbf{q}} C_{b,m}^*(\mathbf{k}) V_{abcd}(\mathbf{p} - \mathbf{k}) C_{d,m}(\mathbf{k}), \quad (3.28)$$

where a, b, c and d labels the Wannier orbitals in the unit cell.

3.4 The Hartree-Fock description of the homogeneous electron gas

For the homogeneous electron gas, the constraint Eq (3.6) on ε_F can be solved easily by introducing the Fermi momentum k_F satisfying

$$\frac{N_{\text{el}}}{V} = \begin{cases} \frac{k_F^3}{6\pi^2} & d = 3, \\ \frac{k_F^2}{4\pi} & d = 2. \end{cases}$$

The Fermi level ε_F is determined by

$$\varepsilon_F = \varepsilon_{k_F} + \Sigma_F(k_F).$$

Using k_F , the self-consistent equation for Σ_F Eq (3.5) is also expressed without Σ_F on the right hand side.

$$\Sigma_F(\mathbf{k}) = \frac{1}{V} \sum_{|\mathbf{p}| < k_F} V(\mathbf{p} - \mathbf{k}).$$

For the long-range Coulomb interaction in the three dimension, the integration in the right-hand side is just an elementary integration and one get

$$\begin{aligned} \Sigma_F^{(3d)}(\mathbf{k}) &= \frac{e^2}{\pi} \int_{-1}^1 dx \int_0^{k_F} \frac{p^2 dp}{p^2 + k^2 - 2pkx} \\ &= \frac{e^2 k_F}{\pi} \left[\frac{1}{2y} \int_0^1 dp p \log \frac{p+y}{|p-y|} \right] \\ &= -\frac{e^2 k_F}{\pi} \left[\frac{1}{2} + \frac{1-y^2}{4y} \log \left| \frac{1+y}{1-y} \right| \right], \end{aligned}$$

with $y = k/k_F$. Here we use the integration by part

$$x \log(x+a) = \frac{1}{2} \frac{d}{dx} x^2 \log(x+a) - \frac{1}{2} \frac{x^2 - a^2}{x+a} - \frac{1}{2} \frac{a^2}{x+a}.$$

For the two dimension, the integration can not be performed analytically and the result is expressed with the complete elliptic integrals respectively of the first and second kind[16]

$$\Sigma_F^{(2d)}(\mathbf{k}) = -\frac{2e^2 k_F}{\pi} \begin{cases} E(y) & y \leq 1, \\ y \left[E\left(\frac{1}{y}\right) - \left(1 - \frac{1}{y^2}\right) K\left(\frac{1}{y}\right) \right] & y \geq 1. \end{cases}$$

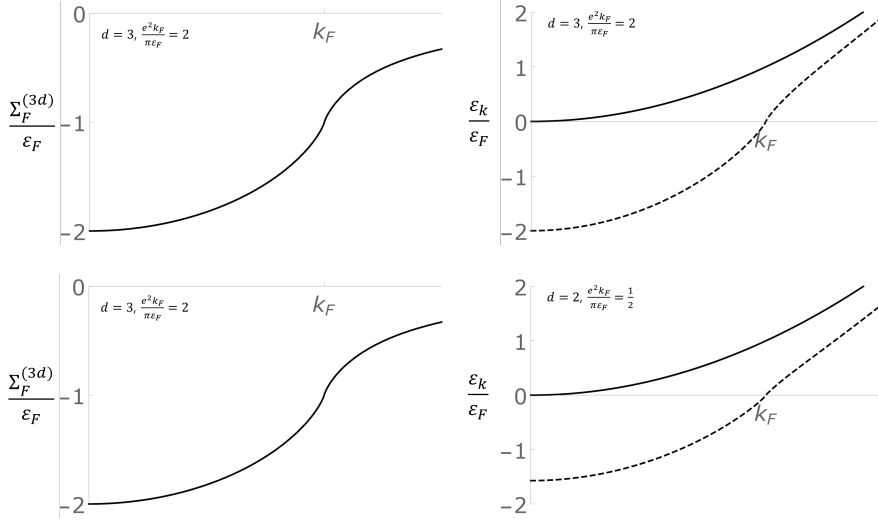


Figure 3.1: The Fock term, or the exchange self energy, and the energy dispersion of the homogeneous two- and three- dimensional electron gases. (a) and (c) : The exchange self-energy in two- and three- dimension divided by the Fermi energy. (b) and (d): Comparison between the non-interacting energy dispersion and the self-energy corrected energy dispersion of the two- and three- dimensional electron gases.

In Figure 3.1(a) and 3.1(c) the plots of $\Sigma_F^{(3d)}$ and $\Sigma_F^{(2d)}$ divided by ε_F are provided for the case of $\frac{e^2 k_F}{\pi \varepsilon_F} = 2$ and $\frac{e^2 k_F}{\pi \varepsilon_F} = \frac{1}{2}$, respectively. And the energy dispersion of electrons in the non-interacting limit and the energy dispersion in the Hartree-Fock approximation are also provided in Figure 3.1(b) and 3.1(d).

The values of the Σ_F at $k = 0$ and $k = k_F$ are

$$\begin{aligned}\Sigma_F^{(3d)}(0) &= -\frac{e^2 k_F}{\pi}, \\ \Sigma_F^{(3d)}(k_F) &= -\frac{e^2 k_F}{2\pi},\end{aligned}$$

and

$$\begin{aligned}\Sigma_F^{(2d)}(0) &= -e^2 k_F, \\ \Sigma_F^{(2d)}(k_F) &= -\frac{2e^2 k_F}{\pi}.\end{aligned}$$

Note that the energy dispersion of electrons is largely modified by $\varepsilon_k \rightarrow \varepsilon_k + \Sigma_F^{(3d)}(0)$.

$\frac{\Sigma^{(3d)}(0)}{\Sigma^{(3d)}(k_F)} = 2$ and $\frac{\Sigma^{(2d)}(0)}{\Sigma^{(2d)}(k_F)} = \frac{1}{2}$ implies that the electrons deep inside the Fermi sea are strongly influenced by the interaction. This conclusion does not coincide with the experimental result and the Landau's Fermi liquid

Chapter 4

Exciton-Polariton condensate in two-dimensional TMDC

4.1 Introduction

Monolayers of TMDC, such as MoS₂ and WSe₂, have attracted widespread interest in recent years as a semiconductor analogue of graphene. Like graphene, they are atomically thin, 2D materials, whose band extrema occurring at the Brillouin zone corners K and K' can be described very well by the Dirac Hamiltonian, that gives rise to the $\pm\pi$ -Berry phase at each valley, but, unlike graphene, possess direct band gaps at K and K' [1].

Given the band structure origin of the valley Berry phase, we may ask whether and how it may be affected by the electron-electron interaction and the electron-photon coupling. The electron-electron interaction in TMDC has been observed to give rise to both the electron-electron pairs, *i.e.* the Cooper pairs [17], and the electron-hole pairs, *i.e.* the excitons [18, 19], with superconductivity, which arises from the condensation of the former, shown to be possibly topologically non-trivial [20, 17, 21].

Meanwhile, the optical valley selection rule for the circularly polarized

light[1, 22, 23] shows the strong effect that the $\pm\pi$ -Berry phase has on the electron-photon coupling with direct band gaps (~ 1.5 to 2 eV) lying within the visible spectrum [8, 9].

The above considerations motivate us to study the condensation of polaritons, emergent bosons from hybridizations of cavity photons and excitons. It is tunable by both the Coulomb electron-electron interaction and the electron-photon coupling for the exciton binding and the photon-exciton hybridization, respectively. The recent years have seen reports in various systems of possible observation of this condensation [24, 25, 26] with progresses underway for TMDC [27, 28]. The room temperature polariton condensation is a possibility, light-matter coupling giving a very small polariton mass [29]. When the polariton lifetime, though limited by the finite lifetimes of both cavity photons and excitons, is much longer than the thermalization time, substantial evidences of superfluidity, such as vortex formation [30], Goldstone modes [31], and the Landau critical velocity [32], have been observed.

In this Chapter, we develop a mean-field theory for exciton-polaritons in gapped Dirac materials such as TMDCs, and demonstrate that due to the effect of the π -Berry phase, the mean-field electronic band structure with the polariton condensate can undergo symmetry-breaking or topological phase transitions¹ driven by the competition between the electron-electron interaction and the electron-photon coupling that can be tuned by the excitation density. We first apply our mean-field theory to the single valley model to show how the phase transitions arise and then extend the calculation on the physical two valley model to obtain various phases and their topological invariants.

¹By contrast, previous studies, *e.g.* [33], dealt with the topology of the effective polariton bands.

4.2 Model

The polariton condensation in our gapped Dirac materials should be derived from the electrons with the Coulomb interaction coupled to coherent photons. Hence the Hamiltonian we consider would be

$$\begin{aligned}
 \hat{H} &= \hat{H}_0 + \hat{H}_{\text{e-e}} + \hat{H}_{\text{ph}} + \hat{H}_{\text{e-ph}} - \mu_X \hat{N}_{\text{tot}}, \tag{4.1} \\
 \hat{H}_0 &= \sum_{\tau=\pm} \sum_{\mathbf{k}} \begin{bmatrix} \hat{c}_{\tau,1,\mathbf{k}}^\dagger & \hat{c}_{\tau,2,\mathbf{k}}^\dagger \end{bmatrix} \mathbf{d}_\tau^{(0)}(\mathbf{k}) \cdot \boldsymbol{\sigma} \begin{bmatrix} \hat{c}_{\tau,1,\mathbf{k}} \\ \hat{c}_{\tau,2,\mathbf{k}} \end{bmatrix}, \\
 \hat{H}_{\text{ph}} &= \hbar\omega_c \sum_I \left(\hat{a}_I^\dagger \hat{a}_I + \frac{1}{2} \right), \\
 \hat{H}_{\text{e-ph}} &= -\frac{1}{c} \vec{A} \cdot \sum_{\tau=\pm} \sum_{\mathbf{k}} \sum_{i,j} [\mathbf{J}^\tau(\mathbf{k})]_{ij} \hat{c}_{\tau,i,\mathbf{k}}^\dagger \hat{c}_{\tau,j,\mathbf{k}}, \\
 \hat{H}_{\text{e-e}} &= \frac{1}{2S} \sum_{\tau,\tau'} \sum_{\mathbf{k}_1,\mathbf{k}_2,\mathbf{q}} \sum_{i,j} V(\mathbf{q}) \hat{c}_{\tau,i,\mathbf{k}_1-\mathbf{q}}^\dagger \hat{c}_{\tau',j,\mathbf{k}_2+\mathbf{q}}^\dagger \hat{c}_{\tau',j,\mathbf{k}_2} \hat{c}_{\tau,i,\mathbf{k}_1},
 \end{aligned}$$

where $\boldsymbol{\sigma}$ represent the Pauli matrices, I the photon polarization index, $\mathbf{d}_\tau^{(0)}(\mathbf{k}) \equiv (\tau\hbar vk_x, \hbar vk_y, E_{\text{gap}}/2)$, with $\tau = \pm$ being the valley index, ω_c the cavity photon frequency and $V(\mathbf{q}) = \frac{2\pi e^2}{\epsilon q}$ the Coulomb interaction, with ϵ being the dielectric constant; note that the exchange terms of the electron-electron interaction are in the orbital rather than the band basis [34, 35, 36]. Meanwhile, the first quantized current operator is given by $\vec{J}_{ij}^\tau(\mathbf{k}) = -e\partial_{\mathbf{k}}[\mathbf{d}_\tau^{(0)}(\mathbf{k}) \cdot \boldsymbol{\sigma}]_{ij}$ ($i, j = 1, 2$) and the gauge field operator by

$$\vec{A} = \sum_I \sqrt{2\pi c^2 \hbar / \epsilon S L_c \omega_c} (\mathbf{e}_I \hat{a}_I e^{-i\omega_c t} + \mathbf{e}_I^* \hat{a}_I^\dagger e^{i\omega_c t}),$$

where \vec{e}_I is the photon polarization vector and S, L_c the cavity area and length, respectively. $\hat{c}_{1(2)}$ and \hat{a}_I are the annihilation operators for the electron in the $L_z = 0$ ($L_z = 2\tau$) orbital and the photon with the polarization I , respectively. Each valley is taken to be completely spin-polarized with opposite spin polarization, *i.e.* $S_z = \tau/2$, due to the transition metal atomic spin-orbit coupling $\mathbf{L} \cdot \mathbf{S}$ removing the spin degeneracy in the $L_z = 2\tau$ orbital; hence,

the dark excitons from intra-valley spin-flip [37] will not be considered. Lastly, $\hat{N}_{\text{tot}} = \sum_I \hat{a}_I^\dagger \hat{a}_I + \hat{N}_{\text{ex}}$ is the total number of excitations, both photons and excitons, in the system and tuned by the chemical potential μ_X . Since the number of exciton \hat{N}_{ex} is the number of electrons excited from the valence band to the conduction band, the band basis for the electrons, $\sum_\alpha [W(\mathbf{k})]_{i,\alpha} \hat{\psi}_{\alpha,\mathbf{k}} = \hat{c}_{i,\mathbf{k}}$ which diagonalizes \hat{H}_0 of Eq. (4.1) with $\hat{\psi}_{c(v)}$ as the annihilation operator of electrons in the conduction (valence) band, can be convenient. This allows to identify the exciton number as $\hat{N}_{\text{ex}} \equiv \sum_{\tau,\mathbf{k}} \hat{n}_{\text{ex},\mathbf{k}}^\tau$ where $\hat{n}_{\text{ex},\mathbf{k}}^\tau \equiv (\hat{\psi}_{\tau,c,\mathbf{k}}^\dagger \hat{\psi}_{\tau,c,\mathbf{k}} + \hat{\psi}_{\tau,v,\mathbf{k}} \hat{\psi}_{\tau,v,\mathbf{k}}^\dagger)/2$. Physically, we are interested in the thermal quasi-equilibrium that is reached after the cooling of a population of hot polaritons initially introduced by a short laser pulse [38]. For simplicity, we shall set the temperature to be zero.

4.3 Self-consistent mean-field equation

We use the BCS variational wave function for the polariton condensate [35, 36]

$$\Psi(\Lambda_\pm) \rangle = \mathcal{N} \prod_{I,\tau=\pm,\mathbf{k}} e^{\Lambda_I \hat{a}_I^\dagger} (u_{\tau,\mathbf{k}} + v_{\tau,\mathbf{k}} \hat{\psi}_{\tau,c,\mathbf{k}}^\dagger \hat{\psi}_{\tau,v,\mathbf{k}}) |0\rangle \quad (4.2)$$

with $\mathcal{N} = e^{-\sum_{I=\pm} \Lambda_I^2/2}$ and $|u_{\tau,\mathbf{k}}|^2 + |v_{\tau,\mathbf{k}}|^2 = 1$, where $I = \pm$ corresponds to the right (left) circularly polarization $\vec{e}_\pm = (1, \pm i)/\sqrt{2}$ and $|0\rangle$ is the ground state of \hat{H}_0 , in which photons are absent and all the valence (conduction) band states are occupied (vacant). In this wave function, the photon component gives the coherent state with the number of photons $\langle \hat{a}_I^\dagger \hat{a}_I \rangle = \Lambda_I^2$ and of excitons $\langle \hat{N}_{\tau,\text{ex}} \rangle = \sum_{\mathbf{k}} |v_{\tau,\mathbf{k}}|^2$; only the excitons with zero center-of-mass momentum are condensed, and the condensation energy arises only from the stronger intra-valley - but not from the weaker inter-valley - electron-electron interaction. To determine Λ_\pm , $u_{\tau,\mathbf{k}}$, $v_{\tau,\mathbf{k}}$ that minimize $\langle \Psi(\Lambda_\pm) | \hat{H} | \Psi(\Lambda_\pm) \rangle$, we obtain the mean-field self-consistency condition not only for the electron-electron interac-

tion through $\hat{H}_{\text{e-e}}^{\text{MF}} = \sum_{\tau,i,j,\mathbf{k}} \tilde{\Delta}_{\tau;ij}(\mathbf{k}) \hat{c}_{\tau,i,\mathbf{k}}^\dagger \hat{c}_{\tau,j,\mathbf{k}}$ where ²

$$\tilde{\Delta}_{\tau;ij}(\mathbf{k}) = -\frac{1}{S} \sum_{\mathbf{p}} V(\mathbf{k} - \mathbf{p}) \left\langle \hat{c}_{\tau,j,\mathbf{p}}^\dagger \hat{c}_{\tau,i,\mathbf{p}} \right\rangle \Big|_{\mu_X=0, \Lambda_\tau=0}^{\mu_X, \Lambda_\tau}, \quad (4.3)$$

but also for $\hat{H}_{\text{ph}} + \hat{H}_{\text{e-ph}}$, by which Λ_I 's are determined as [36]

$$\Lambda_I = -\frac{1}{\hbar\omega_c - \mu_X} \frac{1}{\sqrt{S}} \sum_{\tau,\mathbf{k}} \left(g_{\mathbf{k}}^{I,\tau} \right)^* \langle \hat{\psi}_{\tau,v,\mathbf{k}}^\dagger \hat{\psi}_{\tau,c,\mathbf{k}} \rangle, \quad (4.4)$$

using the rotating wave approximation $\hat{H}_{\text{e-ph}} = \frac{1}{\sqrt{S}} \sum_{\mathbf{k}, I, \tau} g_{\mathbf{k}}^{I,\tau} \hat{a}_I \hat{\psi}_{\tau,c,\mathbf{k}}^\dagger \hat{\psi}_{\tau,v,\mathbf{k}} + \text{h.c.}$ on the electron-photon coupling, where $g_{\mathbf{k}}^{I,\tau} = \sqrt{\frac{\hbar^3}{2\omega_c \epsilon S L_c}} \langle c | \mathbf{e}_I \cdot \mathbf{J}^{(\tau)}(\mathbf{k}) | v \rangle$ is the electron-photon coupling strength, and I the photon circular polarization index. The optical valley selection rule [1] gives us the s -wave electron-photon coupling, *i.e.* $g_{\mathbf{k}}^{I,\tau} = g_0 \delta_{I,\tau} + O(k^2)$.

4.3.1 Details of the optical-valley selection rule

It can be shown $g_{\mathbf{k}}^{I,\tau} = g_0 \delta_{I,\tau}$ under the general consideration of the symmetry of a single-layer transition metal dichalcogenides.

Let us consider $J_i^{(\tau)}(\mathbf{k}) \equiv -e \partial_i H_0^{(\tau)}(\mathbf{k})$. As it is a derivative of a Hamiltonian, a scalar under any $r \in G$, $J_i^{(\tau)}(\mathbf{k})$ should transform like a vector:

$$\Gamma(r) J_j^{(\tau)}(\hat{r}^{-1} \mathbf{k}) \Gamma(r)^\dagger = \hat{r}_{ij} J_i^{(\tau)}(\mathbf{k}), \quad (4.5)$$

and thus $G^{(I,\tau)}(\mathbf{k}) \equiv \mathbf{e}_I \cdot \mathbf{J}^{(\tau)}(\mathbf{k})$ transforms as

$$\Gamma(r) G^{(I,\tau)}(\hat{r}^{-1} \mathbf{k}) \Gamma(r)^\dagger = e^{-iI\alpha} G^{(I,\tau)}(\mathbf{k}), \quad (4.6)$$

when r is the α -rotation along the z -axis:

$$\hat{r} = \begin{pmatrix} \cos \frac{2\pi}{3} & -\sin \frac{2\pi}{3} & 0 \\ \sin \frac{2\pi}{3} & \cos \frac{2\pi}{3} & 0 \\ 0 & 0 & 1 \end{pmatrix}.$$

²The no-photon ground state value in the Fock potential is subtracted off so that $\hat{c}_{\mathbf{k}}$'s can be treated as the non-interacting quasiparticles with our band parameters

Here, we have used $\hat{r}_{ij}(\mathbf{e}_{\pm})_j = (\mathbf{e}_{\pm})_i e^{\mp i\alpha}$. As $g^{(I,\tau)}(\mathbf{k}) \propto \langle c|G^{(I,\tau)}(\mathbf{k})|v\rangle$ is the value of G evaluated using the band basis, we need to rewrite Eq. (4.6) in the band basis:

$$\tilde{\Gamma}_{\mathbf{k}}(r)\tilde{G}^{(I,\tau)}(\hat{r}^{-1}\mathbf{k})\tilde{\Gamma}_{\mathbf{k}}(r)^\dagger = e^{-iI\alpha}\tilde{G}^{(I,\tau)}(\mathbf{k}), \quad (4.7)$$

where $\tilde{\Gamma}_{\mathbf{k}}(r) \equiv W_{\mathbf{k}}^\dagger\Gamma(r)W_{r^{-1}\mathbf{k}}$ and $\tilde{G}^{(I,\tau)}(\mathbf{k}) \equiv W_{\mathbf{k}}^\dagger G^{(I,\tau)}(\mathbf{k})W_{\mathbf{k}}$. It is important to note that $\tilde{\Gamma}_{\mathbf{k}}(r)$ is a diagonal matrix because all bands of interest near the $\tau\mathbf{K}$ valleys are non-degenerate and also does not depend on \mathbf{k} . The proof is as follows. First, the fact that all bands are non-degenerate means the representation matrix $\tilde{\Gamma}_{\mathbf{k}}(r)$ is a direct sum of only one-dimensional irreducible representations, and an one-dimensional irreducible representation coincides with the character of the irreducible representation, which is independent of basis. Since the group we are considering is a crystallographic group such as C_{3h} , the number of all possible values of characters of irreducible representations are finite, while \mathbf{k} varies continuously. Therefore, we arrive at a conclusion that $\tilde{\Gamma}_{\mathbf{k}}(r)$ is independent from \mathbf{k} and must be same with $\Gamma(r)$, which is just $\tilde{\Gamma}_{\mathbf{k}=0}(r)$. Provided with this knowledge, Eq. (4.7) leads us to

$$\frac{[\Gamma(r)]_{ii}}{[\Gamma(r)]_{jj}} \left[\tilde{G}^{(I,\tau)}(\hat{r}^{-1}\mathbf{k}) \right]_{ij} = e^{-iI\alpha} \left[\tilde{G}^{(I,\tau)}(\mathbf{k}) \right]_{ij}, \quad (4.8)$$

which, in turn, informs that the diagonal component $\left[\tilde{G}^{(I,\tau)}(\mathbf{k}) \right]_{ii}$, the intra-band transition amplitude, should be zero at $\mathbf{k} = 0$ for both polarization $I = \pm$. Evaluation of Eq. (4.8) at $\mathbf{k} = 0$ for a single-layer transition metal dichalco-

genide is not difficult provided that

$$\Gamma(C_3) = \left\{ \begin{array}{l} \left(\begin{array}{c|ccc} & c \uparrow & c \downarrow & v \uparrow \\ \hline c \uparrow & 1 & & \\ c \downarrow & & e^{\frac{2\pi i}{3}} & \\ v \uparrow & & & e^{\frac{2\pi i}{3}} \end{array} \right) & \text{for } K \text{ valley} \\ \left(\begin{array}{c|ccc} & c \uparrow & c \downarrow & v \downarrow \\ \hline c \uparrow & 1 & & \\ c \downarrow & & e^{\frac{2\pi i}{3}} & \\ v \downarrow & & & 1 \end{array} \right) & \text{for } -K \text{ valley} \end{array} \right. ,$$

leaving only 4 non-zero $[G^{(I,+)}(0)]_{i,j}$ for $i, j = c \uparrow, c \downarrow, v \uparrow$:

$$\left[\tilde{G}^{(+,+)}(\mathbf{0}) \right]_{c \uparrow, v \uparrow}, \left[\tilde{G}^{(-,+)}(\mathbf{0}) \right]_{v \uparrow, c \uparrow}, \left[\tilde{G}^{(+,+)}(\mathbf{0}) \right]_{c \uparrow, c \downarrow}, \left[\tilde{G}^{(-,+)}(\mathbf{0}) \right]_{c \downarrow, c \uparrow}.$$

(if $\tau = -$, $v \uparrow$ should be replaced with $v \downarrow$.) Among the four, the last three can be neglected within the rotating-wave approximation, which enforces the energy conservation even for the virtual processes of the optical transition. Therefore, the dominant optical excitation from the upper valence band at the K valley is the transition from $v \uparrow$ to $c \uparrow$ by a light polarized in $I = +$ direction.. In a similar reasoning, the dominant contribution to the optical excitation from the $-K$ valley is the transition from $v \downarrow$ to $c \downarrow$ by a light with $I = -$ polarization. Hence, spin, momentum(valley), and the polarization of light are tightly coupled, which makes the family of single layer transition dichalcogenides a good platform of spintronics and valleytronics.

4.4 Competition between s- and p- wave order parameter

From the self-consistency conditions of Eqs. (4.3) and (4.4), we find that there exists the competition between the electron-electron interaction and the electron-photon coupling in the polariton condensation in the Dirac material. We first note that the electron-photon coupling induces only the s -wave excitons at both valleys, as Λ_I in Eq. (4.4) is maximized when the electron-photon coupling $g_{\mathbf{k}}^{I,\tau}$ and the exciton correlation $\langle \hat{\psi}_{\tau,c,\mathbf{k}}^\dagger \hat{\psi}_{\tau,v,\mathbf{k}} \rangle$ are in the same symmetry. On the other hand, the electron-electron interaction may not favor the s -wave exciton when we examine $\hat{H}_{e-e}^{\text{MF}} = \sum_{\tau,\alpha,\beta,\mathbf{k}} \Delta_{\tau;\beta\alpha}(\mathbf{k}) \hat{\psi}_{\tau,\beta,\mathbf{k}}^\dagger \hat{\psi}_{\tau,\alpha,\mathbf{k}}$, given that

$$\begin{aligned} \Delta_{\tau;c,v}(\mathbf{k}) &= \sum_{i,j} [W \tilde{\Delta} W^\dagger]_{\tau;c,v}(\mathbf{k}) \approx \Delta_{\tau;c,v}^s(k) + e^{i\tau\phi_{\mathbf{k}}} \Delta_{\tau;c,v}^p(\mathbf{k}), \\ \Delta_{\tau;c,v}^s(k) &\approx -\frac{1}{S} \cos^2 \frac{\theta_k}{2} \sum_{\mathbf{p}} V(|\mathbf{k} - \mathbf{p}|) \langle \hat{\psi}_{\tau,v,\mathbf{p}}^\dagger \hat{\psi}_{\tau,c,\mathbf{p}} \rangle \cos^2 \frac{\theta_p}{2}, \\ \Delta_{\tau;c,v}^p(k) &\approx \frac{1}{S} \sin \theta_k \sum_{\mathbf{p}} V(|\mathbf{k} - \mathbf{p}|) \end{aligned} \quad (4.9)$$

where $\tan \phi_{\mathbf{k}} \equiv k_y/k_x$, $\tan \theta_k \equiv \hbar v k / (E_{\text{gap}}/2)$. The p -wave components $\Delta_{\tau;c,v}^p(k)$ arises from the $\tau\pi$ Berry phase, as can be seen both from the chiralities of the p -wave components for the two valleys being opposite and $\Delta_{\tau;c,v}^p(k)$ being proportional to $\sin \theta_k$, the integrated Berry curvature of \hat{H}_0 for momenta smaller than k , that vanishes linearly as $k \rightarrow 0$. We see from Eq. (4.9) that the Coulomb electron-electron interaction favors the p -wave (s -wave) exciton at the τ valley when the τ -valley exciton density $\sum_{\mathbf{p}} \langle \hat{n}_{\text{ex},\mathbf{p}}^\tau \rangle$ becomes sufficiently large (small) compared to the critical density set by the average Berry curvature. We will show that when the exciton symmetry of the polariton condensate is predominantly chiral p -wave in the τ valley, the Berry phase sign of τ valley changes in the mean-field Hamiltonian $\hat{H}_{e-e}^{\text{MF}} \equiv \hat{H}_0 + \frac{1}{\sqrt{S}} \sum_{I,\tau,\mathbf{k}} (\Lambda_I g_{\mathbf{k}}^{I,\tau} \hat{\psi}_{\tau,c,\mathbf{k}}^\dagger \hat{\psi}_{\tau,v,\mathbf{k}} + \text{h.c.}) + \hat{H}_{e-e}^{\text{MF}} - \mu_X \hat{N}_{\text{ex}}$ from that of \hat{H}_0 . While Eq. (4.9) also indicates that the chiral

p -wave excitons are due to a component of the electron-electron interaction that violates the N_{tot} conservation (See Appendix A), the N_{tot} fluctuation remains small, *i.e.* $\frac{\langle(\Delta\hat{N}_{\text{tot}})^2\rangle}{N_{\text{tot}}^2} = \frac{\Lambda^2 + \sum_{\mathbf{k}} |u_{\mathbf{k}}|^2 |v_{\mathbf{k}}|^2}{(\Lambda^2 + \sum_{\mathbf{k}} |v_{\mathbf{k}}|^2)^2} \ll 1$.

4.5 Topological phase transition of a single photon–coupled massive Dirac particle system and its Phase diagram

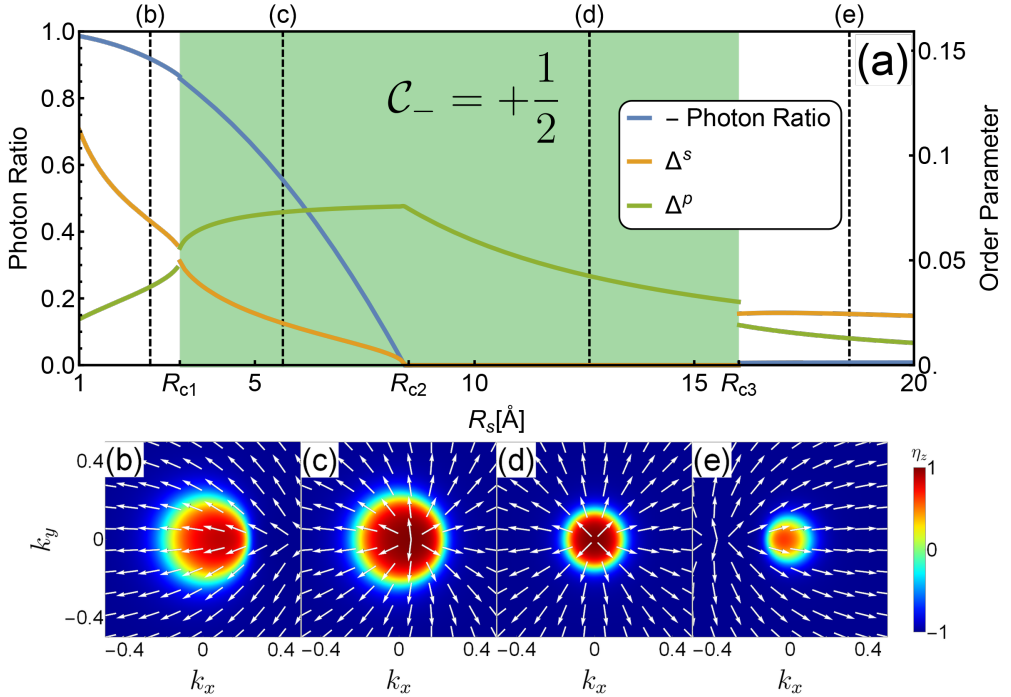


Figure 4.1: (a) Photon fraction and mean-field band exciton gap parameters $\Delta^{s,p}$ averaged over the momentum space as the functions of R_s for the photon frequency $\hbar\omega_c = 2.1\text{eV}\text{\AA}$, the dielectric constant $\epsilon = 10$, the Dirac velocity $\hbar v = 3.7\text{eV}\text{\AA}$, and the band gap of $E_{\text{gap}} = 2.0\text{eV}\text{\AA}$. (b)-(e) Pseudo-spin textures at the R_s values indicated in (a). Arrow represents $\hat{\eta}_{\parallel}$ and false color represents $\eta_z(\mathbf{k})$; for convenience, we have plotted the $\tau = -$ valley coupled to $I = -$ photons.

The essence of the competition between the electron-electron interaction and the electron-photon coupling can emerge clearly from considering only a single

valley, *i.e.* the $\tau = -$ valley coupled to the $I = -$ photons, revealing how the competition can give rise to the phase transition of our polariton condensate. Fig. 4.1(a) shows how the photon fraction $\Lambda^2/(\Lambda^2 + \langle \hat{N}_{\text{ex}} \rangle)$ of the polariton condensate and the exciton gap parameters $\Delta^{s,p}$ of Eq.(4.9) depend on the mean distance $R_s \equiv \sqrt{\frac{S}{N_{\text{tot}}\pi}}$ between excitations, the quantity that determines the total number of excitations N_{tot} . A key feature here is that the p -wave excitons are dark [39], which can be confirmed from Λ vanishing in Eq.(4.4) for the purely p -wave $\langle \hat{\psi}_v^\dagger \hat{\psi}_c \rangle$ because the s -wave symmetry for the electron-photon coupling, *i.e.* $g_{\mathbf{k}} \approx g_0 \delta_{I,\tau}$. Since Δ^p arises solely from the electron-electron interaction, the higher-density discontinuous crossing of $|\Delta^s|$ and $|\Delta^p|$ curves in Fig. 4.1(a) at $R_s = R_{c1}$ can be regarded as a consequence of the competition between the electron-electron interaction and the electron-photon coupling.

Overall, the Fig. 4.2 plots show how the topological phase transition of \hat{H}^{MF} can arise from the competition between the s -wave and the chiral p -wave exciton pairing channels. The Chern number of a single valley can be defined in a manner analogous to that of the topological insulator surface [40], with the understanding that the integer value is obtained when summed with that of the other valley. Note how the Chern number $\mathcal{C}_- = \pm \frac{1}{2}$ coincides exactly with $|\Delta^s| < |\Delta^p|$ ($|\Delta^s| > |\Delta^p|$) in Fig. 4.1 (a). \mathcal{C}_- can be computed equivalently in either the orbital basis obtained from $\boldsymbol{\sigma} \cdot \hat{\mathbf{d}} = W(\boldsymbol{\sigma} \cdot \hat{\boldsymbol{\eta}})W^\dagger$ or the band basis as $\mathcal{C}_- = \frac{1}{4\pi} \int d^2k \hat{\mathbf{d}} \cdot (\partial_{k_x} \hat{\mathbf{d}} \times \partial_{k_y} \hat{\mathbf{d}}) = -\frac{1}{2} + \frac{1}{4\pi} \int d^2k \hat{\boldsymbol{\eta}} \cdot (\partial_{k_x} \hat{\boldsymbol{\eta}} \times \partial_{k_y} \hat{\boldsymbol{\eta}})$, which is consistent with Fig. 4.1 (b)-(e) as it gives $\mathcal{C}_- = \pm \frac{1}{2}$ when the skyrmion is present (absent); note that \hat{H}_0 gives $\mathcal{C}_- = -\frac{1}{2}$. In fact, we may define the overall exciton symmetry to be chiral p -wave when $\mathcal{C}_- = +\frac{1}{2}$. Given that the Δ^p arises from the non-conservation of N_{tot} as can be seen from Eq.(4.9), this is a case of discontinuous phase transitions to excitonic insulator phases in the absence of the N_{tot} conservation, though our case deals with quantum rather than classical phase transitions considered in [41, 42].

The full phase diagrams with respect to R_s and the photon detuning $\delta \equiv \hbar\omega_c - E_{\text{gap}}$ shown as Fig. 4.2 for different values of the dielectric constant ϵ and the band gap E_{gap} can be largely explained by the different energy competitions that give rise to the higher and the lower density phase transition. δ and ϵ are control parameters in the competition between the electron-photon coupling and the electron-electron interaction; the photon self-consistency equation Eq.(4.4) shows that the smaller δ leads to the larger photon fraction, while the smaller ϵ leads to the larger electron-electron interaction. Fig. 4.2 (b) shows that the $\mathcal{C}_- = +\frac{1}{2}$ phase with the chiral p -wave excitons requires sufficiently weak electron-photon coupling, which is naturally larger for the smaller Coulomb interaction of $\epsilon = 15$ shown in red than for the larger Coulomb interaction of $\epsilon = 10$ shown in blue and green. That the lower density (larger R_s) transition depends little on δ confirms its weak dependence on the electron-photon coupling. Meanwhile, the blue curves of Fig. 4.2 (b) shows that for a larger E_{gap} the lower density transition occurring at smaller R_s (larger density) when compared with the lower E_{gap} shown by the green and red curves. This is because of the larger E_{gap} suppressing Δ^p through reducing $\sin \theta_k$ at all momenta, or, equivalently, the Berry curvature integrated over momenta smaller than k .

The phase diagram of Fig. 4.2 (a) shows phase transitions as well as crossovers in contrast to the results for the polariton condensate in the topologically trivial quantum well where only the latter were present [35]. Following the results of Kamide *et al.* for the topologically trivial quantum well, we can define in the $\mathcal{C}_- = -\frac{1}{2}$ region several phases according to the photon fraction as the photon, the polariton and the exciton BEC in the decreasing order, with their boundaries being crossovers (shown as the dotted curves). However, as discussed above, there is a first-order phase transition (shown as the solid curves) between the $\mathcal{C}_- = -\frac{1}{2}$ and the $\mathcal{C}_- = +\frac{1}{2}$ regions. Within the $\mathcal{C}_- = +\frac{1}{2}$ region, the phase with the vanishing photon fraction would be best termed the

electron-hole BCS condensate, R_s being smaller than the p -wave exciton radius³. Inside the $\mathcal{C}_- = +\frac{1}{2}$ region, there is a second-order phase transition (shown as the dashed curves) between the polariton BEC and this electron-hole BCS condensate involving the spontaneous rotational symmetry breaking. Despite photons providing no preferred direction, the rotational symmetry is broken when we have both the s -wave and the chiral p -wave components in $v_{\mathbf{k}}/u_{\mathbf{k}}$ of the exciton wave function Eq.(4.2), which moves the singularity of $\boldsymbol{\eta}_{\parallel}$ textures of Fig. 4.1 (b), (c), (e) away from $\mathbf{k} = 0$. The rotational symmetry in our polariton condensate is restored in Fig. 4.1 (d) on Λ and Δ^s vanishing continuously. Hence, our polariton condensate is always distinct from the \hat{H}_0 ground state in either topology or symmetry.

³Following [43], with the dielectric constant of $\epsilon = 10$ and the band gap of $E_{\text{gap}} = 2.0$ eV, we obtain the exciton radius of $a_{\text{ex}}^{(s)} = 5.2$ Å for the s -wave and $a_{\text{ex}}^{(p)} = 46$ Å for the p -wave.

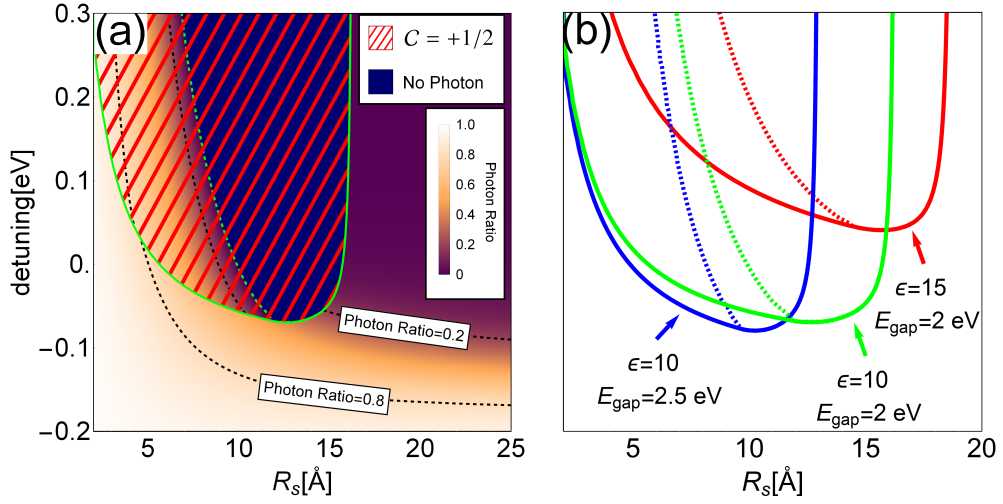


Figure 4.2: (a) The dependence of photon fraction for the single-valley TMDC polariton system on δ and R_s shown with $\hbar\nu = 3.7\text{eV}\text{\AA}$, $\epsilon = 10$ and $E_{\text{gap}} = 2.0$ eV; the green solid, the green dashed and the black dotted curves represent the first-order transitions, the second-order transitions, and the crossovers, respectively. (b) Phase boundaries for the first-order (solid) and second-order (dashed) transitions for $\epsilon=10$ and $E_{\text{gap}}=2$ eV (green), $\epsilon=15$ and $E_{\text{gap}}=2$ eV (red), and $\epsilon=10$ and $E_{\text{gap}}=2.5$ eV (blue).

4.6 Topological phase transition of 2D TMD cavity and its Phase diagram

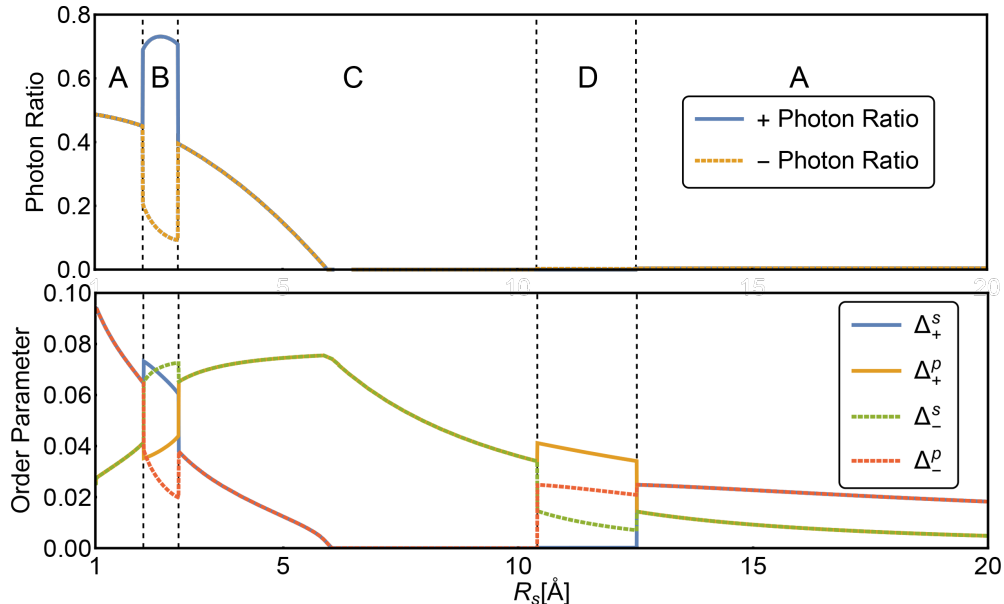


Figure 4.3: Photon fraction (above) and mean-field band exciton gap parameters $\Delta^{s,p}$ (below) for two valleys ($\tau = \pm 1$) as the functions of R_s for the photon frequency $\hbar\omega_c = 2.1\text{eV}$ and other physical parameters following those of Fig. 4.2 (a).

For the two valley TMDC coupled to photons of both circular polarizations shown in Fig. 4.3, we find that the topological phase transitions give rise to both the quantum spin Hall phase (in the region C) and the quantum anomalous Hall phase (in the regions B and D). To analyze this problem, we consider the variational solution of Eq. (4.2) with the phase difference between the two photon polarizations fixed. In the absence of interactions, \hat{H}_0 of Eq. (4.1) gives us the opposite sign for the Chern numbers of $\mathcal{C}_\tau = \frac{\tau}{2}$ for the τ valley. When the exciton symmetry of one valley is the chiral p -wave and that of the other

	$\mathcal{C}_{+\uparrow}$	$\mathcal{C}_{+\downarrow}$	$\mathcal{C}_{-\uparrow}$	$\mathcal{C}_{-\downarrow}$	\mathcal{C}_S	\mathcal{C}_V	\mathcal{C}_{tot}
A	+1/2	+1/2	-1/2	-1/2	0	+1	0
B	$\pm 1/2$	+1/2	-1/2	$\pm 1/2$	-1/2	+1/2	± 1
C	-1/2	+1/2	-1/2	+1/2	-1	0	0
D	$\mp 1/2$	+1/2	-1/2	$\mp 1/2$	-1/2	+1/2	∓ 1

Table 4.1: Phase classification in the two valleys coupled to the photons of both circular polarizations. The alphabet letters in the leftmost column refer to each phase mentioned in Fig. 4.3. $\mathcal{C}_S \equiv \sum_{\tau,\sigma} \sigma \mathcal{C}_{\tau,\sigma}/2$ and $\mathcal{C}_V \equiv \sum_{\tau,\sigma} \tau \mathcal{C}_{\tau,\sigma}/2$ are the spin and the valley Chern numbers respectively. Refer the main text for further details.

valley is the s -wave, we have a net Chern number of $\mathcal{C}_{\text{tot}} \equiv \sum_{\tau,\sigma} \mathcal{C}_{\tau,\sigma} = \pm 1$ for our \hat{H}^{MF} and hence the quantum anomalous Hall phase [44]. Due to the valley polarization that occurs only in this phase, the regions B and D have the elliptic photon polarizations while all the other regions have the linear photon polarizations. Meanwhile, the region C of Fig. 4.3 shows that the photon fraction and the Δ^s at both valleys vanish continuously at the same R_s ⁴. In the region C, we have the quantum spin Hall phase where the time-reversal symmetry is restored by the opposite chirality between the p -wave excitons of the two valleys. Table 1 shows the topological phases for the two-valley TMDC polariton condensate taking into account both spin components at each valley.

⁴The rotational symmetry breaking at two valleys are not independent due to the electron-photon coupling. Therefore, if we take the \hat{H}_0 of Eq.(4.1), *i.e.* with the continuous rotational symmetry, we have for the two valley case the $\text{SO}(2)$ rather than $\text{SO}(2) \times \text{SO}(2)$ symmetry breaking. Given the photon polarization, the vanishing photon fraction is necessary for the rotational symmetry.

4.7 Conclusion

In summary, we found topological phase transitions in the quasi-equilibrium ground state of the TMD monolayer coupled to the cavity photons due to the competition between the electron-photon coupling and the electron-electron interaction tuned by the excitation density. Our approach is expected to work best for the thermal quasi-equilibration time shorter than the polariton lifetime. We may find the regions of our phase diagram with optimal experimental accessibility as the quasi-equilibration time may depend on various physical parameters, *e.g.* R_s . One possible method for triggering our phase transitions may be the terahertz pump which has been shown to induce the *s*-wave to *p*-wave transition in the excitons [45].

Chapter 5

Emergent anisotropic non-Fermi liquid at a topological phase transition in three dimensions

5.1 Introduction

Quantum criticality and topology play key roles in modern condensed matter physics [46, 47, 48, 49, 50], and the two concepts become naturally important near TQPTs. Recently, there has been a surge of interest in TQPTs [51, 52, 53, 54, 55, 56]. The simplest class is described by the weakly interacting Dirac fermions, and it is well understood that the sign of the Dirac mass terms determines adjacent topological phases [57, 58, 59]. Since quasiparticles are well defined, non-interacting tight-binding models are sufficient to describe TQPTs in this class.

Beyond the simplest class, however, our understanding of TQPTs is far from complete. The long-range Coulomb interaction may drastically change the properties of non-interacting fermions near TQPTs, and the non-interacting tight-binding models *cannot* describe some classes of TQPTs. The interplay between critical electronic modes and the Coulomb interaction becomes significant, and quantum critical non-Fermi liquid states may appear with emergent

particle-hole and rotational symmetries [60, 61, 62, 63, 64]. Moreover, the interplay may also give rise to weakly coupled but infinitely anisotropic excitations in a class of TQPTs [65, 66, 67, 68, 69]. Thus, it is vital to deepen our understanding of TQPTs beyond the simplest class.

In this chapter, we uncover a novel class of TQPTs which shows emergent *anisotropic* non-Fermi liquid behaviors in three spatial dimensions (3d) associated with topological nature of electronic wave functions. Our target system is the DWSM adjacent to insulator phases under the long-range Coulomb interaction. The presence of either the four-fold or six-fold rotational symmetry allows a direct phase transition between DWSMs and insulators whose bare Hamiltonian has a quadratic band touching spectrum. Without the symmetries, double-Weyl nodes may split into two Weyl nodes. The long-range Coulomb interaction becomes relevant at the critical point, and thus quasi-particle excitations are expected to be absent. Moreover, the absence of the cubic symmetry indicates a possibility of anisotropic quantum critical behaviors in contrast to most of the fixed points with the full rotational symmetry as in conformal field theories. Using the standard renormalization group (RG) methods, we indeed find novel quantum critical phenomena with emergent *anisotropy*. For example, we find that the power-law dependences of the energy dispersion and the Coulomb interaction on momentum become anisotropic, even though they are initially set to be the same in all directions, and all excitations have anomalous dimensions. Our universality class is one concrete example of strongly interacting fixed points with non-Fermi liquid behaviors beyond the conformal field theory description in 3d. We calculate its experimental signatures in physical observables such as the specific heat, compressibility, diamagnetic susceptibility, and optical conductivity.

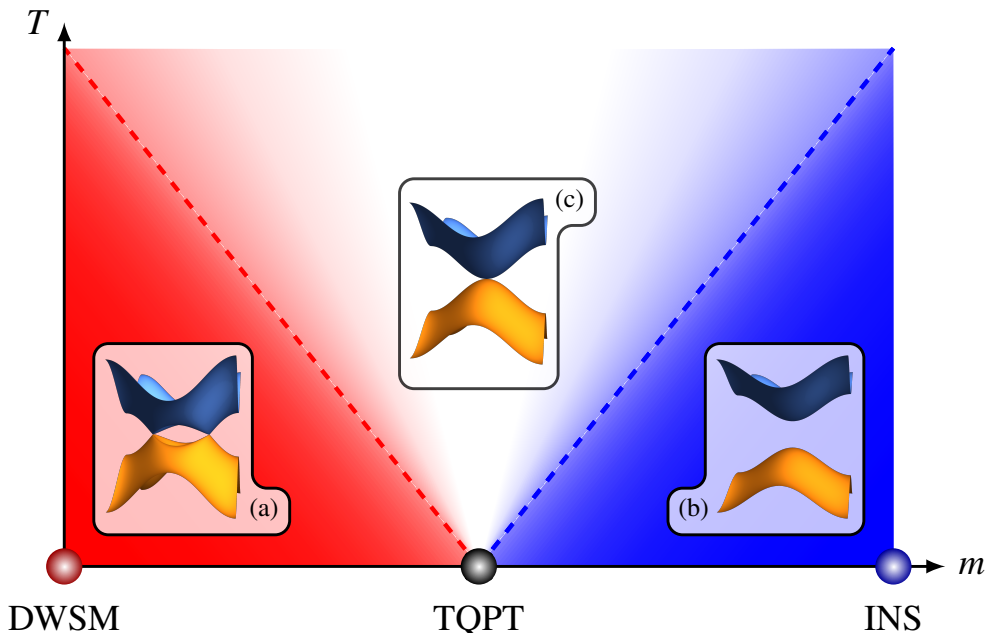


Figure 5.1: Phase diagram for the TQPT between the DWSM and insulator phases with the tuning parameter m . The insets show the energy dispersions for the (a) DWSM, (b) insulator and (c) TQPT.

5.2 Model

We consider a minimal lattice model of DWSMs with a four-fold rotational symmetry C_4 with a rotational axis along the z direction [70, 71, 72, 73, 73],

$$\begin{aligned} \mathcal{H}(\mathbf{k}) = & 2t'_x [\cos(k_y a_0) - \cos(k_x a_0)] \sigma_x \\ & + 2t'_y \sin(k_x a_0) \sin(k_y a_0) \sigma_y + 2M_z(\mathbf{k}) \sigma_z, \end{aligned} \quad (5.1)$$

where $M_z(\mathbf{k}) = m_z - t'_z \cos(k_z a_0) + m_0[2 - \cos(k_x a_0) - \cos(k_y a_0)]$ and a_0 is the lattice constant. In general, C_4 symmetry does not imply $t'_x = t'_y$. However, in the presence of the Coulomb interaction, $t'_x = t'_y$ emerges at low energies Appendix C. For $|m_z| < t'_z$, the Hamiltonian supports two double-Weyl nodes at $\mathbf{k} = (0, 0, \pm k_z^*)$, where $k_z^* = a_0^{-1} \cos^{-1}(m_z/t'_z)$, which are characterized by the

Chern numbers ± 2 around the points [70]. For $|m_z| > t'_z$, the system shows an insulator phase. At $|m_z| = t'_z$, a quantum phase transition occurs between the DWSM and insulator phases, as shown in Fig. 5.1. Neglecting m_0 for simplicity, we obtain the low-energy effective Hamiltonian near the transition point given by

$$\mathcal{H}_0(\mathbf{k}) = t_\perp [(k_x^2 - k_y^2)\sigma_x + 2k_x k_y \sigma_y] + (t_z k_z^2 + m)\sigma_z, \quad (5.2)$$

where $t_\perp = t'_x a_0^2$ and $t_z = t'_z a_0^2$. Here, a tuning parameter of the TQPT, $m \propto |m_z| - t'_z$, is introduced. The energy eigenvalues of the Hamiltonian are given by $E_\pm(\mathbf{k}) = \pm \sqrt{t_\perp^2 (k_x^2 + k_y^2)^2 + (t_z k_z^2 + m)^2}$, and at $m = 0$ the energy dispersion becomes quadratic in all three directions.

The corresponding effective action with the long-range Coulomb interaction is

$$\mathcal{S} = \int d\tau d^3x \psi^\dagger [\partial_\tau - ig\phi + \mathcal{H}_0(-i\nabla)]\psi \quad (5.3)$$

$$+ \int d\tau d^3x \frac{1}{2} \left[a \{ (\partial_x \phi)^2 + (\partial_y \phi)^2 \} + \frac{1}{a} (\partial_z \phi)^2 \right], \quad (5.4)$$

where $g \equiv \frac{\sqrt{4\pi}e_0}{\sqrt{\varepsilon}}$ with e_0 and ε being the bare charge and the dielectric constant, respectively, ψ is a spinor with $2N_f$ components, and ϕ is a bosonic field describing the long-range Coulomb interaction. Note that the topological aspects of Eqn. (5.2) justify the effective action in the sense that the action becomes adiabatically connected to a simple non-mixing two band model without the topological aspects. The parameter a is introduced to characterize the anisotropy ratio of the Coulomb interaction between the xy -plane and the z -axis. For later usage, we define the following dimensionless parameters,

$$\alpha = \frac{A_d - 2g^2}{\sqrt{t_\perp t_z} \Lambda^{4-d}}, \quad \beta = \frac{t_z}{t_\perp}, \quad \gamma = \frac{a\sqrt{\beta}}{2} \quad (5.5)$$

with $A_d = [6\pi(4\pi)^{\frac{d}{2}}\Gamma(\frac{d}{2})]^{-1}$. Here, α represents the ratio of the Coulomb potential and the electron kinetic energy, β^{-1} is the anisotropy parameter for

the fermionic fields, and γ is the combination of the two anisotropy parameters a and β . We assume that all the four-Fermi interactions, $u_{ijkl}\psi_i^\dagger\psi_j^\dagger\psi_k\psi_l$, are set to be small at the lattice-spacing scale and flow into the trivial fixed point as in the literature [74], which is also justified below in Sec 5.6.

5.3 Large N_f calculation

We first use the large N_f method since it is naturally extended from the conventional random phase approximation [75, 76, 65, 77, 66]. The boson self-energy is

$$\Pi(i\Omega, \mathbf{q}) = N_f g^2 \int_{\omega, \mathbf{k}} \text{Tr}[G_0(i\omega + i\Omega, \mathbf{k} + \mathbf{q})G_0(i\omega, \mathbf{k})], \quad (5.6)$$

with the fermion propagator $G_0(i\omega, \mathbf{k}) = (-i\omega + \mathcal{H}_0(\mathbf{k}))^{-1}$. Here, we use the notation $\int_{\omega, \mathbf{k}} = \int \frac{d\omega}{2\pi} \frac{dk_x dk_y}{(2\pi)^2} \int' \frac{dk_z}{2\pi}$, where $\int' \frac{dk_z}{2\pi}$ stands for an integration over $\mu < |k_z| < \Lambda$ with the infrared (IR) cutoff μ and the ultra-violet (UV) cutoff Λ . A detailed exposition of the boson self-energy is presented in Appendix C.

We propose the following ansatz for the boson self-energy at one-loop level:

$$\Pi(i\Omega, \mathbf{q}) = -\frac{N_f g^2 |q_\perp|}{\sqrt{t_\perp t_z}} F\left(\sqrt{\frac{t_\perp}{|\Omega|}} |q_\perp|, \sqrt{\frac{t_z}{t_\perp}} \left|\frac{q_z}{q_\perp}\right|\right), \quad (5.7)$$

where $q_\perp \equiv \sqrt{q_x^2 + q_y^2}$ and

$$F(x, y) = \sqrt{C_{\perp 1}^2 + C_{z_1}^2 y^2} \tanh\left(x \sqrt{C_{\perp 2}^2 + C_{z_2}^2 y^2}\right), \quad (5.8)$$

with $C_{\perp 1} = 0.041$, $C_{\perp 2} = 1.199$, $C_{z_1} = 0.016$, and $C_{z_2} = 1.267$. For the details, see Appendix C

The one-loop boson self-energy modifies the Coulomb potential in momentum space as

$$D(i\Omega, \mathbf{q}) = \frac{1}{D_0^{-1}(\mathbf{q}) - \Pi(i\Omega, \mathbf{q})}, \quad (5.9)$$

where $D_0(\mathbf{q}) = (aq_\perp^2 + \frac{1}{a}q_z^2)^{-1}$ is the bare boson propagator. In the static ($\Omega = 0$) and long wave length ($q \rightarrow 0$) limit, the self-energy dominates the bare propagator since it linearly depends on the momentum in this limit. Thus, we take the boson self-energy as the main contribution to the renormalized Coulomb interaction, $D(i\Omega, \mathbf{q}) \simeq \frac{1}{-\Pi(i\Omega, \mathbf{q})}$. This indicates that the boson is strongly renormalized from the quadratic to a linear momentum dependence, exhibiting the anomalous dimension of order one at the TQPT. This approximation has been well established in large N_f analysis and is checked afterward.

The fermion self-energy with the renormalized Coulomb interaction is

$$\Sigma(i\omega, \mathbf{k}) = (-ig)^2 \int_{\Omega, \mathbf{q}} G_0(i\omega + i\Omega, \mathbf{k} + \mathbf{q}) D(i\Omega, \mathbf{q}), \quad (5.10)$$

and the fermion part of the action is modified by the fermion self-energy as

$$-i\omega + \mathcal{H}_0(\mathbf{k}) \rightarrow -i\omega + \mathcal{H}_0(\mathbf{k}) - \Sigma(i\omega, \mathbf{k}). \quad (5.11)$$

It is straightforward to show that the corrections from the self-energy are logarithmically divergent in both UV and IR cutoffs, respectively, and we find

$$\begin{aligned} \Sigma(i\omega, \mathbf{k}) \approx & \frac{C_\omega}{N_f} (i\omega) \ell - \frac{C_{t_z}}{N_f} \ell (t_z k_z^2) \sigma_z \\ & - \frac{C_{t_\perp}}{N_f} \ell [t_\perp (k_x^2 - k_y^2) \sigma_x + 2t_\perp k_x k_y \sigma_y], \end{aligned} \quad (5.12)$$

where $C_\omega = 0.366$, $C_{t_\perp} = 0.614$, $C_{t_z} = 0.341$, and $\ell = \log \frac{\Lambda}{\mu}$ is the RG parameter. For the details, see Appendix C

We also evaluate the vertex correction at vanishing external momentum and frequency,

$$\delta_g = (-ig)^2 \int_{\Omega, \mathbf{q}} G_0(i\Omega, \mathbf{q})^2 \frac{1}{-\Pi(i\Omega, \mathbf{q})} = \frac{C_g}{N_f} \ell, \quad (5.13)$$

where $C_g = 0.366$, which is *exactly* the same as C_ω . This agreement is not a coincidence but instead a consequence of the Ward identity $\delta_g = \partial\Sigma/\partial(i\omega)$.

Using the logarithmic dependence of the self-energy, one can find various anomalous dimensions. The scale invariance at the critical point forces renormalization of the fermion fields with the anomalous dimension $\eta_f = \frac{C_\omega}{N_f}$. The non-zero anomalous dimension clearly indicates non-Fermi liquid behaviors of the fermionic excitations, which can be understood by the absence of the pole structure in the fermionic Green function.

From Eq. (5.12), the RG equations for t_\perp and t_z are given by

$$\frac{1}{t_\perp} \frac{dt_\perp}{d\ell} = \frac{C_{t_\perp} - C_\omega}{N_f}, \quad \frac{1}{t_z} \frac{dt_z}{d\ell} = \frac{C_{t_z} - C_\omega}{N_f}. \quad (5.14)$$

From Eq. (5.14), we find $\frac{1}{\beta^{-1}} \frac{d\beta^{-1}}{d\ell} = \frac{C_{t_\perp} - C_{t_z}}{N_f} > 0$, indicating that β^{-1} diverges at the TQPT and that the fermionic excitations become highly anisotropic at low energies. Thus, our critical theory is described by an emergent anisotropic non-Fermi liquid.

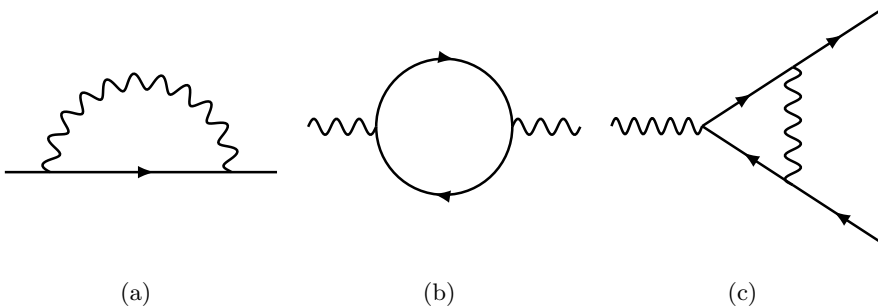


Figure 5.2: Feynman diagrams at one-loop order for the (a) fermion self-energy, (b) boson self-energy, and (c) vertex correction. A straight line with an arrowhead and a wavy line represent the fermion and boson propagators, respectively.

5.4 $\epsilon = 4 - d$ calculation

— Our large N_f calculation is further supported by the standard $\epsilon = 4 - d$ expansion [78, 62, 79, 80]. Here, we introduce a new renormalization scheme

in which the three spatial dimensions are embedded into a manifold that has more coordinates in the direction of the rotational axis (z -direction). Namely, we extend the coordinates as

$$\int \frac{dk_x dk_y}{(2\pi)^2} \int \frac{dk_z}{2\pi} \rightarrow \int \frac{dk_x dk_y}{(2\pi)^2} \int \frac{dk_z d^{d-3}p}{(2\pi)^{d-2}} \quad (5.15)$$

with $k_z^2 \rightarrow k_z^2 + p^2$, and the momentum \mathbf{p} lives in a $(d-3)$ -dimensional manifold. Recalling $[g^2] = z - z_\perp + 3 - d$ with $z = 2$ and $z_\perp = 1$, the coupling constant becomes marginal at $d = 4$ and the quantum fluctuations give logarithmic divergences. To read off these logarithmic divergences, we introduce the parameter $\epsilon = 4 - d$ and employ the standard momentum shell RG analysis with ϵ expansion. For the momentum shell integration, we impose the UV and IR cutoffs on the $(d-2)$ -dimensional space of (k_z, \mathbf{p}) as

$$\int_{\mathbf{k}, \mathbf{p}} = \int \frac{dk_x dk_y}{(2\pi)^2} \int_{\partial\Lambda} \frac{dk_z d^{d-3}p}{(2\pi)^{d-2}} \quad (5.16)$$

where $\partial\Lambda$ represents an infinitesimal momentum shell $\mu < \sqrt{k_z^2 + p^2} < \Lambda$ with $\mu = \Lambda e^{-\ell}$.

By integrating out the high energy modes, we obtain corrections at one-loop order. The fermion self-energy depicted by the diagram in Fig. 5.2(a) is given by

$$\begin{aligned} \Sigma(i\Omega, \mathbf{q}) &= (-ig)^2 \int_{\omega, \mathbf{k}, \mathbf{p}} G_0(i\omega + i\Omega, \mathbf{k} + \mathbf{q}) D_0(i\omega, \mathbf{k}) \\ &\approx -\alpha F_\perp(\gamma) \ell [t_\perp (q_x^2 - q_y^2) \sigma_x + 2t_\perp q_x q_y \sigma_y] \\ &\quad - \alpha F_z(\gamma) \ell (t_z q_z^2) \sigma_z, \end{aligned} \quad (5.17)$$

where F_\perp and F_z are dimensionless functions, whose explicit expressions are presented in Appendix C. Note that the frequency part is not renormalized at the one-loop order because of the instantaneous nature of the bare Coulomb interaction. Then, it is easy to see that the vertex correction [Fig. 5.2(c)]

vanishes due to the Ward identity. For the boson self-energy [Fig. 5.2(b)], we find

$$\begin{aligned}\Pi(\mathbf{q}) &= N_f g^2 \int_{\omega, \mathbf{k}, \mathbf{p}} \text{Tr} [G_0(i\omega, \mathbf{k} + \mathbf{q}/2) G_0(i\omega, \mathbf{k} - \mathbf{q}/2)] \\ &\approx -N_f \alpha \left[\frac{a}{\gamma} q_{\perp}^2 + \frac{\gamma}{a} q_z^2 \right] \ell.\end{aligned}\quad (5.18)$$

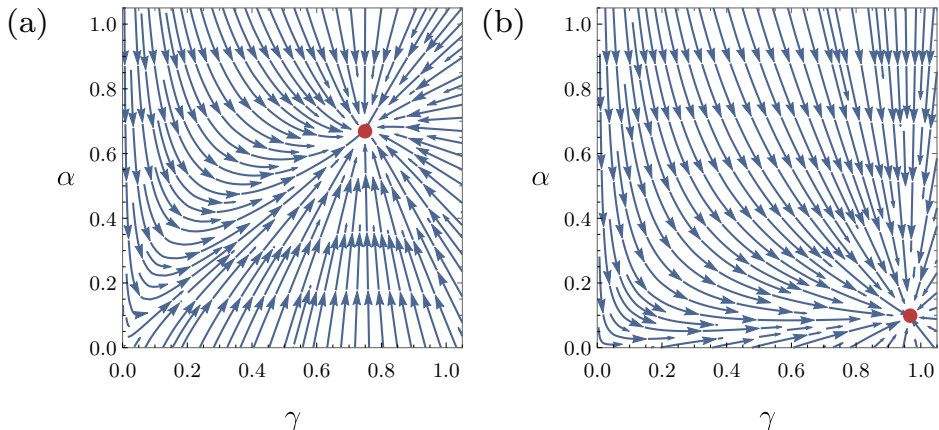


Figure 5.3: RG flows of α and γ for (a) $N_f = 1$ and (b) $N_f = 10$ at $\epsilon = 1$. The red dots represent the fixed points (α^*, γ^*) . For $N_f = 1$, $(\alpha^*, \gamma^*) = (0.671, 0.748)$ and for $N_f = 10$, $(\alpha^*, \gamma^*) = (0.096, 0.966)$ obtained from Eq. (5.19).

Renormalizing the wave functions and the coupling constants, we obtain the RG equations for α and γ as

$$\begin{aligned}\frac{1}{\alpha} \frac{d\alpha}{d\ell} &= \epsilon - \frac{N_f \alpha}{2} \left(\frac{1}{\gamma} + \gamma \right) - \frac{\alpha}{2} F_+(\gamma), \\ \frac{1}{\gamma} \frac{d\gamma}{d\ell} &= \frac{N_f \alpha}{2} \left(\frac{1}{\gamma} - \gamma \right) + \frac{\alpha}{2} F_-(\gamma),\end{aligned}\quad (5.19)$$

where $F_{\pm}(x) = F_z(x) \pm F_{\perp}(x)$. We find two fixed points from the RG equations in Eq. (5.19). The non-interacting fixed point $\alpha^* = 0$ with arbitrary γ^* is unstable, whereas there exists a stable interacting fixed point at (α^*, γ^*) with

$\alpha^* > 0$. For $N_f = 1$ and $\epsilon = 1$, the stable fixed point is located at $(\alpha^*, \gamma^*) = (0.671, 0.748)$, and for large N_f , $(\alpha^*, \gamma^*) \approx (\epsilon/N_f, 1 - 0.358/N_f)$. The RG flows of α and γ are illustrated in Fig. 5.3.

At the stable fixed point, the RG equations for the bosonic and fermionic anisotropy parameters are given by, respectively,

$$\begin{aligned} \left. \frac{1}{a} \frac{da}{d\ell} \right|_{\text{f.p.}} &= \frac{N_f \alpha^*}{2} \left(\frac{1}{\gamma^*} - \gamma^* \right) > 0, \\ \left. \frac{1}{\beta^{-1}} \frac{d\beta^{-1}}{d\ell} \right|_{\text{f.p.}} &= -\alpha^* F_-(\gamma^*) > 0, \end{aligned} \quad (5.20)$$

where f.p. stands for the fixed point. Note that β^{-1} diverges at the stable fixed point as in the large N_f calculation demonstrating an emergent anisotropic non-Fermi liquid, which becomes a sanity check of our analysis giving a consistent result with the large N_f calculation (for details, see Appendix C).

5.5 Physical observables

Recently, several materials [71, 81, 82, 83, 84] have been proposed as possible candidates for DWSMs, in which TQPTs may occur by tuning the system parameters. For example, it has been theoretically demonstrated that SrSi₂ can be tuned by changing the lattice constant through doping or strain, leading to a transition from the DWSM to a trivial insulator phase [84]. Since the anisotropic non-Fermi liquid behavior at the TQPT will provide power-law corrections anisotropically to the scaling of physical observables [76, 85, 86], the anisotropic scaling relations will be valuable to experiments.

First, consider the parameter dependence of physical observables in the non-interacting limit [72, 87, 73, 88, 89]. The details are presented in Appendix C. In the non-interacting limit, the specific heat C_V , compressibility κ , diamagnetic

susceptibility χ_D , and optical conductivity σ are give by

$$\begin{aligned}
C_V &\propto \frac{T^{3/2}}{t_\perp t_z^{1/2}}, & \kappa &\propto \frac{T^{1/2}}{t_\perp t_z^{1/2}}, \\
\chi_{D,\perp} &\propto t_z^{1/2} T^{1/2}, & \chi_{D,z} &\propto \frac{t_\perp}{t_z^{1/2}} T^{1/2}, \\
\sigma_{\perp\perp} &\propto \frac{1}{t_z^{1/2}} \Omega^{1/2}, & \sigma_{zz} &\propto \frac{t_z^{1/2}}{t_\perp} \Omega^{1/2}.
\end{aligned} \tag{5.21}$$

Here, $\chi_{D,x} = \chi_{D,y} = \chi_{D,\perp}$ and $\sigma_{xx} = \sigma_{yy} = \sigma_{\perp\perp}$ because of the C_4 symmetry of the Hamiltonian. We also assume $t_x = t_y = t_\perp$ for simplicity.

Now, consider how the anisotropic non-Fermi liquids change the bare scaling behaviors of the physical observables. From the ϵ expansion, the RG equations for t_\perp and t_z are given by

$$\begin{aligned}
\frac{1}{t_\perp} \frac{dt_\perp}{d \ln b} &= z - 2z_\perp + \alpha F_\perp(\gamma), \\
\frac{1}{t_z} \frac{dt_z}{d \ln b} &= z - 2 + \alpha F_z(\gamma),
\end{aligned} \tag{5.22}$$

where $\ln b \equiv \ell$. Let us choose $z = 2$ and $z_\perp = 1$ so that t_\perp and t_z are marginal at the tree level. Since $\frac{d\mathcal{O}}{d \ln b} = z\mathcal{O}$ for $\mathcal{O} = \omega, T$ with $z = 2$, $\mathcal{O}(b) = \mathcal{O}b^2$. Let b^* be the cutoff value defined as $\mathcal{O}(b^*) = \Lambda$, then $b^* = (\Lambda/\mathcal{O})^{1/2}$. Combining this with Eq. (5.22), we find that $t_i(b^*) = t_{i,0}(b^*)^{\alpha^* F_i(\gamma^*)} \propto \mathcal{O}^{-c_i}$ where $i = \perp, z$, $c_i = \frac{1}{2} \left. \frac{d \ln t_i}{d \ln b} \right|_{\text{f.p.}} = \alpha^* F_i(\gamma^*)/2$, $c_\perp \approx 0.402/N_f$, and $c_z \approx 0.044/N_f$ in the large N_f approximation.

Then, near the interacting fixed point, the scaling relations of the physical observables with respect to either temperature or frequency become

$$\begin{aligned}
C_V &\propto T^{3/2+\eta_1}, & \kappa &\propto T^{1/2+\eta_1}, \\
\chi_{D,\perp} &\propto T^{1/2-\eta_2}, & \chi_{D,z} &\propto T^{1/2-\eta_3}, \\
\sigma_{\perp\perp} &\propto \Omega^{1/2+\eta_2}, & \sigma_{zz} &\propto \Omega^{1/2+\eta_3},
\end{aligned} \tag{5.23}$$

where $\eta_1 \equiv c_\perp + c_z/2 \approx 0.423/N_f$, $\eta_2 \equiv c_z/2 \approx 0.022/N_f$, and $\eta_3 \equiv c_\perp - c_z/2 \approx 0.380/N_f$. (Equivalently, we can obtain the same results by including all the

effects of renormalization in the coordinates rather than the system parameters, as presented in Appendix C.) Thus, it is easily seen that the diamagnetic susceptibility and optical conductivity show anisotropic scaling behaviors, $\chi_{D,z}/\chi_{D,\perp} \propto T^{\eta_2-\eta_3}$ and $\sigma_{\perp\perp}/\sigma_{zz} \propto \Omega^{\eta_2-\eta_3}$. In addition, the permittivity tensor characterizing the charge screening also exhibits the anisotropic behavior, $\varepsilon_{\perp}/\varepsilon_z = a^2 \propto \Omega^{\eta_2-\eta_3}$. By measuring these ratios, we can clearly see the anisotropic scaling behaviors at the TQPT.

5.6 Short-range interaction and the stability of anisotropic non-Fermi liquid fixed point

In this section, we study the effects of short-range interactions which was reported to destroy the non-Fermi liquid phase in the pyrochlore iridates $A_2\text{Ir}_2\text{O}_7$ [90, 91] and show that the non-Fermi liquid phase of DWSM at TQPT remains stable in a realizable range of N_f in $d = 3$.

To investigate how short-range interactions affects the non-Fermi liquid we have found, we first use the following identity

$$\left(\psi^\dagger\sigma_0\psi\right)^2 = -\left(\psi^\dagger\sigma_i\psi\right)^2 = \frac{1}{2}\left(\psi^\dagger\sigma_y\psi^*\right)\left(\psi^\dagger\sigma_y\psi\right) \quad (5.24)$$

for $i = x, y, z$. Using this identity, we can study the effects of all possible short-range interactions in particle-particle channel and particle-hole channels by adding just the following interaction to the action in Eq. (5.4):

$$S_u = \frac{u}{2} \int d^d x dt \left(\psi^\dagger\sigma_0\psi\right)_{(t,x)}^2 \quad (5.25)$$

In contrast to Ref. [90, 91] where the 4 by 4 gamma matrices are used and the vector-type short-range interactions appear, only the scalar-type interaction is needed in the present case.

To obtain the corrections generated by the short-range interaction and the combination of the short-range and Coulomb interaction up to one-loop order,

we evaluate the Feynman diagrams in Fig. 5.4.

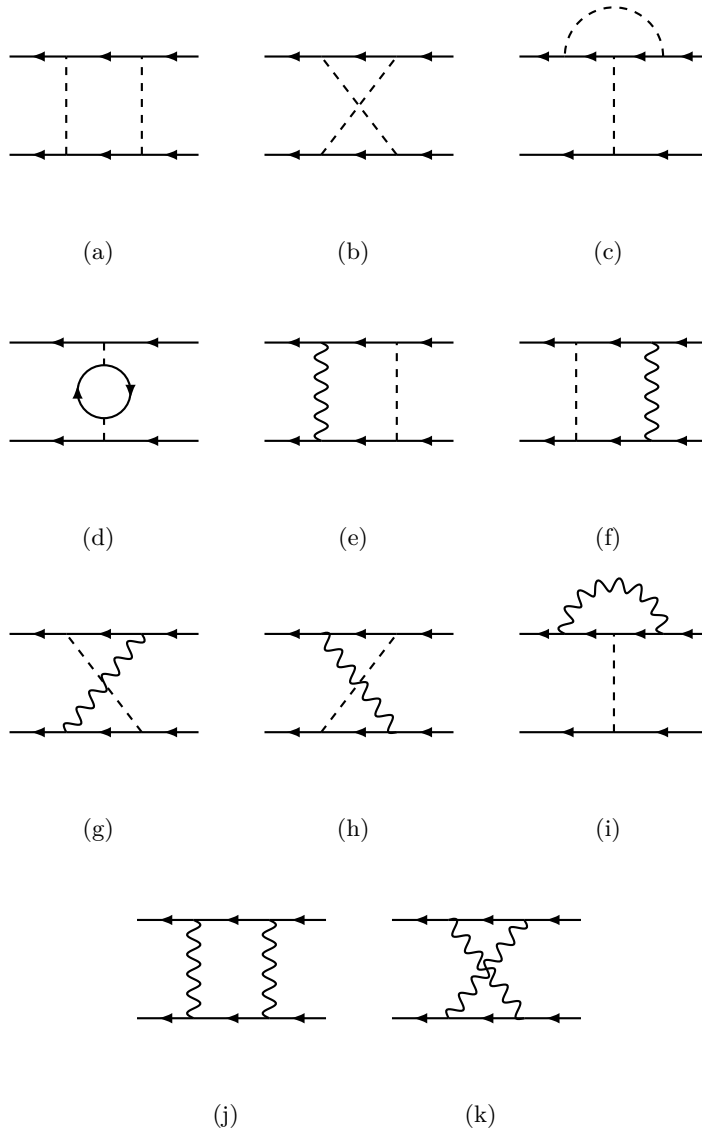


Figure 5.4: Feynman diagrams generated by the short-range interaction and long-range Coulomb interactions. The dashed and wavy lines stand for the short-range interaction and long-range Coulomb interaction, respectively. The solid line with arrow tip stands for the fermion.

Among the diagrams in Fig. 5.4, only the diagrams Fig. 5.4(b), 5.4(g),

5.4(h), and 5.4(k) give us the following non-zero corrections to the short-range interaction,

$$\begin{aligned}\delta u^{(b)} dl &= -u^2 \int_{\partial\Lambda} \frac{d\Omega d^d q}{(2\pi)^{d+1}} \eta_{\mu\nu} \frac{\text{Tr}[\sigma_0 G(i\Omega, \mathbf{q}) \sigma_0 \sigma_\mu]}{\text{Tr}[\sigma_\mu \sigma_\mu]} \frac{\text{Tr}[\sigma_0 G(i\Omega, \mathbf{q}) \sigma_0 \sigma_\mu]}{\text{Tr}[\sigma_\mu \sigma_\mu]}, \\ \delta u^{(g),(h)} dl &= u (ig)^2 \int_{\partial\Lambda} \frac{d\Omega d^d q}{(2\pi)^{d+1}} \eta_{\mu\nu} \\ &\quad \times \frac{\text{Tr}[\sigma_0 G(i\Omega, \mathbf{q}) \sigma_0 \sigma_\mu]}{\text{Tr}[\sigma_\mu \sigma_\mu]} \frac{\text{Tr}[\sigma_0 G(i\Omega, \mathbf{q}) \sigma_0 \sigma_\mu]}{\text{Tr}[\sigma_\mu \sigma_\mu]} D_0(i\Omega, \mathbf{q}), \\ \delta u^{(k)} dl &= - (ig)^4 \int_{\partial\Lambda} \frac{d\Omega d^d q}{(2\pi)^{d+1}} \eta_{\mu\nu} \\ &\quad \times \frac{\text{Tr}[\sigma_0 G(i\Omega, \mathbf{q}) \sigma_0 \sigma_\mu]}{\text{Tr}[\sigma_\mu \sigma_\mu]} \frac{\text{Tr}[\sigma_0 G(i\Omega, \mathbf{q}) \sigma_0 \sigma_\mu]}{\text{Tr}[\sigma_\mu \sigma_\mu]} D_0(i\Omega, \mathbf{q})^2,\end{aligned}$$

where $\eta_{\mu\nu} \equiv \text{diag}(1, -1, -1, 1)$ and the repeated indices are summed over. Here, by using Eq. 5.24, we convert the corrections to ‘vector-type’ short-range interaction such as $(\psi^\dagger \sigma_i \psi)^2$ ($i = x, y, z$) into the corrections to the ‘scalar-type’ short-range interaction such as $(\psi^\dagger \sigma_0 \psi)^2$ and it is reflected in $\eta_{\mu\nu}$. As a result, we obtain the following correction δu to u :

$$\delta u dl = \delta u^{(b)} dl + \delta u^{(g)} dl + \delta u^{(h)} dl + \delta u^{(k)} dl \quad (5.26)$$

$$\begin{aligned}&= - \sum_{a,b=u,g} \int_{\partial\Lambda} \frac{d\Omega d^d q}{(2\pi)^{d+1}} \eta_{\mu\nu} \\ &\quad \times \frac{\text{Tr}[\sigma_0 G(i\Omega, \mathbf{q}) \sigma_0 \sigma_\mu]}{\text{Tr}[\sigma_\mu \sigma_\mu]} \frac{\text{Tr}[\sigma_0 G(i\Omega, \mathbf{q}) \sigma_0 \sigma_\mu]}{\text{Tr}[\sigma_\mu \sigma_\mu]} I_a(\mathbf{q}) I_b(\mathbf{q})\end{aligned} \quad (5.27)$$

$$\begin{aligned}&= \frac{u^2}{4} \int_{\partial\Lambda} \frac{d^d q}{(2\pi)^d} \frac{1}{\varepsilon_{\mathbf{q}}} + \frac{ug^2}{2} \int_{\partial\Lambda} \frac{d^d q}{(2\pi)^d} \frac{1}{aq_\perp^2 + \frac{1}{a} q_z^2} \frac{1}{\varepsilon_{\mathbf{q}}} \\ &\quad + \frac{g^4}{4} \int_{\partial\Lambda} \frac{d^d q}{(2\pi)^d} \frac{1}{(aq_\perp^2 + \frac{1}{a} q_z^2)^2} \frac{1}{\varepsilon_{\mathbf{q}}},\end{aligned} \quad (5.28)$$

where $I_u(\mathbf{q}) = u$ and $I_g(\mathbf{q}) = \frac{g^2}{a(k_x^2 + k_y^2) + k_z^2/a}$. Introducing a dimensionless parameter

$$\bar{u} = \frac{S_{d-2}}{4\pi (2\pi)^{d-2} \Lambda^{2-d} |t_\perp|} u,$$

the correction δu to the dimensionless \bar{u} is obtained from Eq. (5.28),

$$\delta u = \bar{u}^2 H_1(\lambda) + \bar{u} \alpha H_2(\gamma, \lambda) + \alpha^2 H_3(\gamma, \lambda), \quad (5.29)$$

with

$$\begin{aligned}
H_1(\gamma, \lambda) &= \int_0^{\Lambda_\rho} \frac{\rho d\rho}{\sqrt{\rho^4 + (1 + \lambda\rho^2)^2}} \tag{5.30} \\
&= \frac{1}{2\sqrt{1 + \lambda^2}} \log \left[1 + \frac{\sqrt{1 + (\sqrt{1 + \lambda^2} + \lambda)^2}}{\sqrt{1 + \lambda^2} + \lambda} \right],
\end{aligned}$$

$$\begin{aligned}
H_2(\gamma, \lambda) &= 12\gamma \int_0^\infty \frac{\rho d\rho}{(1 + 4\gamma^2\rho^2)\sqrt{\rho^4 + (1 + \lambda\rho^2)^2}} \tag{5.31} \\
&= \frac{6\gamma}{\sqrt{1 + (4\gamma^2 - \lambda)^2}} \log \left[\frac{4\gamma^2 \left(4\gamma^2 - \lambda + \sqrt{1 + (4\gamma^2 - \lambda)^2} \right)}{\sqrt{1 + \lambda^2} \sqrt{1 + (4\gamma^2 - \lambda)^2} + \lambda(4\gamma^2 - \lambda) - 1} \right],
\end{aligned}$$

$$\begin{aligned}
H_3(\gamma, \lambda) &= 36\gamma^2 \int_0^\infty \frac{\rho d\rho}{(1 + 4\gamma^2\rho^2)^2 \sqrt{\rho^4 + (1 + \lambda\rho^2)^2}} \tag{5.32} \\
&= 18\gamma^2 \left[\frac{4\gamma^2 - \sqrt{1 + \lambda^2}}{1 + (4\gamma^2 - \lambda)^2} + \frac{(4\gamma^2 - \lambda)\lambda - 1}{(1 + (4\gamma^2 - \lambda)^2)^{3/2}} \right. \\
&\quad \left. \times \log \left[\frac{4\gamma^2 \left\{ \sqrt{1 + (4\gamma^2 - \lambda)^2} - (4\gamma^2 - \lambda) \right\}}{1 - \lambda(4\gamma^2 - \lambda) + \sqrt{(1 + \lambda^2)(1 + (4\gamma^2 - \lambda)^2)}} \right] \right],
\end{aligned}$$

where $\Lambda_\rho = (1 + \lambda^2)^{-1/4}$ is introduced to regulate the UV divergence in Eq. (5.30).

After rescaling the fields and space-time coordinates, we finally obtain the

RG flow functions for α , γ , λ and \bar{u} :

$$\frac{1}{\alpha} \frac{d\alpha}{d\ell} = \epsilon - \frac{\alpha}{2} \left[N_f \left\{ \frac{1}{\gamma} \left(\frac{2 + \lambda^2}{2} - \frac{\lambda(5 + 2\lambda^2)}{4\sqrt{1 + \lambda^2}} \right) + \gamma \left(\frac{1 + 2\lambda^2}{\sqrt{1 + \lambda^2}} - 2\lambda \right) \right\} \right] \quad (5.33)$$

$$\begin{aligned} & - \frac{\alpha}{2} F_+(\gamma, \lambda) \\ \frac{1}{\gamma} \frac{d\gamma}{d\ell} = & \frac{\alpha}{2} \left[N_f \left\{ \frac{1}{\gamma} \left(\frac{2 + \lambda^2}{2} - \frac{\lambda(5 + 2\lambda^2)}{4\sqrt{1 + \lambda^2}} \right) - \gamma \left(\frac{1 + 2\lambda^2}{\sqrt{1 + \lambda^2}} - 2\lambda \right) \right\} + \right] \quad (5.34) \\ & + \frac{\alpha}{2} F_-(\gamma, \lambda) \end{aligned}$$

$$\frac{1}{\lambda} \frac{d\lambda}{d\ell} = - \frac{\alpha}{\lambda} \left[4\gamma^2 F_z(\gamma, \lambda) + \lambda F_{\perp}(\gamma, \lambda) \right], \quad (5.35)$$

$$\begin{aligned} \frac{d\bar{u}}{d\ell} &= (\epsilon - 2 - \alpha F_{\perp}(\gamma, \lambda)) \bar{u} + \delta \bar{u} \\ &= (\epsilon - 2 - \alpha F_{\perp}(\gamma, \lambda) + \alpha H_2(\gamma, \lambda)) \bar{u} + H_1(\gamma, \lambda) \bar{u}^2 + H_3(\gamma, \lambda) \alpha^2. \quad (5.36) \end{aligned}$$

Note that no modification arises in Eqs. (5.33), (5.34), and (5.35) even if we include u , because u does not yield self-energy correction to the fermion ψ and boson ϕ at leading order. And for the particle-particle channel, it has the same RG flow equations as the particle-hole channel because they have the same operator form.

The RG function Eq. (5.36) of \bar{u} includes a term proportional to α^2 . This α^2 correction generates \bar{u} during RG flow even if we start with an initial condition $\bar{u}(\ell = 0) = 0$. Consequently, we find no stable fixed point with $N_f = 1$ in $d = 3$. Figure 5.5 shows RG flow for $N_f = 4, 4.775$, and 5 in $d = 3$ when we ignore λ in the RG functions Eq. (5.33, 5.34, 5.35, 5.36), where stable (unstable) fixed points are denoted by red (blue) points. The green point is the NFL fixed point. The lower bound of N_f , N_c , above which a stable fixed point begins to appear is approximately $N_c = 4.775$ as it is seen. The results seems to show that the non-Fermi liquid phase of DWSM at TQPT is not realizable in a real experiment since $N_f \geq 5$ is not likely to be achievable. However, if we take λ into account, we get a qualitatively different consequence. Fig. 5.6 shows RG flow when λ is

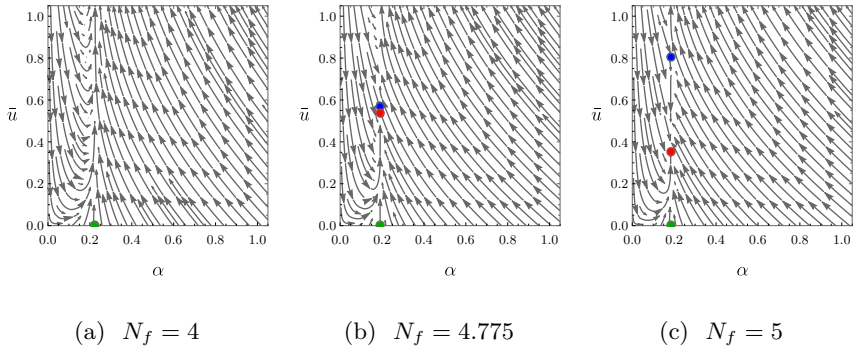


Figure 5.5: RG flow diagrams in terms of N_f when s_{\perp} is ignored.

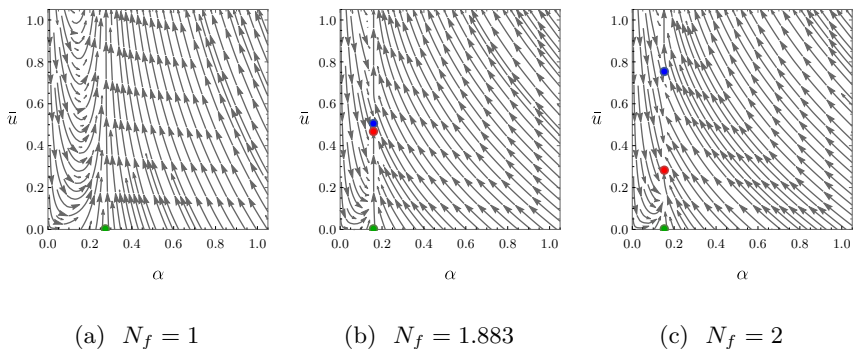


Figure 5.6: RG flow diagrams in terms of N_f when s_{\perp} is allowed.

kept. The estimated lower bound of N_f is about $N_c = 1.883$. Thus, a stable fixed point appear for $N_f = 2$ which is much smaller and compared to that obtained when λ is neglected. We expect that dWSM at TQPT with $N_f = 2$ is accessible in an experiment with SrSi_2 [82]. Although the estimated values of the lower bounds of N_f are found to depend on the renormalization scheme, s_{\perp} -term in DWSM at TQPT seems to stabilize the non-Fermi liquid phase.

So far, we consider the corrections up to one-loop order diagrams. However, in the ϵ expansion, we find the anisotropic NFL fixed point up to order of $\mathcal{O}(\epsilon)$. In that reason, near our anisotropic NFL fixed point, α^2 will give us the correction of $\mathcal{O}(\epsilon^2)$. So, if we carefully consider the order of ϵ , we can ignore α^2 contribution in Eq. (5.36) near our anisotropic NFL fixed point. In this

situation, the short-range interaction is irrelevant in $d = 3$ when $N_f > N_c = 2.279$ when λ is neglected, while N_c become 0.952 if λ is kept. Thus, keeping λ , we find that the non-Fermi liquid phase of DWSM at TQPT with $N_f = 1$ remains stable in the presence of the short-range interaction up to the accuracy of $\mathcal{O}(\epsilon)$. Note that to properly keep $\mathcal{O}(\epsilon^2)$ contribution, we need to calculate the two-loop order calculations, but that is out of our scope.

5.7 Discussion

Through out this chapter, for simplicity we ignored m_0 in Eq. (5.1) and the corresponding $s_\perp(k_x^2 + k_y^2)\sigma_z$ term with $s_\perp = m_0 a_0^2$ in \mathcal{H}_0 , which is allowed by symmetry. If we include the effect of this term, we find that there still exists a stable non-Gaussian fixed point at $(\alpha^*, \gamma^*, \lambda^*) = (0.336\epsilon/N_f, 0.821 - 0.083/N_f, -\text{sgn}(\beta)(0.866 + 0.035/N_f))$ in the ϵ expansion ($\lambda \equiv s_\perp/t_\perp$), indicating that the anisotropic non-Fermi liquid behavior is robust against the $s_\perp(k_x^2 + k_y^2)\sigma_z$ term. The details are presented in Appendix C. Note that for a TQPT between triple-Weyl semimetals [89], we believe that similar symmetry-allowed parabolic term should be considered.

There are studies about the instability of NFL in the quadratic dispersions under the presence of the short-range interactions [90, 91]. Our calculations are controlled by either ϵ or $1/N_f$. Thus, the scaling dimensions of the four-point short-range interactions at the stable fixed point are the same as the bare one at the leading order, $[u_{ijkl}] = -d + 2 + \mathcal{O}(\epsilon \text{ or } 1/N_f)$, which indicates that our fixed point is stable under the short-range interactions.

We stress that our emergent anisotropic non-Fermi liquid fixed point is distinct from previously studied non-Fermi liquid fixed points. Our fixed point is in 3d in sharp contrast to most of the previously studied fixed points including the very nice work by Sur and Lee where anisotropic non-Fermi liquid below 3d was found [79]. In 3d, quantum fluctuations are typically marginal or even

irrelevant, so quasi-particles are usually well-defined. However, the interplay between the topology and C_4 rotational symmetry in our systems protects the quadratic band touching at the topological phase transition, and the anisotropic non-Fermi liquid fixed point appears. As discussed above, the absence of the cubic symmetry makes the anisotropy even emergent in terms of the anomalous dimensions. Furthermore, the characteristic interplay between topology and symmetry is crucial in addition to the long-range Coulomb interaction to realize our universality class.

5.8 Conclusion

We studied TQPTs between DWSMs and insulators using the large N_f theory and $\epsilon = 4 - d$ expansion. We found that a novel class of quantum criticality appears at the TQPT characterized by emergent anisotropic non-Fermi liquid behaviors in which critical electronic modes and the long-range Coulomb interaction are strongly coupled, and the system becomes infinitely anisotropic. The anisotropic behaviors at the TQPT may be observed experimentally by measuring the power-law corrections to the diamagnetic susceptibility $\chi_{D,z}/\chi_{D,\perp} \propto T^{\eta_2 - \eta_3}$ and optical conductivity $\sigma_{\perp\perp}/\sigma_{zz} \propto \Omega^{\eta_2 - \eta_3}$, which we propose as smoking-gun signals of our TQPTs.

Chapter 6

Conclusion

It is the effects of interactions in the newly discovered topological materials that my doctoral research has been focused on. The researches are started with an anticipation that the Coulomb interaction between electrons are not well screened in some topological materials as much as it is in the conventional three dimensional materials. Hence, the initial aims of my researches are to reveal what phenomena can occur, which is rarely expected in the conventional material, and how it is related to the topological character of the new materials. To solve this curiosity, we have studied two electronic systems with non-trivial topological characters in which electrons are interacting via the long-range Coulomb interaction. In the following paragraphs, we summarize what we have studied in this doctoral thesis.

One of the two is an exciton-polariton system in a microcavity with a transition metal dichalcogenide. To deal with a wide range of excitation density, we treat an exciton as a composite particle of an electron in the conduction band and a hole created when a state in the valence band is emptied, rather than a bosonic particle. To deal with the condensation of excitons and photons, we introduce an ansatz for the mean-field ground state which is just the direct product of the coherent state of photon and the coherent state of exciton.

Solving the self-consistent mean-field equations numerically in a system with a single species of massive Dirac fermion, or just the single valley problem, we find that the s-wave and p-wave excitonic order parameters compete and there are topological phase transitions owing to the competition between them. Furthermore, we show that the p-wave order parameter is generated due to non-zero Berry curvature around the band extremum, which is an intrinsic properties of the massive Dirac fermion. Applying the same method to the two-valley problem, in which electrons in both valleys effectively interact through the cavity photon, we get a result showing the possibility that various topological phases can appear in a microcavity with a monolayer transition metal dichalcogenide.

The next subject is related to a three-dimensional topological semimetal, called a double-Weyl semimetal. A double-Weyl semimetal is characterized by double-Weyl nodes near the Fermi energy which can come true because crystallographic systems are thought not to be subject to the relativistic Lorentz symmetry. When two double-Weyl nodes merge, called the topological phase transition point, there appears a band structure whose dispersion is quadratic in all directions. Abrikosov proposed that systems with quadratic band touchings can show a singular response to the external fields because the Coulomb interaction is not screened well and preserves its long-range nature in the long-wavelength limit. To examine the proposal of Abrikosov in a double-Weyl semimetal at its topological phase transition point, we employ two renormalization group approaches, the large N_f method and the $\epsilon = 4 - d$ expansion. The approaches yield a consistent result implying that a double-Weyl semimetal at the topological phase transition is an anisotropic non-Fermi liquid. We also check whether weak short-range interactions destroy this anisotropic non-Fermi liquid phase, and get a result that if more than two merging points of double-Weyl nodes exist simultaneously in the first Brillouin zone, the anisotropic non-Fermi liquid phase survives the short-range interaction.

Bibliography

- [1] D. Xiao, G.-B. Liu, W. Feng, X. Xu, and W. Yao, [Phys. Rev. Lett. **108**, 196802 \(2012\)](#).
- [2] C. K. Chiu, J. C. Teo, A. P. Schnyder, and S. Ryu, [Rev Mod Phys **88**, 1 \(2016\)](#).
- [3] C. L. Kane and E. J. Mele, [Phys. Rev. Lett. **95**, 146802 \(2005\)](#).
- [4] C. L. Kane and E. J. Mele, [Phys. Rev. Lett. **95**, 226801 \(2005\)](#).
- [5] L. Fu and C. L. Kane, [Phys. Rev. B **74**, 195312 \(2006\)](#).
- [6] L. Fu, C. L. Kane, and E. J. Mele, [Phys. Rev. Lett. **98**, 106803 \(2007\)](#).
- [7] K. S. Novoselov, A. K. Geim, S. V. Morozov, D. Jiang, Y. Zhang, S. V. Dubonos, I. V. Grigorieva, and A. A. Firsov, [Science **306**, 666 \(2004\)](#).
- [8] A. Splendiani, L. Sun, Y. Zhang, T. Li, J. Kim, C.-Y. Chim, G. Galli, and F. Wang, [Nano Lett. **10**, 1271 \(2010\)](#).
- [9] K. F. Mak, C. Lee, J. Hone, J. Shan, and T. F. Heinz, [Phys. Rev. Lett. **105**, 136805 \(2010\)](#).
- [10] M. König, S. Wiedmann, C. Brüne, A. Roth, H. Buhmann, L. W. Molenkamp, X.-L. Qi, and S.-C. Zhang, [Science **318**, 766 \(2007\)](#).

- [11] Y. Xia, D. Qian, D. Hsieh, L. Wray, A. Pal, H. Lin, A. Bansil, D. Grauer, Y. S. Hor, R. J. Cava, *et al.*, [Nature physics](#) **5**, 398 (2009).
- [12] J. Zak, [Phys. Rev. Lett.](#) **62**, 2747 (1989).
- [13] J. Jung, F. Zhang, Z. Qiao, and A. H. MacDonald, [Phys. Rev. B](#) **84**, 075418 (2011).
- [14] S. Y. Xu, I. Belopolski, N. Alidoust, M. Neupane, G. Bian, C. Zhang, R. Sankar, G. Chang, Z. Yuan, C. C. Lee, S. M. Huang, H. Zheng, J. Ma, D. S. Sanchez, B. K. Wang, A. Bansil, F. Chou, P. P. Shibayev, H. Lin, S. Jia, and M. Z. Hasan, [Science \(80- \)](#) **349**, 613 (2015).
- [15] L. F. Mattheiss, [Phys. Rev. B](#) **8**, 3719 (1973).
- [16] G. Giuliani and G. Vignale, *Quantum theory of the electron liquid* (Cambridge university press, 2005).
- [17] J. M. Lu, O. Zheliuk, I. Leermakers, N. F. Q. Yuan, U. Zeitler, K. T. Law, and J. T. Ye, [Science](#) **350**, 1353 (2015).
- [18] D. Y. Qiu, F. H. da Jornada, and S. G. Louie, [Phys. Rev. Lett.](#) **111**, 216805 (2013).
- [19] M. M. Ugeda, A. J. Bradley, S.-F. Shi, F. H. da Jornada, Y. Zhang, D. Y. Qiu, W. Ruan, S.-K. Mo, Z. Hussain, Z.-X. Shen, F. Wang, S. G. Louie, and M. F. Crommie, [Nat. Mater.](#) **13**, 1091 (2014).
- [20] N. F. Q. Yuan, K. F. Mak, and K. T. Law, [Phys. Rev. Lett.](#) **113**, 097001 (2014).
- [21] Y.-T. Hsu, A. Vaezi, M. H. Fischer, and E.-A. Kim, [Nat. Commun.](#) **8**, 14985 (2017).

- [22] T. Cao, G. Wang, W. Han, H. Ye, C. Zhu, J. Shi, Q. Niu, P. Tan, E. Wang, B. Liu, and J. Feng, [Nat. Commun.](#) **3**, 887 (2012).
- [23] H. Zeng, J. Dai, W. Yao, D. Xiao, and X. Cui, [Nat. Nanotech.](#) **7**, 490 (2012).
- [24] H. Deng, G. Weihs, C. Santori, J. Bloch, and Y. Yamamoto, [Science](#) **298**, 199 (2002).
- [25] J. Kasprzak, M. Richard, S. Kundermann, A. Baas, P. Jeambrun, J. M. J. Keeling, F. M. Marchetti, M. H. Szymańska, R. André, J. L. Staehli, V. Savona, P. B. Littlewood, B. Deveaud, and L. S. Dang, [Nature](#) **443**, 409 (2006).
- [26] R. Balili, V. Hartwell, D. Snoke, L. Pfeiffer, and K. West, [Science](#) **316**, 1007 (2007).
- [27] X. Liu, T. Galfsky, Z. Sun, F. Xia, E.-c. Lin, Y.-H. Lee, S. Kéna-Cohen, and V. M. Menon, [Nat. Photon.](#) **9**, 30 (2015).
- [28] Y.-J. Chen, J. D. Cain, T. K. Stanev, V. P. Dravid, and N. P. Stern, [Nat. Photon.](#) **11**, 431 (2017).
- [29] J. J. Baumberg, A. V. Kavokin, S. Christopoulos, A. J. D. Grundy, R. Butté, G. Christmann, D. D. Solnyshkov, G. Malpuech, G. Baldassarri Höger von Högersthal, E. Feltin, J.-F. Carlin, and N. Grandjean, [Phys. Rev. Lett.](#) **101**, 136409 (2008).
- [30] K. G. Lagoudakis, M. Wouters, M. Richard, A. Baas, I. Carusotto, R. André, L. S. Dang, and B. Deveaud-Plédran, [Nature Physics](#) **4**, 706 (2008).
- [31] S. Utsunomiya, L. Tian, G. Roumpos, C. W. Lai, N. Kumada, T. Fujisawa, M. Kuwata-Gonokami, A. Löffler, S. Höfling, A. Forchel, and Y. Yamamoto, [Nature Physics](#) **4**, 700 (2008).

- [32] A. Amo, J. Lefrère, S. Pigeon, C. Adrados, C. Ciuti, I. Carusotto, R. Houdré, E. Giacobino, and A. Bramati, [Nature Physics](#) **5**, 805 (2009).
- [33] T. Karzig, C.-E. Bardyn, N. H. Lindner, and G. Refael, [Phys. Rev. X](#) **5**, 031001 (2015).
- [34] F. M. Marchetti, J. Keeling, M. H. Szymańska, and P. B. Littlewood, [Phys. Rev. Lett.](#) **96**, 066405 (2006).
- [35] K. Kamide and T. Ogawa, [Phys. Rev. Lett.](#) **105**, 056401 (2010).
- [36] T. Byrnes, T. Horikiri, N. Ishida, and Y. Yamamoto, [Phys. Rev. Lett.](#) **105**, 186402 (2010).
- [37] J. P. Echeverry, B. Urbaszek, T. Amand, X. Marie, and I. C. Gerber, [Phys. Rev. B](#) **93**, 121107 (2016).
- [38] T. Byrnes, N. Y. Kim, and Y. Yamamoto, [Nat. Phys.](#) **10**, 803 (2014).
- [39] Z. Ye, T. Cao, K. O'Brien, H. Zhu, X. Yin, Y. Wang, S. G. Louie, and X. Zhang, [Nature](#) **513**, 214 (2014).
- [40] X.-L. Qi, T. L. Hughes, and S.-C. Zhang, [Phys. Rev. B](#) **78**, 195424 (2008).
- [41] L. Keldysh and Y. V. KopaeV, [Sov. Phys. Solid State](#) **6**, 2219 (1965).
- [42] M. J. Rice and S. Strässler, [Solid State Commun.](#) **13**, 1931 (1973).
- [43] X. L. Yang, S. H. Guo, F. T. Chan, K. W. Wong, and W. Y. Ching, [Phys. Rev. A](#) **43**, 1186 (1991).
- [44] F. D. M. Haldane, [Phys. Rev. Lett.](#) **61**, 2015 (1988).
- [45] J. M. Ménard, C. Poellmann, M. Porer, U. Leierseder, E. Galopin, A. Lemaître, A. Amo, J. Bloch, and R. Huber, [Nat. Commun.](#) **5**, 4648 (2014).

- [46] X.-L. Qi and S.-C. Zhang, [Rev. Mod. Phys. **83**, 1057 \(2011\)](#).
- [47] S. Sachdev and B. Keimer, [Physics Today **64**, 29 \(2011\)](#).
- [48] N. P. Armitage, E. J. Mele, and A. Vishwanath, [Rev. Mod. Phys. **90**, 015001 \(2018\)](#).
- [49] M. Vojta, [Reports on Progress in Physics **81**, 064501 \(2018\)](#).
- [50] M. Z. Hasan and C. L. Kane, [Rev. Mod. Phys. **82**, 3045 \(2010\)](#).
- [51] M. König, S. Wiedmann, C. Brüne, A. Roth, H. Buhmann, L. W. Molenkamp, X.-L. Qi, and S.-C. Zhang, [Science **318**, 766 \(2007\)](#).
- [52] S.-Y. Xu, Y. Xia, L. A. Wray, S. Jia, F. Meier, J. H. Dil, J. Osterwalder, B. Slomski, A. Bansil, H. Lin, R. J. Cava, and M. Z. Hasan, [Science **332**, 560 \(2011\)](#).
- [53] Z. Wang, Y. Sun, X.-Q. Chen, C. Franchini, G. Xu, H. Weng, X. Dai, and Z. Fang, [Phys. Rev. B **85**, 195320 \(2012\)](#).
- [54] L. Wu, M. Brahlek, R. Valdés Aguilar, A. V. Stier, C. M. Morris, Y. Lubashevsky, L. S. Bilbro, N. Bansal, S. Oh, and N. P. Armitage, [Nature Physics **9**, 410 \(2013\)](#).
- [55] Q. Faure, S. Takayoshi, S. Petit, V. Simonet, S. Raymond, L.-P. Regnault, M. Boehm, J. S. White, M. Månsson, C. Rüegg, P. Lejay, B. Canals, T. Lorenz, S. C. Furuya, T. Giamarchi, and B. Grenier, [Nature Physics **14**, 716 \(2018\)](#).
- [56] B. A. Bernevig, T. L. Hughes, and S.-C. Zhang, [Science **314**, 1757 \(2006\)](#).
- [57] F. D. M. Haldane, [Phys. Rev. Lett. **61**, 2015 \(1988\)](#).
- [58] C. L. Kane and E. J. Mele, [Phys. Rev. Lett. **95**, 226801 \(2005\)](#).

- [59] L. Fu, C. L. Kane, and E. J. Mele, [Phys. Rev. Lett. **98**, 106803 \(2007\)](#).
- [60] J. M. Luttinger, [Phys. Rev. **102**, 1030 \(1956\)](#).
- [61] S. Murakami, N. Nagosa, and S.-C. Zhang, [Phys. Rev. B **69**, 235206 \(2004\)](#).
- [62] E.-G. Moon, C. Xu, Y. B. Kim, and L. Balents, [Phys. Rev. Lett. **111**, 206401 \(2013\)](#).
- [63] N. Zerf, L. N. Mihaila, P. Marquard, I. F. Herbut, and M. M. Scherer, [Phys. Rev. D **96**, 096010 \(2017\)](#).
- [64] M. Hermele, T. Senthil, and M. P. A. Fisher, [Phys. Rev. B **72**, 104404 \(2005\)](#).
- [65] Y. Huh and S. Sachdev, [Phys. Rev. B **78**, 064512 \(2008\)](#).
- [66] L. Savary, E.-G. Moon, and L. Balents, [Phys. Rev. X **4**, 041027 \(2014\)](#).
- [67] B.-J. Yang, E.-G. Moon, H. Isobe, and N. Nagaosa, [Nature Physics **10**, 774 \(2014\)](#).
- [68] G. Y. Cho and E.-G. Moon, [Scientific Reports **6**, 19198 \(2016\)](#).
- [69] S. Han, G. Y. Cho, and E.-G. Moon, [Phys. Rev. B **98**, 085149 \(2018\)](#).
- [70] B. Roy, P. Goswami, and V. Juričić, [Phys. Rev. B **95**, 201102 \(2017\)](#).
- [71] C. Fang, M. J. Gilbert, X. Dai, and B. A. Bernevig, [Phys. Rev. Lett. **108**, 266802 \(2012\)](#).
- [72] S. Ahn, E. J. Mele, and H. Min, [Phys. Rev. B **95**, 161112 \(2017\)](#).
- [73] S.-K. Jian and H. Yao, [Phys. Rev. B **92**, 045121 \(2015\)](#).
- [74] D. T. Son, [Phys. Rev. B **75**, 235423 \(2007\)](#).

- [75] L. Janssen and I. F. Herbut, *Phys. Rev. B* **93**, 165109 (2016).
- [76] H. Isobe, B.-J. Yang, A. Chubukov, J. Schmalian, and N. Nagaosa, *Phys. Rev. Lett.* **116**, 076803 (2016).
- [77] S.-S. Lee, *Phys. Rev. B* **80**, 165102 (2009).
- [78] S. Sachdev, *Quantum Phase Transitions*, 2nd ed. (Cambridge University Press, Cambridge, 2011).
- [79] S. Sur and S.-S. Lee, *Phys. Rev. B* **94**, 195135 (2016).
- [80] S.-S. Lee, *Annual Review of Condensed Matter Physics* **9**, 227 (2018).
- [81] G. Xu, H. Weng, Z. Wang, X. Dai, and Z. Fang, *Phys. Rev. Lett.* **107**, 186806 (2011).
- [82] S.-M. Huang, S.-Y. Xu, I. Belopolski, C.-C. Lee, G. Chang, T.-R. Chang, B. Wang, N. Alidoust, G. Bian, M. Neupane, D. Sanchez, H. Zheng, H.-T. Jeng, A. Bansil, T. Neupert, H. Lin, and M. Z. Hasan, *Proceedings of the National Academy of Sciences* **113**, 1180 (2016).
- [83] Z. Yan and Z. Wang, *Phys. Rev. B* **96**, 041206 (2017).
- [84] B. Singh, G. Chang, T.-R. Chang, S.-M. Huang, C. Su, M.-C. Lin, H. Lin, and A. Bansil, *Scientific Reports* **8**, 10540 (2018).
- [85] D. E. Sheehy and J. Schmalian, *Phys. Rev. Lett.* **99**, 226803 (2007).
- [86] P. Hosur, S. A. Parameswaran, and A. Vishwanath, *Phys. Rev. Lett.* **108**, 046602 (2012).
- [87] H.-H. Lai, *Phys. Rev. B* **91**, 235131 (2015).
- [88] H. Fukuyama, *Physics Letters A* **32**, 111 (1970).

- [89] J.-R. Wang, G.-Z. Liu, and C.-J. Zhang, *Phys. Rev. B* **99**, 195119 (2019).
- [90] I. F. Herbut and L. Janssen, *Phys. Rev. Lett.* **113**, 106401 (2014).
- [91] L. Janssen and I. F. Herbut, *Phys. Rev. B* **92**, 045117 (2015).

Appendix A

Coulomb interaction in the band basis

The self-consistent equation for the Fock term in the band basis is expressed as

$$\begin{aligned}
 \Delta_{\tau;\beta\alpha}(\mathbf{k}) &= -\frac{1}{S} \sum_{\mathbf{p}} \sum_{i,j} V(\mathbf{k} - \mathbf{p}) W_{i\beta}^*(\mathbf{k}) \langle \hat{c}_{\tau,j,\mathbf{p}}^\dagger \hat{c}_{\tau,i,\mathbf{p}} \rangle W_{j\alpha}(\mathbf{k}) \\
 &= -\frac{1}{S} \sum_{\mathbf{p}} \sum_{\alpha',\beta',i,j} V(\mathbf{k} - \mathbf{p}) W_{i\beta}^*(\mathbf{k}) W_{j\beta'}^*(\mathbf{p}) \rho_{\tau;\alpha'\beta'}(\mathbf{p}) W_{i\alpha'}(\mathbf{p}) W_{j\alpha}(\mathbf{k}),
 \end{aligned} \tag{A.1}$$

with

$$W(\mathbf{k}) = \begin{pmatrix} \cos \frac{\theta_{\mathbf{k}}}{2} & -\sin \frac{\theta_{\mathbf{k}}}{2} e^{i\tau\phi_{\mathbf{k}}} \\ \sin \frac{\theta_{\mathbf{k}}}{2} e^{i\tau\phi_{\mathbf{k}}} & \cos \frac{\theta_{\mathbf{k}}}{2} \end{pmatrix},$$

where $\phi_{\mathbf{k}} = \arctan(k_y/k_x)$ and $\theta_{\mathbf{k}} = \arctan \frac{\hbar v \sqrt{k_x^2 + k_y^2}}{E_{\text{gap}}/2}$. Here, we introduce the one-particle density matrix $\rho_{\tau;\alpha'\beta'}(\mathbf{p}) \equiv \langle \hat{\psi}_{\tau,\beta',\mathbf{p}}^\dagger \hat{\psi}_{\tau,\alpha',\mathbf{p}} \rangle$ for the notational convenience. And we neglect Hartree terms with $V(\mathbf{q} = 0)$ which vanishes due to overall charge neutrality. In the second line in (A.1), under an assumption that the translational symmetry remains unbroken, $\langle \hat{c}_{\tau,i,\mathbf{k}_1-\mathbf{q}}^\dagger | \hat{c}_{\tau',j,\mathbf{k}_2} \rangle = \delta_{\tau,\tau'} \delta_{\mathbf{k}_1-\mathbf{q},\mathbf{k}_2} \langle \hat{c}_{\tau,i,\mathbf{k}_2}^\dagger | \hat{c}_{\tau',j,\mathbf{k}_2} \rangle$ is used. It can also be shown that $\Delta_{\tau;vc}(\mathbf{k}) = \Delta_{\tau;cv}^*(\mathbf{k})$ and $\Delta_{\tau;vv}(\mathbf{k}) = -\Delta_{\tau;cc}(\mathbf{k})$. The latter relation is from the electron number conservation.

We solved (4.4) and (A.1) numerically with the fixed excitation density

constraint. We used the triangular mesh of 256 by 256 with the momentum cutoff 1 Å to minimize the number of the mesh outside of the cutoff momentum while keeping the rotational symmetry as much as possible. Instead of imposing excitation density constraint explicitly, we solved the self-consistent equation changing the chemical potential for the excitation density.

The partial wave decomposition in Eq. (4.9) of the main text is extracted from Eq. (A.1). To make notation simple, let us assume $\tau = +1$. For $\Delta_{1;cc}$ and $\Delta_{1;cv}$,

$$\begin{aligned} \Delta_{1;cc}(\mathbf{k}) = & -\frac{1}{S} \sum_{\mathbf{p}} V(\mathbf{k} - \mathbf{p}) [n_{1;eh}(\mathbf{p}) \{\sin \theta_{\mathbf{k}} \sin \theta_{\mathbf{p}} \cos(\phi_{\mathbf{k}} - \phi_{\mathbf{p}}) + \cos \theta_{\mathbf{k}} \cos \theta_{\mathbf{p}}\} \\ & + \frac{e^{i\phi_{\mathbf{p}}}}{2} \rho_{1;cv}(\mathbf{p}) \{\sin \theta_{\mathbf{k}} \cos \theta_{\mathbf{p}} \cos(\phi_{\mathbf{k}} - \phi_{\mathbf{p}}) + i \sin(\phi_{\mathbf{k}} - \phi_{\mathbf{p}}) - \cos \theta_{\mathbf{k}} \sin \theta_{\mathbf{p}}\} \\ & + \frac{e^{-i\phi_{\mathbf{p}}}}{2} \rho_{1;vc}(\mathbf{p}) \{\sin \theta_{\mathbf{k}} \cos \theta_{\mathbf{p}} \cos(\phi_{\mathbf{k}} - \phi_{\mathbf{p}}) - i \sin(\phi_{\mathbf{k}} - \phi_{\mathbf{p}}) - \cos \theta_{\mathbf{k}} \sin \theta_{\mathbf{p}}\}] , \end{aligned} \quad (\text{A.2})$$

$$\begin{aligned} \Delta_{1;cv}(\mathbf{k}) = & \frac{1}{S} \sum_{\mathbf{p}} V(\mathbf{k} - \mathbf{p}) \left[e^{-i\phi_{\mathbf{k}}} n_{1;eh}(\mathbf{p}) \left\{ \sin \theta_{\mathbf{k}} \cos \theta_{\mathbf{p}} \right. \right. \\ & \left. \left. + \sin \theta_{\mathbf{p}} \left(e^{i(\phi_{\mathbf{p}} - \phi_{\mathbf{k}})} \sin^2 \frac{\theta_{\mathbf{k}}}{2} - e^{-i(\phi_{\mathbf{p}} - \phi_{\mathbf{k}})} \cos^2 \frac{\theta_{\mathbf{k}}}{2} \right) \right\} \right. \\ & \left. - e^{-2i\phi_{\mathbf{k}}} \rho_{1;cv}(\mathbf{p}) \left\{ e^{i\phi_{\mathbf{p}}} \sin \frac{\theta_{\mathbf{k}}}{2} \sin \frac{\theta_{\mathbf{p}}}{2} + e^{i\phi_{\mathbf{k}}} \cos \frac{\theta_{\mathbf{k}}}{2} \cos \frac{\theta_{\mathbf{p}}}{2} \right\}^2 \right. \\ & \left. + e^{-2i(\phi_{\mathbf{k}} + \phi_{\mathbf{p}})} \rho_{1;vc}(\mathbf{p}) \left\{ e^{i\phi_{\mathbf{p}}} \sin \frac{\theta_{\mathbf{k}}}{2} \cos \frac{\theta_{\mathbf{p}}}{2} - e^{i\phi_{\mathbf{k}}} \cos \frac{\theta_{\mathbf{k}}}{2} \sin \frac{\theta_{\mathbf{p}}}{2} \right\}^2 \right] , \end{aligned} \quad (\text{A.3})$$

where $n_{1;eh}(\mathbf{p}) = \{\rho_{1;cc}(\mathbf{p}) - \rho_{1;vv}(\mathbf{p}) + 1\} / 2$.

By Fourier transformation, we can get the partial waves of $\Delta_{\tau;cv}(\mathbf{k})$, $\Delta_{\tau;cv}^{(m)}(k) = \int_{0,|\mathbf{k}|=k}^{2\pi} \frac{d\phi_{\mathbf{k}}}{2\pi} \Delta_{\tau;cv}(\mathbf{k}) e^{-im\phi_{\mathbf{k}}}$ for $m = 0, \pm 1, \pm 2, \dots$. Also, we have subtracted the contribution from non-excited states ($\rho_{\tau;\alpha\beta}(\mathbf{k}) = 0$ but $\rho_{\tau;vv}(\mathbf{k}) = 1$) as only

excited quasiparticles are assumed to interact with each other.

$$\begin{aligned}
\Delta_{1;cc}^{(m)}(k) = & \frac{1}{4\pi} \int_0^\infty dp p \left[-n_{1;eh}^{(m)}(p) \left\{ f_{p,k}^{(|m-1|)} \sin \theta_{\mathbf{p}} \sin \theta_{\mathbf{k}} \right. \right. \\
& + 2f_{p,k}^{(|m|)} \cos \theta_{\mathbf{p}} \cos \theta_{\mathbf{k}} + f_{p,k}^{(|m+1|)} \sin \theta_{\mathbf{p}} \sin \theta_{\mathbf{k}} \left. \left. \right\} \right. \\
& + \rho_{1;cv}^{(m-1)}(p) \left\{ -f_{p,k}^{(|m-1|)} \cos^2 \frac{\theta_{\mathbf{p}}}{2} \sin \theta_{\mathbf{k}} \right. \\
& + f_{p,k}^{(|m|)} \sin \theta_{\mathbf{p}} \cos \theta_{\mathbf{k}} + f_{p,k}^{(|m+1|)} \sin^2 \frac{\theta_{\mathbf{p}}}{2} \sin \theta_{\mathbf{k}} \left. \right\} \\
& + \left[\rho_{1;cv}^{(-m-1)}(p) \right]^* \left\{ f_{p,k}^{(|m-1|)} \sin^2 \frac{\theta_{\mathbf{p}}}{2} \sin \theta_{\mathbf{k}} \right. \\
& \left. \left. + f_{p,k}^{(|m+1|)} \sin \theta_{\mathbf{p}} \cos \theta_{\mathbf{k}} - f_{p,k}^{(|m+2|)} \cos^2 \frac{\theta_{\mathbf{p}}}{2} \sin \theta_{\mathbf{k}} \right\} \right], \tag{A.4}
\end{aligned}$$

$$\begin{aligned}
\Delta_{1;cv}^{(m)}(k) = & \frac{1}{2\pi} \int_0^\infty dp p \left[n_{1;eh}^{(m+1)}(p) \left\{ -f_{p,k}^{(|m|)} \sin \theta_{\mathbf{p}} \cos^2 \frac{\theta_{\mathbf{k}}}{2} \right. \right. \\
& + f_{p,k}^{(|m+1|)} \cos \theta_{\mathbf{p}} \sin \theta_{\mathbf{k}} + f_{p,k}^{(|m+2|)} \sin \theta_{\mathbf{p}} \sin^2 \frac{\theta_{\mathbf{k}}}{2} \left. \left. \right\} \right. \\
& - \rho_{1;cv}^{(m)}(p) \left\{ f_{p,k}^{(|m|)} \cos^2 \frac{\theta_{\mathbf{p}}}{2} \cos^2 \frac{\theta_{\mathbf{k}}}{2} \right. \\
& + \frac{1}{2} f_{p,k}^{(|m+1|)} \sin \theta_{\mathbf{p}} \sin \theta_{\mathbf{k}} + f_{p,k}^{(|m+2|)} \sin^2 \frac{\theta_{\mathbf{p}}}{2} \sin^2 \frac{\theta_{\mathbf{k}}}{2} \left. \right\} \\
& + \left[\rho_{1;cv}^{(-2-m)}(p) \right]^* \left\{ f_{p,k}^{(|m|)} \sin^2 \frac{\theta_{\mathbf{p}}}{2} \cos^2 \frac{\theta_{\mathbf{k}}}{2} \right. \\
& \left. \left. - \frac{1}{2} f_{p,k}^{(|m+1|)} \sin \theta_{\mathbf{p}} \sin \theta_{\mathbf{k}} + f_{p,k}^{(|m+2|)} \cos^2 \frac{\theta_{\mathbf{p}}}{2} \sin^2 \frac{\theta_{\mathbf{k}}}{2} \right\} \right], \tag{A.5}
\end{aligned}$$

$$\begin{aligned}
f_{p,k}^{(m)} = & \int_0^{2\pi} \frac{d\phi}{2\pi} (p^2 + k^2 - 2pk \cos \phi)^{-1/2} e^{-im\phi} \\
= & \frac{1}{k+p} {}_3F_2 \left(\left\{ \frac{1}{2}, \frac{1}{2}, 1 \right\}, \{1-m, 1+m\}; \frac{4kp}{(k+p)^2} \right), \tag{A.6}
\end{aligned}$$

$$O^{(m)}(p) = \int_{0,|\mathbf{p}|=p}^{2\pi} \frac{d\phi_{\mathbf{p}}}{2\pi} O(\mathbf{p}) e^{-im\phi_{\mathbf{p}}}, \tag{A.7}$$

where ${}_3F_2$ is the generalized hypergeometric function. In general, we expect to have $\rho_{\tau;cv}^{(m)} \neq 0$ for every m as the self-consistent equations relate terms with angular momentum m and $-m-2$. But $m = -1$ is the only exception as $(-1) = -(-1) - 2$. Therefore, we get a solution with $\rho_{\tau;cv}^{(-1)} \neq 0$ and $n_{\tau;eh}^{(0)} \neq 0$,

and all other terms vanish. Actually, this is the solution which satisfies the rotational symmetry as both $\rho_{\tau;cv}^{(-1)}$ and $n_{\tau;eh}^{(0)}$ keep the symmetry. Therefore, to describe the rotational symmetry breaking, we should include other pairing terms.

We used a truncated equation which includes only the *s-wave* ($m = 0$) and the *p-wave* ($m = -1$) terms of contributions in the main text to describe the phase transition. The *p-wave* term should be included as it is the only pairing term which preserves the rotational symmetry of the Hamiltonian. And the *s-wave* is also crucial as it is induced by the cavity photon and breaks the rotational symmetry. Also, we kept terms with factor $f_{p,k}^{(0)}$ only in the truncated equation as it gives the largest contribution. Lastly, the *s-wave* is expected to dominate in the low excitation density regime as mentioned in the main text. This choice for the truncation is also supported by Fig. SA.1.

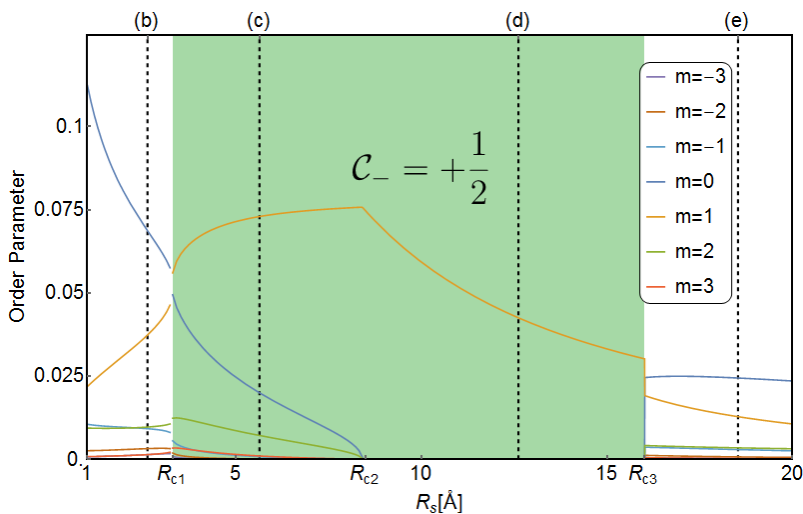


Figure A.1: Pairing terms with various m integrated along the radial direction with the condition in Fig. 1 of the main text. The rotational symmetry preserving solution appears in $R_{c2} < R_s < R_{c3}$.

We have mentioned in the main text that the particle-hole pair non-conserving

term induces $\Delta_{\tau;\alpha\beta}^{(-1)}(\mathbf{k})$. The first term of (A.7) with $m = -1$ contains $n_{\tau;eh}(\mathbf{p}) = \{\rho_{\tau;cc}(\mathbf{p}) - \rho_{\tau;vv}(\mathbf{p}) + 1\} / 2$. Therefore, in the mean field Hamiltonian such term appears due to contribution like $\psi_{c,\mathbf{k}}^\dagger \psi_{c,\mathbf{p}}^\dagger \psi_{v,\mathbf{p}} \psi_{c,\mathbf{k}}$ or $\psi_{c,\mathbf{k}}^\dagger \psi_{v,\mathbf{p}}^\dagger \psi_{v,\mathbf{p}} \psi_{v,\mathbf{k}}$ which apparently breaks particle-hole pair number conservation.

Appendix B

Relation between the Chern number in the normal phase and the Skyrmion number of Hartree-Fock quasiparticle bands

In this chapter of Appendix, we are going to prove the relation between the Chern number in the orbital basis and the Skyrmion number in the quasiparticle band basis. For convenience, we list some notations used in this chapter of Appendix.

- $|i\rangle$: Orbitals basis.
- $|\psi_n(\mathbf{k})\rangle = W_{in}(\mathbf{k})|i\rangle$: Eigenstates of \hat{H}_0 . Here $n = c$ is the upper energy band and $n = v$ is the lower band
- $|u_\alpha(\mathbf{k})\rangle = V_{n\alpha}(\mathbf{k})|\psi_n(\mathbf{k})\rangle = U_{i\alpha}(\mathbf{k})|i\rangle$: Eigenstates of

$$\hat{H}_{MF} = \sum_{m,n,\mathbf{k}} \psi_m^\dagger(\mathbf{k}) [\vec{\eta}(\mathbf{k}) \cdot \vec{\sigma}]_{mn} \psi_n(\mathbf{k}),$$

where the diagonalization $\sum_n [\vec{\eta}(\mathbf{k}) \cdot \vec{\sigma}]_{mn} V_{n\alpha}(\mathbf{k}) = E_\alpha(\mathbf{k})V_{m\alpha}(\mathbf{k})$ is done by $V(\mathbf{k})$. $\alpha = \tilde{c}$ is the upper mean-field energy band and $\alpha = \tilde{v}$ is the lower mean-field energy band.

To obtain $\mathcal{C}_\tau = \frac{\tau}{2} + \frac{i}{2\pi} \iint \hat{z} \cdot [\nabla V^\dagger \times \nabla V]_{\bar{v}\bar{v}} d^2k$, Let us start from the usual definition of Berry curvature $\vec{\mathcal{F}}_{\bar{v}\bar{v}} = i\nabla \times \langle u_{\bar{v}}(\mathbf{k}) | \nabla | u_{\bar{v}}(\mathbf{k}) \rangle$,

$$\begin{aligned}
-i [\mathcal{F}_r]_{\bar{v}\bar{v}} &= \epsilon_{pqr} \partial_p \langle u_{\bar{v}}(\mathbf{k}) | \partial_q | u_{\bar{v}}(\mathbf{k}) \rangle \\
&= \epsilon_{pqr} \partial_p \langle \psi_m(\mathbf{k}) | V_{m\bar{v}}^* \partial_q V_{n\bar{v}} | \psi_n(\mathbf{k}) \rangle \\
&= \epsilon_{pqr} \langle \partial_p \psi_m(\mathbf{k}) | V_{m\bar{v}}^* \partial_q V_{n\bar{v}} | \psi_n(\mathbf{k}) \rangle + \epsilon_{pqr} \langle \psi_m(\mathbf{k}) | \partial_p V_{m\bar{v}}^* \partial_q V_{n\bar{v}} | \psi_n(\mathbf{k}) \rangle \\
&= \epsilon_{pqr} V_{m\bar{v}}^* \partial_q V_{n\bar{v}} \langle \partial_p \psi_m(\mathbf{k}) | \psi_n(\mathbf{k}) \rangle + \epsilon_{pqr} V_{m\bar{v}}^* V_{n\bar{v}} \langle \partial_p \psi_m(\mathbf{k}) | \partial_q \psi_n(\mathbf{k}) \rangle \\
&\quad + \epsilon_{pqr} \partial_p V_{m\bar{v}}^* \partial_q V_{n\bar{v}} \langle \psi_m(\mathbf{k}) | \psi_n(\mathbf{k}) \rangle + \epsilon_{pqr} \partial_p V_{m\bar{v}}^* V_{n\bar{v}} \langle \psi_m(\mathbf{k}) | \partial_q \psi_n(\mathbf{k}) \rangle \\
&= \epsilon_{pqr} V_{m\bar{v}}^* \partial_q V_{n\bar{v}} \langle \partial_p \psi_m(\mathbf{k}) | \psi_n(\mathbf{k}) \rangle + \epsilon_{pqr} \partial_q V_{m\bar{v}}^* V_{n\bar{v}} \langle \partial_p \psi_m(\mathbf{k}) | \psi_n(\mathbf{k}) \rangle \\
&\quad + \epsilon_{pqr} V_{m\bar{v}}^* V_{n\bar{v}} \langle \partial_p \psi_m(\mathbf{k}) | \partial_q \psi_n(\mathbf{k}) \rangle + \epsilon_{pqr} \partial_p V_{m\bar{v}}^* \partial_q V_{n\bar{v}} \langle \psi_m(\mathbf{k}) | \psi_n(\mathbf{k}) \rangle \\
&= \epsilon_{pqr} \partial_p V_{m\bar{v}}^* \partial_q V_{n\bar{v}} + \epsilon_{pqr} \partial_p [V_{m\bar{v}}^* \langle \psi_m(\mathbf{k}) | \partial_q \psi_n(\mathbf{k}) \rangle V_{n\bar{v}}], \\
\therefore \vec{\mathcal{F}}_{\bar{v}\bar{v}} &= \left[\nabla V^\dagger \times i\nabla V \right]_{\bar{v}\bar{v}} + \nabla \times \left[V^\dagger \vec{\mathcal{A}}^{(0)} V \right]_{\bar{v}\bar{v}}. \tag{B.1}
\end{aligned}$$

Using Eq (B.1), the Chern number is divided into two parts,

$$\begin{aligned}
\mathcal{C}_\tau &= \frac{1}{2\pi} \iint [\mathcal{F}_z]_{\bar{v}\bar{v}} d^2k \\
&= \frac{1}{2\pi} \iint \hat{z} \cdot \left(\nabla \times \left[V^\dagger \vec{\mathcal{A}}^{(0)} V \right]_{\bar{v}\bar{v}} \right) d^2k + \frac{1}{2\pi} \iint \hat{z} \cdot \left[\nabla V^\dagger \times i\nabla V \right]_{\bar{v}\bar{v}} d^2k \\
&= \frac{1}{2\pi} \oint \left[V^\dagger \vec{\mathcal{A}}^{(0)} V \right]_{\bar{v}\bar{v}} \cdot d\mathbf{k} + \frac{1}{2\pi} \iint \hat{z} \cdot \left[\nabla V^\dagger \times i\nabla V \right]_{\bar{v}\bar{v}} d^2k, \tag{B.2}
\end{aligned}$$

where $\left[\vec{\mathcal{A}}^{(0)} \right]_{mn} = \langle \psi_m(\mathbf{k}) | i\nabla \psi_n(\mathbf{k}) \rangle$ is the matrix-valued Berry connection. If the interaction is not strong enough or our momentum space is larger enough, then we can assume $\lim_{|\mathbf{k}| \rightarrow \infty} V_{m\bar{v}}(\mathbf{k}) = \delta_{m\bar{v}}$. In that case, the line integration of the first term can be reduced to $\frac{1}{2\pi} \oint \left[\vec{\mathcal{A}}^{(0)} \right]_{\bar{v}\bar{v}} \cdot d\mathbf{k}$ which is the Berry phase of non-interacting valence band.

Taking that $V(\mathbf{k})$ diagonalizes $\vec{\eta}(\mathbf{k}) \cdot \vec{\sigma}$ into consideration, we can express $\Omega_{xy} = \hat{z} \cdot [\nabla V^\dagger \times i\nabla V]_{\bar{v}\bar{v}}$ by $\frac{1}{2} \int \vec{\eta} \cdot (\partial_x \vec{\eta} \times \partial_y \vec{\eta}) d^2k$. To prove this statement, let us first consider the manifestly gauge invariant form of Berry curvature

$$\Omega_{xy} = i \frac{\langle \tilde{v} | \partial_x H | \tilde{c} \rangle \langle \tilde{c} | \partial_y H | \tilde{v} \rangle - (x \leftrightarrow y)}{(E_{\tilde{v}} - E_{\tilde{c}})^2}$$

for Hamiltonian $H(\mathbf{k}) = \vec{\eta}(\mathbf{k}) \cdot \vec{\sigma}$. Noting $\langle v | \partial_x H | c \rangle$ is equal to $\eta \langle v | \partial_x \hat{\eta} \cdot \vec{\sigma} | c \rangle$, where $\hat{\eta}$ denotes the unit vector along the direction of $\vec{\eta}$, we can show that Ω_{xy} becomes $\frac{1}{2} \hat{\eta} \cdot (\partial_x \hat{\eta} \times \partial_y \hat{\eta})$ as follows.

$$\begin{aligned} \Omega_{xy} &= i \frac{\langle v | \partial_x H | c \rangle \langle c | \partial_y H | v \rangle - (x \leftrightarrow y)}{(E_v - E_c)^2} \\ &= i \frac{\eta^2 [\langle v | \partial_x \hat{\eta}_i \cdot \sigma_i | c \rangle \langle c | \partial_y \hat{\eta}_j \cdot \sigma_j | v \rangle - (x \leftrightarrow y)]}{4\eta^2} \\ &= i \frac{\partial_x \hat{\eta}_i \partial_y \hat{\eta}_j \langle v | [\sigma_i, \sigma_j] | v \rangle}{4} \end{aligned} \quad (\text{B.3})$$

$$= \frac{1}{2} \hat{\eta} \cdot (\partial_x \hat{\eta} \times \partial_y \hat{\eta}), \quad (\text{B.4})$$

where we use $[\sigma_i, \sigma_j] = 2i\epsilon_{ijk}\sigma_k$ between Eq (B.3) and (B.4).

Consequently, we obtain the following final result

$$\begin{aligned} \mathcal{C}_\tau &= \frac{\tau}{2} + \frac{1}{2\pi} \iint \hat{z} \cdot [\nabla V^\dagger \times \nabla V]_{\bar{v}\bar{v}} d^2k \\ &= \frac{\tau}{2} + \frac{1}{4\pi} \int \hat{\eta} \cdot (\partial_x \hat{\eta} \times \partial_y \hat{\eta}) d^2k, \end{aligned} \quad (\text{B.5})$$

where $\tau = \pm$ denotes the valley index.

Appendix C

Details of calculation of the renormalization group calculation

C.1 Details of the $\epsilon = 4 - d$ method

In this section, we provide detailed calculations of the $\epsilon = 4 - d$ method. First, we prove that $t_x = t_y$ and $a_x = a_y$ at low energies. Next, we derive the renormalization group (RG) equations using the $\epsilon = 4 - d$ expansion. Then we discuss the effect of the symmetry-allowed parabolic term, which is neglected in the main text, demonstrating that the TQPT is still characterized by anisotropic non-Fermi liquids.

Consider the leading-order self-energy corrections for fermions and bosons:

$$\Sigma(0, \mathbf{k}) = (-ig)^2 \int_{\Omega, \mathbf{q}} G_0(i\Omega, \mathbf{q} + \mathbf{k}) D_0(i\Omega, \mathbf{q}), \quad (\text{C.1})$$

$$\Pi(i\Omega, \mathbf{q}) = -N_f (-ig)^2 \int_{\omega, \mathbf{k}} \text{Tr}[G_0(i\Omega + i\omega, \mathbf{k} + \mathbf{q}/2) G_0(i\omega, \mathbf{k} - \mathbf{q}/2)], \quad (\text{C.2})$$

where $\int_{\Omega, \mathbf{q}, \mathbf{p}} = \int_{\Omega} \frac{d\Omega}{2\pi} \int \frac{dq_x dq_y}{(2\pi)} \int_{\partial\Lambda} \frac{dq_z d^{d-3}p}{(2\pi)^{d-2}}$ with $\partial\Lambda$ being the region $\mu < \sqrt{q_z^2 + p^2} <$

Λ. Here,

$$G_0(i\Omega, \mathbf{k}) = \frac{1}{-i\Omega + \varepsilon_x(\mathbf{k})\sigma_x + \varepsilon_y(\mathbf{k})\sigma_y + \varepsilon_z(\mathbf{k})\sigma_z} \\ = \frac{i\Omega + \varepsilon_x(\mathbf{k})\sigma_x + \varepsilon_y(\mathbf{k})\sigma_y + \varepsilon_z(\mathbf{k})\sigma_z}{\Omega^2 + E(\mathbf{k})^2}, \quad (\text{C.3})$$

$$D_0(i\Omega, \mathbf{q}) = \frac{1}{a_x q_x^2 + a_y q_y^2 + a_z q_z^2}, \quad (\text{C.4})$$

where $\varepsilon_x(\mathbf{k}) = t_x(k_x^2 - k_y^2)$, $\varepsilon_y(\mathbf{k}) = 2t_y k_x k_y$, $\varepsilon_z(\mathbf{k}) = t_z k_z^2$, and $E(\mathbf{k}) = \sqrt{\varepsilon_x(\mathbf{k})^2 + \varepsilon_y(\mathbf{k})^2 + \varepsilon_z(\mathbf{k})^2}$.

C.1.1 Proof of the emergent rotational symmetry along the k_z -axis

C.1.1.1 Proof of $a_x = a_y$

First, let us prove that $a_x = a_y$ at low energies. From the self-energy of the Coulomb interaction at $\Omega = 0$,

$$\Pi(0, \mathbf{k}) = -N_f(-ig)^2 \int_{\omega, \mathbf{q}} \text{Tr}[G_0(i\omega, \mathbf{q} + \mathbf{k}/2)G_0(i\omega, \mathbf{q} - \mathbf{k}/2)] \\ = -N_f g^2 \int_{\mathbf{q}, \mathbf{p}} \left(1 - \frac{\vec{\varepsilon}_+ \cdot \vec{\varepsilon}_-}{E_+ E_-}\right) \frac{1}{E_+ + E_-} \\ \approx -N_f g^2 \int_{\mathbf{q}, \mathbf{p}} \left[\frac{1}{a_x} \frac{(q_x^2 + q_y^2)(t_x^2 t_y^2 (q_x^2 + q_y^2)^2 + t_z^2 (t_x^2 + t_y^2)(q_z^2 + p^2)^2)}{2(t_x^2 (q_x^2 - q_y^2)^2 + 4t_y^2 q_x^2 q_y^2 + t_z^2 (q_z^2 + p^2)^2)^{5/2}} a_x k_x^2 \right. \\ \left. + \frac{1}{a_y} \frac{(q_x^2 + q_y^2)(t_x^2 t_y^2 (q_x^2 + q_y^2)^2 + t_z^2 (t_x^2 + t_y^2)(q_z^2 + p^2)^2)}{2(t_x^2 (q_x^2 - q_y^2)^2 + 4t_y^2 q_x^2 q_y^2 + t_z^2 (q_z^2 + p^2)^2)^{5/2}} a_y k_y^2 \right] \\ \left. + \frac{1}{a_z} \frac{t_z^2 q_z^2 (t_x^2 (q_x^2 - q_y^2)^2 + 4t_y^2 q_x^2 q_y^2)}{(t_x^2 (q_x^2 - q_y^2)^2 + 4t_y^2 q_x^2 q_y^2 + t_z^2 (q_z^2 + p^2)^2)^{5/2}} a_z k_z^2 \right], \quad (\text{C.5})$$

where $\varepsilon_{i\pm} = \varepsilon_i(\mathbf{q} \pm \mathbf{k}/2)$ and $E_{\pm} = \sqrt{\sum_i \varepsilon_{i\pm}^2}$.

We find that the coefficients of the k_x^2 and k_y^2 terms are the same, which we

denote as C_a , are given by

$$C_a = -N_f g^2 \int_{\mathbf{q}, \mathbf{p}} \frac{(q_x^2 + q_y^2) [t_x^2 t_y^2 (q_x^2 + q_y^2)^2 + t_z^2 (t_x^2 + t_y^2) (q_z^2 + p^2)^2]}{2 [t_x^2 (q_x^2 - q_y^2)^2 + 4 t_y^2 q_x^2 q_y^2 + t_z^2 (q_z^2 + p^2)^2]^{5/2}} \\ \propto -\frac{N_f g^2}{\Lambda^{4-d}} \ell, \quad (\text{C.6})$$

where $\ell = \ln(\Lambda/\mu)$. Let $C'_a = -C_a/\ell$, which is positive regardless of t_x , t_y and t_z . Then, the beta function of a_x/a_y is

$$\frac{1}{a_x/a_y} \frac{d(a_x/a_y)}{d\ell} = C'_a a_y \left(1 - \frac{a_x}{a_y}\right). \quad (\text{C.7})$$

Since C'_a is positive, $a_x = a_y$ at low energies.

C.1.1.2 Proof of $t_x = t_y$

From now on, we employ the following form of the Coulomb interaction propagator with $a_x = a_y \equiv a$ and $a_z = 1/a$,

$$D_0(i\Omega, \mathbf{q}) = \frac{1}{a(q_x^2 + q_y^2) + (q_z^2 + p^2)/a}. \quad (\text{C.8})$$

Then

$$\Sigma(i\omega, \mathbf{k}) = (-ig)^2 \int_{\Omega, \mathbf{q}, \mathbf{p}} G_0(i\omega + i\Omega, \mathbf{k} + \mathbf{q}) D_0(i\Omega, \mathbf{q}), \\ = -\frac{g^2}{2} \int_{\mathbf{q}, \mathbf{p}} \frac{\varepsilon_x(\mathbf{k} + \mathbf{q})\sigma_x + \varepsilon_y(\mathbf{k} + \mathbf{q})\sigma_y + \varepsilon_z(\mathbf{k} + \mathbf{q})\sigma_z}{E(\mathbf{k} + \mathbf{q})} \\ \times \frac{1}{a(q_x^2 + q_y^2) + (q_z^2 + p^2)/a}, \quad (\text{C.9})$$

$$\approx -\delta_{t_x} \varepsilon_x(\mathbf{k})\sigma_x - \delta_{t_y} \varepsilon_y(\mathbf{k})\sigma_y - \delta_{t_z} \varepsilon_z(\mathbf{k})\sigma_z, \quad (\text{C.10})$$

where

$$\delta_{t_x} = \frac{g^2}{2} \int_{\mathbf{q}, \mathbf{p}} \frac{\varepsilon_x^2 t_y^2 (q_x^4 + 6q_x^2 q_y^2 + q_y^4) - 2\varepsilon_y^2 t_x^2 (q_x^4 + q_y^4) - (2 - t_y^2/t_x^2) \varepsilon_x^2 \varepsilon_z^2 + \varepsilon_z^4}{(\varepsilon_x^2 + \varepsilon_y^2 + \varepsilon_z^2)^{5/2} (a(q_x^2 + q_y^2) + (q_z^2 + p^2)/a)}, \quad (\text{C.11})$$

$$\delta_{t_y} = \frac{g^2}{2} \int_{\mathbf{q}, \mathbf{p}} \frac{-\varepsilon_x^2 t_x^2 (q_x^4 + 6q_x^2 q_y^2 + q_y^4) + 2\varepsilon_y^2 t_x^2 (q_x^4 + q_y^4) - (2 - t_x^2/t_y^2) \varepsilon_y^2 \varepsilon_z^2 + \varepsilon_z^4}{(\varepsilon_x^2 + \varepsilon_y^2 + \varepsilon_z^2)^{5/2} (a(q_x^2 + q_y^2) + (q_z^2 + p^2)/a)}, \quad (\text{C.12})$$

$$\delta_{t_z} = \frac{g^2}{2} \int_{\mathbf{q}, \mathbf{p}} \frac{(\varepsilon_x^2 + \varepsilon_y^2)(\varepsilon_x^2 + \varepsilon_y^2 - \varepsilon_z t_z (5q_z^2 - p^2))}{(\varepsilon_x^2 + \varepsilon_y^2 + \varepsilon_z^2)^{5/2}} \frac{1}{a(q_x^2 + q_y^2) + (q_z^2 + p^2)/a}. \quad (\text{C.13})$$

To prove $t_x = t_y$ at low energies, let us define $T = t_x/t_y$. Then, the beta function of T is given by

$$\frac{1}{T} \frac{dT}{d\ell} = \frac{\delta_{t_x} - \delta_{t_y}}{\ell}. \quad (\text{C.14})$$

From Eqs. (C.11) and (C.12), $\delta_{t_x} - \delta_{t_y}$ is given by

$$\delta_{t_x} - \delta_{t_y} = \frac{g^2}{2} \int_{\mathbf{q}, \mathbf{p}} \frac{(t_x^2 + t_y^2) \varepsilon_x^2 (q_x^4 + 6q_x^2 q_y^2 + q_y^4) - 2(t_x^2 + t_y^2) \varepsilon_y^2 (q_x^4 + q_y^4)}{(\varepsilon_x^2 + \varepsilon_y^2 + \varepsilon_z^2)^{5/2} (a(q_x^2 + q_y^2) + (q_z^2 + p^2)/a)} - \frac{((2 - t_y^2/t_x^2) \varepsilon_x^2 - (2 - t_x^2/t_y^2) \varepsilon_y^2) \varepsilon_z^2}{(\varepsilon_x^2 + \varepsilon_y^2 + \varepsilon_z^2)^{5/2} (a(q_x^2 + q_y^2) + (q_z^2 + p^2)/a)} \quad (\text{C.15})$$

$$= \frac{g^2}{2t_y} \int_{\mathbf{q}, \mathbf{p}} \frac{(1 + T^2) ((q_x^2 - q_y^2)^2 (q_x^4 + 6q_x^2 q_y^2 + q_y^4) T^2 - 8q_x^2 q_y^2)}{(T^2 (q_x^2 - q_y^2)^2 + 4q_x^2 q_y^2 + \beta^2 (q_z^2 + p^2)^2)^{5/2} (a(q_x^2 + q_y^2) + (q_z^2 + p^2)/a)} + \frac{g^2}{2t_y} \int_{\mathbf{q}, \mathbf{p}} \frac{\beta^2 (q_z^2 + p^2)^2 (q_x^4 + 6q_x^2 q_y^2 + q_y^4 - 2(q_x^4 + q_y^4) T^2)}{(T^2 (q_x^2 - q_y^2)^2 + 4q_x^2 q_y^2 + \beta^2 (q_z^2 + p^2)^2)^{5/2} (a(q_x^2 + q_y^2) + (q_z^2 + p^2)/a)}, \quad (\text{C.16})$$

where $\beta \equiv t_z/t_y$.

Expanding $\delta_{t_x} - \delta_{t_y}$ in terms of $\delta T = T - 1$, then we have

$$\begin{aligned}
\delta_{t_x} - \delta_{t_y} &\approx \frac{g^2}{2t_y} \int_{\mathbf{q}, \mathbf{p}} \frac{(q_x^4 - 6q_x^2q_y^2 + q_y^4)(2(q_x^2 + q_y^2)^2 - (q_z^2 + p^2)^2\beta^2)}{((q_x^2 + q_y^2)^2 + \beta^2(q_z^2 + p^2)^2)^{5/2}(a(q_x^2 + q_y^2) + (q_z^2 + p^2)/a)} \\
&\quad - \frac{g^2}{2t_y} \delta T \int_{\mathbf{q}, \mathbf{p}} \frac{4(q_x^2 + q_y^2)^2(q_x^8 - 22q_x^6q_y^2 + 50q_x^4q_y^4 - 22q_x^2q_y^6 + q_y^8)}{((q_x^2 + q_y^2)^2 + \beta^2(q_z^2 + p^2)^2)^{7/2}(a(q_x^2 + q_y^2) + (q_z^2 + p^2)/a)} \\
&\quad + \frac{g^2}{2t_y} \delta T \int_{\mathbf{q}, \mathbf{p}} \frac{\beta^2(q_z^2 + p^2)^2(7q_x^8 - 40q_x^6q_y^2 + 2q_x^4q_y^4 - 40q_x^2q_y^6 + 7q_y^8)}{((q_x^2 + q_y^2)^2 + \beta^2(q_z^2 + p^2)^2)^{7/2}(a(q_x^2 + q_y^2) + (q_z^2 + p^2)/a)} \\
&\quad - \frac{g^2}{2t_y} \delta T \int_{\mathbf{q}, \mathbf{p}} \frac{4\beta^4(q_x^4 + q_y^4)(q_z^2 + p^2)^4}{((q_x^2 + q_y^2)^2 + \beta^2(q_z^2 + p^2)^2)^{7/2}(a(q_x^2 + q_y^2) + (q_z^2 + p^2)/a)} \\
&= - \frac{A_{d-2}g^2}{12\pi\sqrt{t_y t_z} \Lambda^{4-d}} \left(\frac{9a^5\beta^{5/2}}{4} \int_0^\infty dr \frac{r^5(4a^4\beta^2 - r^4)}{(r^4 + a^4\beta^2)^{7/2}(r^2 + 1)} \right) \delta T \ell \\
&= - \alpha G_T(\gamma) \delta T \ell, \tag{C.17}
\end{aligned}$$

where $\alpha = \frac{A_{d-2}g^2}{\sqrt{t_\perp t_z} \Lambda^{4-d}}$, $\gamma = \frac{a\sqrt{\beta}}{2}$, and $A_d = \frac{1}{6\pi(4\pi)^{d/2}\Gamma(d/2)}$. Here, we introduce the function $G_T(x)$ defined by

$$\begin{aligned}
G_T(x) &= 72x^5 \int_0^\infty dr \frac{r^5(64x^4 - r^4)}{(r^4 + 16x^4)^{7/2}(r^2 + 1)} \\
&= \frac{3x}{4(1 + 16x^4)^{7/2}} \left[\sqrt{1 + 16x^4}(1 + 160x^4 - 832x^6 - 1536x^8 + 2048x^{10}) \right. \\
&\quad \left. + 48x^4(-1 + 64x^4) \ln \left(\frac{4x^2(4x^2 + \sqrt{1 + 16x^4})}{-1 + \sqrt{1 + 16x^4}} \right) \right]. \tag{C.18}
\end{aligned}$$

Note that $G_T(\gamma)$ is positive for all γ . Then, we see

$$\frac{1}{\delta T} \frac{d\delta T}{d\ell} \approx - \alpha G_T(\gamma) \delta T \tag{C.19}$$

is negative (positive) for positive (negative) δT . Therefore, δT flows to 0, which means $T = 1$ is a stable fixed point and we arrive at the conclusion that $t_x = t_y \equiv t_\perp$ at the low energies. Combining the results of Secs. C.1.1.1 and

C.1.1.2, we can use the following form of action at low energies,

$$\mathcal{S} = \int d\tau d^d x \left[\psi^\dagger (\partial_\tau - ig\phi + \hat{\mathcal{H}}_0(-i\nabla))\psi + \frac{1}{2} \left(a \{ (\partial_x \phi)^2 + (\partial_y \phi)^2 \} + \frac{1}{a} (\partial_z \phi)^2 \right) \right], \quad (\text{C.20})$$

where

$$\mathcal{H}_0(\mathbf{k}) = t_\perp (k_x^2 - k_y^2) \sigma_x + 2t_\perp k_x k_y \sigma_y + t_z k_z^2 \sigma_z. \quad (\text{C.21})$$

C.1.2 Renormalization group equations in the $\epsilon = 4 - d$ expansion

In this section, we will show the details of the RG analysis using the $\epsilon = 4 - d$ expansion. From Eqs. (C.5) and (C.11)–(C.13) with $t_x = t_y = t_\perp$ and $a_x = a_y = a_z^{-1} = a$, we obtain the fermion and boson self-energies, respectively, given by

$$\begin{aligned} \Sigma(i\Omega, \mathbf{q}) &= (-ig)^2 \int_{\omega, \mathbf{k}, \mathbf{p}} G_0(i\omega + i\Omega, \mathbf{k} + \mathbf{q}) D_0(i\omega, \mathbf{k}) \\ &\approx -\alpha F_\perp(\gamma) \ell \left[t_\perp (q_x^2 - q_y^2) \sigma_x + 2t_\perp q_x q_y \sigma_y \right] - \alpha F_z(\gamma) \ell (t_z q_z^2) \sigma_z, \end{aligned} \quad (\text{C.22})$$

$$\begin{aligned} \Pi(\mathbf{q}) &= g^2 \int_{\omega, \mathbf{k}, \mathbf{p}} \text{Tr} [G_0(i\omega, \mathbf{k} + \mathbf{q}/2) G_0(i\omega, \mathbf{k} - \mathbf{q}/2)] \\ &\approx -N_f \alpha \left[\frac{a}{\gamma} q_\perp^2 + \frac{\gamma}{a} q_z^2 \right] \ell, \end{aligned} \quad (\text{C.23})$$

where $F_{\perp}(\gamma)$ and $F_z(\gamma)$ are given by

$$\begin{aligned}
F_{\perp}(x) &\equiv \frac{\delta_x}{\alpha\ell} \Big|_{t_x=t_y=t_{\perp}, a_x=a_y=a_z^{-1}=a} \\
&= 48x^5 \int_0^{\infty} dr \frac{r(32x^4 - r^4)}{(r^4 + 16x^4)^{5/2}(r^2 + 1)} \\
&= \frac{3x}{2(1 + 16x^4)^{5/2}} \left[\sqrt{1 + 16x^4}(1 + 64x^4 - 192x^6) \right. \\
&\quad \left. - 16x^4(1 - 32x^4) \ln \left(\frac{4x^2(4x^2 + \sqrt{1 + 16x^4})}{-1 + \sqrt{1 + 16x^4}} \right) \right], \tag{C.24}
\end{aligned}$$

$$\begin{aligned}
F_z(x) &\equiv \frac{\delta_z}{\alpha\ell} \Big|_{t_x=t_y=t_{\perp}, a_x=a_y=a_z^{-1}=a} \\
&= 6x \int_0^{\infty} dr \frac{r^5(r^4 - 32x^4)}{(r^4 + 16x^4)^{5/2}(r^2 + 1)} \\
&= \frac{3x}{(1 + 16x^4)^{5/2}} \left[\sqrt{1 + 16x^4}(-2 + 12x^2 + 16x^4) \right. \\
&\quad \left. + (1 - 32x^4) \ln \left(\frac{4x^2(4x^2 + \sqrt{1 + 16x^4})}{-1 + \sqrt{1 + 16x^4}} \right) \right]. \tag{C.25}
\end{aligned}$$

Figure C.1 shows the plots of $F_{\perp}(x)$ and $F_z(x)$. Then, after rescaling $z \rightarrow ze^{\ell}$, $(x, y) \rightarrow (x, y)e^{z_{\perp}\ell}$, and $\tau \rightarrow e^{z\ell}\tau$, and introducing the renormalization constant, $\psi \rightarrow \psi/Z_{\psi}^{1/2}$, $\phi \rightarrow \phi/Z_{\phi}^{1/2}$, $t_{\perp} \rightarrow t_{\perp}/Z_{t_{\perp}}$, $t_z \rightarrow t_z/Z_{t_z}$, $a \rightarrow a/Z_a$,

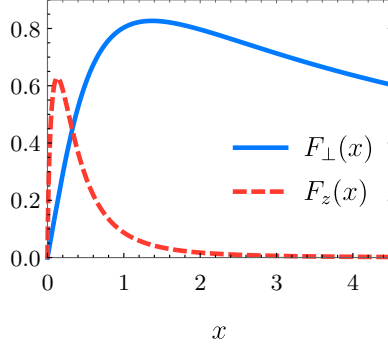


Figure C.1: Plots of $F_{\perp}(x)$ and $F_z(x)$. The blue solid line and red dashed line represent $F_{\perp}(x)$ and $F_z(x)$, respectively.

and $g \rightarrow g/Z_g$, we arrive at the following renormalized action,

$$\begin{aligned}
\mathcal{S}_{\text{renorm}} &= \int d\tau d^d x \left[\psi^\dagger \left(\partial_\tau - ig\phi + \mathcal{H}_0(-i\nabla) - \Sigma(-i\nabla) \right) \psi \right. \\
&\quad \left. + \frac{1}{2} \left(a \{ (\partial_x \phi)^2 + (\partial_y \phi)^2 \} + \frac{1}{a} (\partial_z \phi)^2 \right) - \frac{1}{2} \phi \Pi(-i\nabla) \phi \right] \\
&= \int d\tau d^d x \frac{e^{(z+2z_{\perp}+d-2)\ell}}{Z_{\psi}} \psi^\dagger \left[e^{-z\ell} \partial_\tau - \frac{1}{Z_g Z_{\phi}^{1/2}} ig\phi \right. \tag{C.26}
\end{aligned}$$

$$\begin{aligned}
&\quad + \frac{e^{-2z_{\perp}\ell}}{Z_{t_{\perp}}} (1 + \alpha F_{\perp}(\gamma)\ell) t_{\perp} ((\partial_y^2 - \partial_x^2)\sigma_x - 2\partial_x \partial_y \sigma_y) \\
&\quad - \frac{e^{-2\ell}}{Z_{t_z}} (1 + \alpha F_z(\gamma)) t_z \partial_z^2 \sigma_z \left. \right] \psi \\
&\quad + \int d\tau d^3 x \frac{e^{(z+2z_{\perp}+d-2)\ell}}{2Z_{\phi}} \left[\frac{e^{-2z_{\perp}\ell}}{Z_a} 2 \left(1 + N_f \frac{\alpha}{\gamma} \ell \right) a ((\partial_x \phi)^2 + (\partial_y \phi)^2) \right. \\
&\quad \left. + e^{-2\ell} Z_a (1 + N_f \alpha \gamma \ell) \frac{1}{a} (\partial_z \phi)^2 \right] \tag{C.27}
\end{aligned}$$

Requiring the scaling invariance of the action, we obtain the renormalization

constants as follows:

$$Z_\psi = 1 + [2z_\perp + (d-2)] \ell, \quad (\text{C.28})$$

$$Z_{t_\perp} = 1 + [z - 2z_\perp + \alpha F_\perp(\gamma)] \ell, \quad (\text{C.29})$$

$$Z_{t_z} = 1 + [z - 2 + \alpha F_z(\gamma)] \ell, \quad (\text{C.30})$$

$$Z_\phi = 1 + \left[z + z_\perp + (d-3) + \frac{N_f \alpha}{2} \left(\frac{1}{\gamma} + \gamma \right) \right] \ell, \quad (\text{C.31})$$

$$Z_a = 1 + \left[1 - z_\perp + \frac{N_f \alpha}{2} \left(\frac{1}{\gamma} - \gamma \right) \right] \ell, \quad (\text{C.32})$$

$$Z_g = 1 + \left[\frac{z - z_\perp - (d-3)}{2} - \frac{N_f \alpha}{4} \left(\frac{1}{\gamma} + \gamma \right) \right] \ell. \quad (\text{C.33})$$

From these renormalization constants, we can obtain the following RG equations for $d = 4 - \epsilon$,

$$\frac{1}{t_\perp} \frac{dt_\perp}{d\ell} = z - 2z_\perp + \alpha F_\perp(\gamma), \quad (\text{C.34})$$

$$\frac{1}{t_z} \frac{dt_z}{d\ell} = z - 2 + \alpha F_z(\gamma), \quad (\text{C.35})$$

$$\frac{1}{a} \frac{da}{d\ell} = 1 - z_\perp + \frac{N_f \alpha}{2} \left(\frac{1}{\gamma} - \gamma \right), \quad (\text{C.36})$$

$$\frac{1}{g^2} \frac{dg^2}{d\ell} = z - z_\perp - 1 + \epsilon - \frac{N_f \alpha}{2} \left(\frac{1}{\gamma} + \gamma \right). \quad (\text{C.37})$$

Thus, we find the RG equations for the dimensionless parameters α and γ as follows:

$$\frac{1}{\alpha} \frac{d\alpha}{d\ell} = \epsilon - \frac{N_f \alpha}{2} \left(\frac{1}{\gamma} + \gamma \right) - \frac{\alpha}{2} \left(F_z(\gamma) + F_\perp(\gamma) \right), \quad (\text{C.38})$$

$$\frac{1}{\gamma} \frac{d\gamma}{d\ell} = \frac{N_f \alpha}{2} \left(\frac{1}{\gamma} - \gamma \right) + \frac{\alpha}{2} \left(F_z(\gamma) - F_\perp(\gamma) \right). \quad (\text{C.39})$$

C.1.3 Effects of the symmetry-allowed parabolic term

If we include the symmetry-allowed parabolic term, $s_\perp(k_x^2 + k_y^2)\sigma_z$, the non-interacting Hamiltonian \mathcal{H}_0 is modified as

$$\mathcal{H}_0 = t_\perp(k_x^2 - k_y^2)\sigma_x + 2t_\perp k_x k_y \sigma_y + [Bt_z k_z^2 + s_\perp(k_x^2 + k_y^2)] \sigma_z, \quad (\text{C.40})$$

where $B = \pm 1$ for the topologically trivial and nontrivial insulator phases, respectively.

C.1.3.1 Boson self-energy

Similarly as in Eq. (C.23), we can obtain the boson self-energy in the presence of the symmetry-allowed parabolic term as

$$\begin{aligned}\Pi(i\Omega, \mathbf{q}) &= -N_f (ig)^2 \int_{\omega, \mathbf{k}, \mathbf{p}} \text{Tr}[G_0(i\Omega + i\omega, \mathbf{k} + \mathbf{q})G_0(i\omega, \mathbf{k})] \\ &\approx -N_f \alpha \left[\frac{1}{\gamma} \left(\frac{2 + \lambda^2}{2} - B \frac{\lambda(5 + 2\lambda^2)}{4\sqrt{1 + \lambda^2}} \right) a q_{\perp}^2 + \gamma \left(\frac{1 + 2\lambda^2}{\sqrt{1 + \lambda^2}} - 2B\lambda \right) \frac{1}{a} q_z^2 \right],\end{aligned}\tag{C.41}$$

where $\lambda = \frac{s_{\perp}}{t_{\perp}}$.

C.1.3.2 Fermion self-energy

Similarly as in Eq. (C.22), we can obtain the fermion self-energy as

$$\begin{aligned}\Sigma(i\omega, \mathbf{k}) &= (ig)^2 \int_{\Omega, \mathbf{q}, \mathbf{p}} G_0(i\omega + i\Omega, \mathbf{k} + \mathbf{q})D_0(i\Omega, \mathbf{q}) \\ &\approx -\delta_{t_{\perp}} [t_{\perp}(k_x^2 - k_y^2)\sigma_x + 2t_{\perp}k_x k_y \sigma_y] - [\delta_{t_z} B t_z k_z^2 + \delta_{s_{\perp}} s_{\perp}(k_x^2 + k_y^2)] \sigma_z,\end{aligned}\tag{C.42}$$

where δ_{t_\perp} , δ_{t_z} and δ_{s_\perp} are, respectively, given by

$$\begin{aligned}
\delta_{t_\perp} &= \frac{g^2}{2} \int_{\mathbf{k}, \mathbf{p}} \frac{t_z^2 k_\perp k_z^{d+1} (2(Bt_z k_z^2 + s_\perp k_\perp^2)^2 - t_\perp^2 k_\perp^4)}{2(t_\perp^2 k_\perp^4 + (Bt_z k_z^2 + s_\perp k_\perp^2)^2)^{5/2} (ak_\perp^2 + \frac{1}{a}k_z^2)} \\
&= \frac{A_{d-2} g^2 \ell}{\sqrt{t_\perp t_z} \Lambda^{4-d}} \int dr \frac{3(2\gamma)^5 r (-r^4 + 2(4B\gamma^2 + \lambda r^2)^2)}{2(1+r^2)(r^4 + (4B\gamma^2 + \lambda r^2)^2)^{5/2}} \\
&= \alpha F_\perp(\gamma, \lambda) \ell, \tag{C.43}
\end{aligned}$$

$$\begin{aligned}
\delta_{t_z} &= \frac{g^2}{2} \int_{\mathbf{k}, \mathbf{p}} \frac{t_\perp^3 k_\perp^5 k_z^{d-3} (t_\perp^2 k_\perp^4 - (2Bt_z k_z^2 - s_\perp k_\perp^2)(Bt_z k_z^2 + s_\perp k_\perp^2))}{(t_\perp^2 k_\perp^4 + (Bt_z k_z^2 + s_\perp k_\perp^2)^2)^{5/2} (ak_\perp^2 + \frac{1}{a}k_z^2)} \\
&= \frac{A_{d-2} g^2 \ell}{\sqrt{t_\perp t_z} \Lambda^{4-d}} \int dr \frac{6\gamma r^5 (r^4 - (8B\gamma^2 - \lambda r^2)(2B\gamma^2 + \lambda r^2))}{(1+r^2)(r^4 + (4B\gamma^2 + \lambda r^2)^2)^{5/2}} \\
&= \alpha F_z(\gamma, \lambda) \ell, \tag{C.44}
\end{aligned}$$

$$\begin{aligned}
\delta_{s_\perp} &= \frac{g^2}{2} \int_{\mathbf{k}, \mathbf{p}} \frac{B t_\perp^2 t_z k_\perp^3 k_z^{d-1} (t_\perp^2 k_\perp^4 - (2Bt_z k_z^2 - s_\perp k_\perp^2)(Bt_z k_z^2 + s_\perp k_\perp^2))}{s_\perp 2(t_\perp^2 k_\perp^4 + (Bt_z k_z^2 + s_\perp k_\perp^2)^2)^{5/2} (ak_\perp^2 + \frac{1}{a}k_z^2)} \\
&= \frac{B}{\lambda} \frac{A_{d-2} g^2 \ell}{\sqrt{t_\perp t_z} \Lambda^{4-d}} \int dr \frac{3(2\gamma)^3 r^3 (r^4 - (8B\gamma^2 - \lambda r^2)(4B\gamma^2 + \lambda r^2))}{(1+r^2)(r^4 + (4B\gamma^2 + \lambda r^2)^2)^{5/2}} \\
&= \frac{B}{\lambda} \alpha F_s(\gamma, \lambda) \ell. \tag{C.45}
\end{aligned}$$

Here, we introduce the following dimensionless functions,

$$\begin{aligned}
F_\perp(\gamma, \lambda) &= \int_0^\infty dr \frac{48\gamma^5 r (-r^4 + 2(4B\gamma^2 + \lambda r^2)^2)}{(1+r^2)(r^4 + (4B\gamma^2 + \lambda r^2)^2)^{5/2}} \\
&= \frac{3\gamma}{2(1 + (4B\gamma^2 - \lambda)^2)^2} \left[(1 + \lambda^2)^{3/2} + 64\gamma^4 (-3\gamma^2 + \sqrt{1 + \lambda^2}) \right. \\
&\quad \left. - 4B\gamma^2 \lambda (-12\gamma^2 + 5\sqrt{1 + \lambda^2}) - \frac{16\gamma^4 (1 - 2(4B\gamma^2 - \lambda)^2)}{\sqrt{1 + (4B\gamma^2 - \lambda)^2}} \right. \\
&\quad \left. \times \ln \left(\frac{4\gamma^2 (4\gamma^2 - B\lambda + \sqrt{1 + (4B\gamma^2 - \lambda)^2})}{-1 + 4B\gamma^2 \lambda - \lambda^2 + \sqrt{1 + \lambda^2} \sqrt{1 + (4B\gamma^2 - \lambda)^2}} \right) \right], \tag{C.46}
\end{aligned}$$

$$\begin{aligned}
F_z(\gamma, \lambda) &= \int_0^\infty dr \frac{6\gamma r^5 (r^4 - (8B\gamma^2 - \lambda r^2)(4B\gamma^2 + \lambda r^2))}{(1+r^2)(r^4 + (4B\gamma^2 + \lambda r^2)^2)^{5/2}} \\
&= \frac{3\gamma}{(1 + (4B\gamma^2 - \lambda))^2} \left[- \left(16B\gamma^4\lambda - 4\gamma^2(3 + 2\lambda^2) + B\lambda(1 + \lambda^2) \right) \right. \\
&\quad + \sqrt{1 + \lambda^2}(-2 + (4B\gamma^2 - \lambda)^2) + \frac{1 - 32\gamma^4 + 4B\gamma^2\lambda + \lambda^2}{\sqrt{1 + (4B\gamma^2 - \lambda)^2}} \\
&\quad \left. \times \ln \left(\frac{4\gamma^2(4\gamma^2 - B\lambda + \sqrt{1 + (4B\gamma^2 - \lambda)^2})}{-1 + 4B\gamma^2\lambda - \lambda^2 + \sqrt{1 + \lambda^2}\sqrt{1 + (4B\gamma^2 - \lambda)^2}} \right) \right], \quad (\text{C.47})
\end{aligned}$$

$$\begin{aligned}
F_s(\gamma, \lambda) &= \int_0^\infty dr \frac{24\gamma^3 r^3 (r^4 - (8B\gamma^2 - \lambda r^2)(4B\gamma^2 + \lambda r^2))}{(1+r^2)(r^4 + (4B\gamma^2 + \lambda r^2)^2)^{5/2}} \\
&= \frac{-12\gamma}{(1 + (4B\gamma^2 - \lambda))^2} \left[- \left(16B\gamma^4\lambda - 4\gamma^2(3 + 2\lambda^2) + B\lambda(1 + \lambda^2) \right) \right. \\
&\quad + \sqrt{1 + \lambda^2}(-2 + (4B\gamma^2 - \lambda)^2) - \frac{1 - 32\gamma^4 + 4B\gamma^2\lambda + \lambda^2}{\sqrt{1 + (4B\gamma^2 - \lambda)^2}} \\
&\quad \left. \times \ln \left(\frac{4\gamma^2(4\gamma^2 - B\lambda + \sqrt{1 + (4B\gamma^2 - \lambda)^2})}{-1 + 4B\gamma^2\lambda - \lambda^2 + \sqrt{1 + \lambda^2}\sqrt{1 + (4B\gamma^2 - \lambda)^2}} \right) \right] \\
&= -4\gamma^2 F_z(\gamma, \lambda). \quad (\text{C.48})
\end{aligned}$$

Note that in the limit $\lambda = 0$, $F_\perp(\gamma, \lambda) = F_\perp(\gamma)$, and $F_z(\gamma, \lambda) = F_z(\gamma)$.

C.1.3.3 RG flow equation

From Sec. C.1.3.1 and Sec. C.1.3.2, we can obtain the following RG flow equations,

$$\frac{1}{t_{\perp}} \frac{dt_{\perp}}{d\ell} = z - 2z_{\perp} + \alpha F_{\perp}(\gamma, \lambda), \quad (\text{C.49})$$

$$\frac{1}{t_z} \frac{dt_z}{d\ell} = z - 2 + \alpha F_z(\gamma, \lambda), \quad (\text{C.50})$$

$$\frac{1}{s_{\perp}} \frac{ds_{\perp}}{d\ell} = z - 2z_{\perp} - 4b \frac{\alpha}{\lambda} \gamma^2 F_z(\gamma, \lambda), \quad (\text{C.51})$$

$$\begin{aligned} \frac{1}{a} \frac{da}{d\ell} = & 1 - z_{\perp} + \frac{N_f \alpha}{2\gamma} \left(\frac{2 + \lambda^2}{2} - B \frac{\lambda(5 + 2\lambda^2)}{4\sqrt{1 + \lambda^2}} \right) \\ & - \frac{N_f \gamma \alpha}{2} \left(\frac{1 + 2\lambda^2}{\sqrt{1 + \lambda^2}} - 2B\lambda \right), \end{aligned} \quad (\text{C.52})$$

$$\begin{aligned} \frac{1}{g^2} \frac{dg^2}{d\ell} = & z - z_{\perp} - 1 + \epsilon - \frac{N_f \alpha}{2\gamma} \left(\frac{2 + \lambda^2}{2} - B \frac{\lambda(5 + 2\lambda^2)}{4\sqrt{1 + \lambda^2}} \right) \\ & - \frac{N_f \gamma \alpha}{2} \left(\frac{1 + 2\lambda^2}{\sqrt{1 + \lambda^2}} - 2B\lambda \right), \end{aligned} \quad (\text{C.53})$$

Then, the RG equations for the dimensionless parameters, α , γ and λ are given by

$$\begin{aligned} \frac{1}{\alpha} \frac{d\alpha}{d\ell} = & \epsilon - \frac{\alpha}{2} \left[N_f \left\{ \frac{1}{\gamma} \left(\frac{2 + \lambda^2}{2} - B \frac{\lambda(5 + 2\lambda^2)}{4\sqrt{1 + \lambda^2}} \right) + \gamma \left(\frac{1 + 2\lambda^2}{\sqrt{1 + \lambda^2}} - 2B\lambda \right) \right\} \right. \\ & \left. + F_z(\gamma, \lambda) + F_{\perp}(\gamma, \lambda) \right], \end{aligned} \quad (\text{C.54})$$

$$\begin{aligned} \frac{1}{\gamma} \frac{d\gamma}{d\ell} = & \frac{\alpha}{2} \left[N_f \left\{ \frac{1}{\gamma} \left(\frac{2 + \lambda^2}{2} - B \frac{\lambda(5 + 2\lambda^2)}{4\sqrt{1 + \lambda^2}} \right) - \gamma \left(\frac{1 + 2\lambda^2}{\sqrt{1 + \lambda^2}} - 2B\lambda \right) \right\} \right. \\ & \left. + F_z(\gamma, \lambda) - F_{\perp}(\gamma, \lambda) \right], \end{aligned} \quad (\text{C.55})$$

$$\frac{1}{\lambda} \frac{d\lambda}{d\ell} = - \frac{\alpha}{\lambda} [4B\gamma^2 F_z(\gamma, \lambda) + \lambda F_{\perp}(\gamma, \lambda)]. \quad (\text{C.56})$$

For given N_f , the RG equations have unstable fixed point, $\alpha^* = 0$ with arbitrary γ^* and λ^* , and stable interacting fixed point, $(\alpha^*, \gamma^*, \lambda^*) = (0.342\epsilon/N_f, 0.799-$

$0.079/N_f, -B(0.875+0.032/N_f))$ for large N_f . Then, near the interacting fixed point,

$$\begin{aligned} \left. \frac{1}{a} \frac{da}{d\ell} \right|_{\text{f.p.}} &= \frac{N_f \alpha^*}{2} \left[\frac{1}{\gamma^*} \left(\frac{2 + \lambda^{*2}}{2} - B \frac{\lambda^*(5 + 2\lambda^{*2})}{4\sqrt{1 + \lambda^{*2}}} \right) \right. \\ &\quad \left. - \gamma^* \left(\frac{1 + 2\lambda^{*2}}{\sqrt{1 + \lambda^{*2}}} - 2B\lambda^* \right) \right] > 0, \end{aligned} \quad (\text{C.57})$$

$$\left. \frac{1}{\beta^{-1}} \frac{d\beta^{-1}}{d\ell} \right|_{\text{f.p.}} = -\alpha^* \left(F_z(\gamma^*, \lambda^*) - F_\perp(\gamma^*, \lambda^*) \right) > 0. \quad (\text{C.58})$$

Thus, the bosonic and fermionic anisotropy parameters a and β^{-1} diverge at the stable interacting fixed point. Therefore, even if we keep $s_\perp(k_x^2 + k_y^2)\sigma_z$, the interacting fixed point still exhibits anisotropic non-Fermi liquid behaviors.

C.2 Details of the large N_f calculation

In this section, we will show the detailed calculations of the large N_f method.

C.2.1 Boson self-energy

Consider the self-energy of the Coulomb interaction given by

$$\begin{aligned} \Pi(i\Omega, \mathbf{q}) &= -N_f (-ig)^2 \int_{\omega, \mathbf{k}} \text{Tr}[G_0(i\Omega + i\omega, \mathbf{k} + \mathbf{q})G_0(i\omega, \mathbf{k})] \\ &= -N_f g^2 \int_{\mathbf{k}} \frac{E_+ + E_-}{(E_+ + E_-)^2 + \Omega^2} \left(1 - \frac{\vec{\varepsilon}_+ \cdot \vec{\varepsilon}_-}{E_+ E_-} \right), \end{aligned} \quad (\text{C.59})$$

where $\varepsilon_{i\pm} = \varepsilon_i(\mathbf{k} \pm \mathbf{q}/2)$ and $E_\pm = \sqrt{\sum_i \varepsilon_{i\pm}^2}$.

C.2.1.1 q_\perp dependence

Let us find the q_\perp dependence in $\Pi(i\Omega, \mathbf{q})$ with non-zero $i\Omega$. Because of the emergent rotational symmetry along the k_z -axis, we put $\mathbf{q}_\perp = q_\perp \hat{x}$ for simplicity. After changing the integration variables, $k_x \rightarrow q_\perp x, k_y \rightarrow q_\perp y, k_z \rightarrow$

$(t_\perp/t_z)^{1/2}q_\perp z$, we get

$$\begin{aligned}
\Pi(i\Omega, q_\perp) &= -\frac{N_f g^2 |q_\perp|}{8\pi^3 \sqrt{t_\perp t_z}} \\
&\times \int d^3x \left[\frac{\sqrt{\left((x+1)^2 + y^2\right)^2 + z^4}}{\left[\sqrt{\left((x+1)^2 + y^2\right)^2 + z^4} + \sqrt{\left(x^2 + y^2\right)^2 + z^4} \right]^2 + \left(\frac{\Omega}{t_\perp |q_\perp|^2}\right)^2} \right. \\
&+ \left. \frac{\sqrt{\left(x^2 + y^2\right)^2 + z^4}}{\left[\sqrt{\left((x+1)^2 + y^2\right)^2 + z^4} + \sqrt{\left(x^2 + y^2\right)^2 + z^4} \right]^2 + \left(\frac{\Omega}{t_\perp |q_\perp|^2}\right)^2} \right] \\
&\times \left[1 - \frac{\left((x+1)^2 - y^2\right)\left(x^2 - y^2\right) + 4(x+1)xy^2 + z^4}{\sqrt{\left((x+1)^2 + y^2\right)^2 + z^4} \sqrt{\left(x^2 + y^2\right)^2 + z^4}} \right] \\
&= -\frac{C_{\perp 1} N_f g^2}{\sqrt{t_\perp^2 t_z}} \sqrt{t_\perp q_\perp^2} \tanh(C_{\perp 2} \xi_r), \tag{C.60}
\end{aligned}$$

where $\xi_r = \sqrt{\frac{t_\perp}{|\Omega|}} |q_\perp|$, $C_{\perp 1} = 0.042$, and $C_{\perp 2} = 1.199$. The final result is a fitting function using an ansatz obtained from $\Pi(i\Omega, q_\perp) \propto \xi_r^2$ for $\xi_r \ll 1$, and $\Pi(i\Omega, q_\perp) \propto \xi_r$ for $\xi_r \gg 1$.

C.2.1.2 q_z dependence

Similarly, after changing the integration variables, $k_\perp \rightarrow (t_z/t_\perp)^{1/2}q_\perp r$, $k_z \rightarrow q_z z$, we get

$$\begin{aligned}
\Pi(i\Omega, q_z) &= -\frac{N_f g^2 |q_z|}{4\pi^2 t_\perp} \int_0^\infty dr r \int_{-\infty}^\infty dz \frac{\sqrt{r^4 + (z+1)^4} + \sqrt{r^4 + z^4}}{\left[\sqrt{r^4 + (z+1)^4} + \sqrt{r^4 + z^4} \right]^2 + \left(\frac{\Omega}{t_z q_z^2}\right)^2} \\
&\times \left[1 - \frac{r^4 + (z+1)^2 z^2}{\sqrt{r^4 + (z+1)^4} \sqrt{r^4 + z^4}} \right] \\
&= -\frac{C_{z 1} N_f g^2}{\sqrt{t_\perp^2 t_z}} \sqrt{t_z q_z^2} \tanh(C_{z 2} \xi_z), \tag{C.61}
\end{aligned}$$

where $\xi_z = \sqrt{\frac{t_z}{|\Omega|}}|q_z|$, $C_{z_1} = 0.016$, and $C_{z_2} = 1.267$. The final result is a fitting function using an ansatz obtained from $\Pi(i\Omega, q_z) \propto \xi_z^2$ for $\xi_z \ll 1$, and $\Pi(i\Omega, q_z) \propto \xi_z$ for $\xi_z \gg 1$.

C.2.1.3 Arbitrary q dependence

For arbitrary \mathbf{q} ,

$$\begin{aligned}
\Pi(i\Omega, \mathbf{q}) &= -\frac{N_f g^2 |q_\perp| \xi_z}{8\pi^3 \sqrt{t_\perp t_z} \xi_r} \\
&\times \int d^3x \left[\frac{\sqrt{\left((x+1)^2 + y^2\right)^2 + \frac{\xi_z^4}{\xi_r^4} (z+1)^4}}{\left[\sqrt{\left((x+1)^2 + y^2\right)^2 + \frac{\xi_z^4}{\xi_r^4} (z+1)^4} + \sqrt{\left(x^2 + y^2\right)^2 + \frac{\xi_z^4}{\xi_r^4} z^4} \right]^2 + \left(\frac{\Omega}{t_\perp q_\perp^2}\right)^2} \right. \\
&+ \left. \frac{\sqrt{\left(x^2 + y^2\right)^2 + \frac{\xi_z^4}{\xi_r^4} z^4}}{\left[\sqrt{\left((x+1)^2 + y^2\right)^2 + \frac{\xi_z^4}{\xi_r^4} (z+1)^4} + \sqrt{\left(x^2 + y^2\right)^2 + \frac{\xi_z^4}{\xi_r^4} z^4} \right]^2 + \left(\frac{\Omega}{t_\perp q_\perp^2}\right)^2} \right] \\
&\times \left[1 - \frac{\left((x+1)^2 - y^2\right)\left(x^2 - y^2\right) + 4(x+1)xy^2 - \frac{\xi_z^4}{\xi_r^4} (z+1)z}{\sqrt{\left((x+1)^2 + y^2\right)^2 + \frac{\xi_z^4}{\xi_r^4} (z+1)^4} \sqrt{\left(x^2 + y^2\right)^2 + \frac{\xi_z^4}{\xi_r^4} z^4}} \right] \\
&= -\frac{N_f g^2}{\sqrt{t_\perp^2 t_z}} \sqrt{C_{\perp 1}^2 t_\perp q_\perp^2 + C_{z_1}^2 t_z q_z^2} \tanh\left(\sqrt{C_{\perp 2}^2 \xi_r^2 + C_{z_2}^2 \xi_z^2}\right). \quad (\text{C.62})
\end{aligned}$$

The comparison between the exact numerical values and ansatz for the Coulomb interaction self-energy is presented in Fig. 1 in the main text.

C.2.2 Fermion self-energy

Using the boson self-energy obtained in Sec. C.2.1, we can obtain the fermion self-energy as follows:

$$\begin{aligned}
\Sigma(i\omega, \mathbf{k}) &= (ig)^2 \int_{\Omega, \mathbf{q}} G_0(i\Omega + i\omega, \mathbf{q} + \mathbf{k}) D(i\Omega, \mathbf{q}) \\
&= -g^2 \int_{\Omega, \mathbf{q}} \frac{i(\Omega + \omega) + \varepsilon_x(\mathbf{k} + \mathbf{q})\sigma_x + \varepsilon_y(\mathbf{k} + \mathbf{q})\sigma_y + \varepsilon_z(\mathbf{k} + \mathbf{q})\sigma_z}{(\Omega + \omega)^2 + \varepsilon_x^2(\mathbf{k} + \mathbf{q}) + \varepsilon_y^2(\mathbf{k} + \mathbf{q}) + \varepsilon_z^2(\mathbf{k} + \mathbf{q})} \\
&\quad \times \frac{1}{a(q_x^2 + q_y^2) + q_z^2/a - \Pi(i\Omega, \mathbf{q})} \\
&\approx -g^2 \int_{\Omega, \mathbf{q}} \frac{i(\Omega + \omega) + \varepsilon_x(\mathbf{k} + \mathbf{q})\sigma_x + \varepsilon_y(\mathbf{k} + \mathbf{q})\sigma_y + \varepsilon_z(\mathbf{k} + \mathbf{q})\sigma_z}{(\Omega + \omega)^2 + \varepsilon_x^2(\mathbf{k} + \mathbf{q}) + \varepsilon_y^2(\mathbf{k} + \mathbf{q}) + \varepsilon_z^2(\mathbf{k} + \mathbf{q})} \\
&\quad \times \frac{1}{-\Pi(i\Omega, \mathbf{q})} \\
&\approx i\omega\delta_\omega - \delta_{t_\perp} (\varepsilon_x(\mathbf{k})\sigma_x + \varepsilon_y(\mathbf{k})\sigma_y) - \delta_{t_z}\varepsilon_z(\mathbf{k})\sigma_z.
\end{aligned} \tag{C.63}$$

The corrections δ_ω , δ_{t_\perp} , and δ_{t_z} are evaluated in the following subsections.

C.2.2.1 ω correction δ_ω

The correction δ_ω is given by

$$\begin{aligned}
\delta_\omega &= -g^2 \int_{\Omega, \mathbf{q}} \frac{t_\perp^2 (q_x^2 + q_y^2)^2 + t_z^2 q_z^4 - \Omega^2}{[t_\perp^2 (q_x^2 + q_y^2)^2 + t_z^2 q_z^4 + \Omega^2]^2} \frac{\coth\left(\frac{\sqrt{C_{\perp 2}^2 (q_x^2 + q_y^2) + C_{z 2}^2 \beta q_z^2}}{(\Omega/t_\perp)^{1/2}}\right)}{\frac{N_f e^2}{(t_\perp t_z)^{1/2}} \sqrt{C_{\perp 1}^2 (q_x^2 + q_y^2) + C_{z 1}^2 \beta q_z^2}} \\
&= -\frac{(t_\perp t_z)^{1/2}}{8\pi^3 N_f} \frac{1}{t_\perp^2} \int_{-\infty}^{\infty} d\Omega \int_{\mu < |q_z| < \Lambda} dq_z \int_{-\infty}^{\infty} dq_\perp q_\perp \frac{q_\perp^4 + \beta^2 q_z^4 - \Omega^2/t_\perp^2}{[q_\perp^4 + \beta^2 q_z^4 + \Omega^2/t_\perp^2]^2} \\
&\quad \times \frac{\coth\left(\frac{\sqrt{C_{\perp 2}^2 q_\perp^2 + C_{z 2}^2 \beta q_z^2}}{(\Omega/t_\perp)^{1/2}}\right)}{\sqrt{C_{\perp 1}^2 q_\perp^2 + C_{z 1}^2 \beta q_z^2}}.
\end{aligned} \tag{C.64}$$

After changing the integration variables, $q_\perp \rightarrow \sqrt{\beta}q_z a$ and $\Omega \rightarrow \beta t_\perp q_z^2 b$, we have

$$\begin{aligned}\delta_\omega &= \frac{(t_\perp t_z)^{1/2}}{N_f} \frac{1}{t_\perp^2} \frac{t_\perp \beta^2}{\beta^{5/2}} \ln(\Lambda/\mu) \int_0^\infty da \int_0^\infty db \frac{a}{2\pi^3} \frac{-a^2 - 1 + b^2}{(a^4 + 1 + b^2)^2} \\ &\quad \times \frac{\coth\left(\sqrt{(C_{\perp 2}^2 a^2 + C_{z 2}^2)}/b\right)}{\sqrt{C_{\perp 1}^2 a^2 + C_{z 1}^2}} \\ &= \frac{C_\omega}{N_f} \ln(\Lambda/\mu),\end{aligned}\tag{C.65}$$

where $C_\omega = 0.366072$. Note that δ_ω has a logarithmic divergence both in the UV and IR cutoffs.

C.2.2.2 t_\perp correction δ_{t_\perp}

The correction δ_{t_\perp} is given by

$$\begin{aligned}\delta_{t_\perp} &= g^2 \int_{\Omega, q} \frac{(\Omega^2 + t_z^2 q_z^4)(\Omega^2 - 3t_\perp^2 (q_x^2 + q_y^2)^2 + t_z^2 q_z^4)}{[\Omega^2 + t_\perp^2 (q_x^2 + q_y^2)^2 + t_z^2 q_z^4]^3} \frac{\coth\left(\frac{\sqrt{C_{\perp 2}^2 (q_x^2 + q_y^2) + C_{z 2}^2 \beta q_z^2}}{(\Omega/t_\perp)^{1/2}}\right)}{\frac{N_f e^2}{(t_\perp t_z)^{1/2}} \sqrt{C_{\perp 1}^2 (q_x^2 + q_y^2) + C_{z 1}^2 \beta q_z^2}} \\ &= \frac{(t_\perp t_z)^{1/2}}{8\pi^3 t_\perp^2 N_f} \int_{-\infty}^\infty d\Omega \int_{\mu < |q_z| < \Lambda} dq_z \int_{-\infty}^\infty dq_\perp q_\perp \frac{(\Omega^2/t_\perp^2 + \beta^2 q_z^4)(\Omega^2/t_\perp^2 - 3q_\perp^4 + \beta^2 q_z^4)}{[\Omega^2/t_\perp^2 + q_\perp^4 + \beta^2 q_z^4]^3} \\ &\quad \times \frac{\coth\left(\frac{\sqrt{C_{\perp 2}^2 q_\perp^2 + C_{z 2}^2 \beta q_z^2}}{(\Omega/t_\perp)^{1/2}}\right)}{\sqrt{C_{\perp 1}^2 q_\perp^2 + C_{z 1}^2 \beta q_z^2}}.\end{aligned}\tag{C.66}$$

After changing the integration variables, $q_\perp \rightarrow \sqrt{\beta}q_z a$ and $\Omega \rightarrow \beta t_\perp q_z^2 b$, we have

$$\begin{aligned}\delta_{t_\perp} &= \frac{(t_\perp t_z)^{1/2}}{t_\perp^2 N_f} \frac{t_\perp \beta^2}{\beta^{5/2}} \ln(\Lambda/\mu) \int_0^\infty da \int_0^\infty db \frac{a}{2\pi^3} \frac{(1 + b^2)(-3a^4 + 1 + b^2)}{(a^4 + 1 + b^2)^3} \\ &\quad \times \frac{\coth\left(\sqrt{(C_{\perp 2}^2 a^2 + C_{z 2}^2)}/b\right)}{\sqrt{C_{\perp 1}^2 a^2 + C_{z 1}^2}} \\ &= \frac{C_{t_\perp}}{N_f} \ln(\Lambda/\mu),\end{aligned}\tag{C.67}$$

where $C_{t_\perp} = 0.614362$. Note that δ_{t_\perp} has a logarithmic divergence both in the UV and IR cutoffs.

C.2.2.3 t_z correction δ_{t_z}

The correction δ_{t_z} is given by

$$\delta_{t_z} = g^2 \int_{\Omega, q} \frac{16t_z^4 q_z^8 + \left(\Omega^2 + t_\perp^2 (q_x^2 + q_y^2)^2 + t_z^2 k_z^4\right) \left(\Omega^2 + t_\perp^2 (q_x^2 + q_y^2)^2 - 13t_z^2 k_z^4\right)}{[\Omega^2 + t_\perp^2 (q_x^2 + q_y^2)^2 + t_z^2 q_z^4]^3} \coth \left(\frac{\sqrt{C_{\perp 2}^2 (q_x^2 + q_y^2) + C_{z 2}^2 \beta q_z^2}}{(\Omega/t_\perp)^{1/2}} \right) \times \frac{N_f e^2}{(t_\perp t_z)^{1/2} \sqrt{C_{\perp 1}^2 (q_x^2 + q_y^2) + C_{z 1}^2 \beta q_z^2}} \quad (\text{C.68})$$

$$= \frac{(t_\perp t_z)^{1/2}}{8\pi^3 t_\perp^2 N_f} \int_{-\infty}^{\infty} d\Omega \int_{\mu < |q_z| < \Lambda} dq_z \int_{-\infty}^{\infty} dq_\perp q_\perp \left[\frac{16\beta^4 q_z^8}{[\Omega^2/t_\perp^2 + q_\perp^4 + \beta^2 q_z^4]^3} + \frac{\left(\Omega^2/t_\perp^2 + q_\perp^4 + \beta^2 k_z^4\right) \left(\Omega^2/t_\perp^2 + q_\perp^4 - 13\beta^2 k_z^4\right)}{[\Omega^2/t_\perp^2 + q_\perp^4 + \beta^2 q_z^4]^3} \right] \coth \left(\frac{\sqrt{C_{\perp 2}^2 q_\perp^2 + C_{z 2}^2 \beta q_z^2}}{(\Omega/t_\perp)^{1/2}} \right) \times \frac{1}{\sqrt{C_{\perp 1}^2 q_\perp^2 + C_{z 1}^2 \beta q_z^2}}. \quad (\text{C.69})$$

After changing the integration variables, $q_\perp \rightarrow \sqrt{\beta} q_z a$ and $\Omega \rightarrow \beta t_\perp q_z^2 b$, we have

$$\delta_{t_z} = \frac{(t_\perp t_z)^{1/2} t_\perp \beta^2}{t_\perp^2 N_f \beta^{5/2}} \ln(\Lambda/\mu) \int_0^\infty da \int_0^\infty db \frac{a}{2\pi^3} \frac{16 + (a^4 + 1 + b^2)(a^4 - 13 + b^2)}{(a^4 + 1 + b^2)^3} \times \frac{\coth \left(\sqrt{(C_{\perp 2}^2 a^2 + C_{z 2}^2)}/b \right)}{\sqrt{C_{\perp 1}^2 a^2 + C_{z 1}^2}} = \frac{C_{t_z}}{N_f} \ln(\Lambda/\mu), \quad (\text{C.70})$$

where $C_{t_z} = 0.341231$. Note that δ_{t_z} has a logarithmic divergence both in the UV and IR cutoffs.

C.2.3 Vertex correction

The correction δ_g is given by

$$\begin{aligned}
\delta_g &= (ig)^2 \int_{\Omega, \mathbf{q}} \frac{1}{2} \text{Tr}[G_0(i\omega, \mathbf{q})G_0(i\omega, \mathbf{q})]D(i\omega, \mathbf{q}) \\
&= -g^2 \int_{\Omega, \mathbf{q}} \frac{-\Omega^2 + t_\perp^2(q_x^2 + q_y^2)^2 + t_z^2 q_z^4}{[\Omega^2 + t_\perp^2(q_x^2 + q_y^2)^2 + t_z^2 q_z^4]^2} \frac{\coth\left(\sqrt{(C_{\perp 2}^2(q_x^2 + q_y^2) + C_{z 2}^2 \beta q_z^2)t_\perp/\Omega}\right)}{\frac{N_f e^2}{\sqrt{t_\perp t_z}} \sqrt{C_{\perp 1}^2(q_x^2 + q_y^2) + C_{z 1}^2 \beta q_z^2}} \\
&= -\frac{\sqrt{t_\perp t_z}}{8\pi^3 N_f t_\perp^2} \int_{-\infty}^{\infty} d\Omega \int_{\mu < |q_z| < \Lambda} dq_z \int_{-\infty}^{\infty} dq_\perp q_\perp \frac{-\Omega^2/t_\perp^2 + q_\perp^4 + \beta^2 q_z^4}{(\Omega^2/t_\perp^2 + q_\perp^4 + \beta^2 q_z^4)^2} \\
&\quad \times \frac{\coth\left(\sqrt{(C_{\perp 2}^2 q_\perp^2 + C_{z 2}^2 \beta q_z^2)t_\perp/\Omega}\right)}{\sqrt{C_{\perp 1}^2 q_\perp^2 + C_{z 1}^2 \beta q_z^2}}. \tag{C.71}
\end{aligned}$$

After changing the integration variables, $q_\perp \rightarrow \sqrt{\beta} q_z a$ and $\Omega \rightarrow \beta t_\perp q_z^2 b$, we have

$$\begin{aligned}
\delta_g &= \frac{(t_\perp t_z)^{1/2}}{N_f} \frac{1}{t_\perp^2} \frac{t_\perp \beta^2}{\beta^{5/2}} \ln(\Lambda/\mu) \int_0^\infty da \int_0^\infty db \frac{a}{2\pi^3} \frac{-a^2 - 1 + b^2}{(a^4 + 1 + b^2)^2} \\
&\quad \times \frac{\coth\left(\sqrt{(C_{\perp 2}^2 a^2 + C_{z 2}^2)/b}\right)}{\sqrt{C_{\perp 1}^2 a^2 + C_{z 1}^2}} \\
&= \frac{C_g}{N_f} \ln(\Lambda/\mu), \tag{C.72}
\end{aligned}$$

where $C_g = C_\omega$, which is consistent with the Ward identity.

C.3 Consistency between the large N_f calculation and ϵ expansion

In this section, we will show the correspondence between the large N_f calculation and the ϵ expansion.

In the static ($\Omega = 0$) and long wavelength limit ($q \rightarrow 0$), the boson propagator in the large N_f approximation has the following form for the momentum

dependence:

$$D(i\omega = 0, \mathbf{q} \rightarrow 0)^{-1} \sim q_{\perp} + |q_z|. \quad (\text{C.73})$$

Let us consider the ϵ expansion case. In the ϵ expansion, near the interacting fixed point,

$$\alpha^* \gamma^* = \frac{\epsilon}{N_f} \left(1 - \frac{c_{N_f}}{N_f} \right) \approx \frac{\epsilon}{N_f}, \quad (\text{C.74})$$

$$\frac{\alpha^*}{\gamma^*} = \frac{\epsilon}{N_f} \frac{1}{1 - c_{N_f}/N_f} \approx \frac{\epsilon}{N_f} \left(1 + \frac{c_{N_f}}{N_f} \right) \approx \frac{\epsilon}{N_f}, \quad (\text{C.75})$$

where we only keep up to N_f^{-1} order because we consider the large N_f limit.

Using these results,

$$\begin{aligned} D(i\omega = 0, \mathbf{q} \rightarrow 0)^{-1} &= a q_{\perp}^2 + \frac{1}{a} q_z^2 - \Pi(i\omega, \mathbf{q}) \\ &= a \left(1 + N_f \frac{\alpha^*}{\gamma^*} \ell \right) q_{\perp}^2 + \frac{1}{a} (1 + N_f \alpha^* \gamma^* \ell) q_z^2 \\ &\approx a (1 + \epsilon \ell) q_{\perp}^2 + \frac{1}{a} (1 + \epsilon \ell) q_z^2 \\ &\sim e^{\epsilon \ell} q_{\perp}^2 + e^{\epsilon \ell} q_z^2 \\ &\approx q_{\perp}^{2-\epsilon/z_{\perp}} + |q_z|^{2-\epsilon}. \end{aligned} \quad (\text{C.76})$$

Here, in the fourth line, we absorbed the momentum dependence of a into q_{\perp} and q_z . For a sufficiently large N_f , $z_{\perp} \approx 1$, thus for $\epsilon = 1$ with $d = 3$, $D(0, \mathbf{q})^{-1} \sim q_{\perp} + |q_z|$. Therefore, the result of the ϵ expansion is consistent with the large N_f calculation.

C.4 Physical observables in the non-interacting limit

In this section, we will calculate the physical observables such as the specific heat, compressibility, diamagnetic susceptibility, and optical conductivity at the TQPT between DWSM and insulating phases in the non-interacting limit. For simplicity, we assume $t_x = t_y = t_{\perp}$, the rotational symmetry along the k_z -axis.

C.4.1 Density of states

Through the analytic continuation $i\omega \rightarrow \omega + i\delta$ in $G_0(i\omega, \mathbf{k})$, the retarded Green's function G_0^{ret} is obtained as

$$G_0^{\text{ret}}(\omega + i\delta, \mathbf{k}) = \frac{1}{-(\omega + i\delta) + \mathcal{H}_0(\mathbf{k})}, \quad (\text{C.77})$$

and the imaginary part of G_0^{ret} and the spectral function are

$$\text{Im}[G_0^{\text{ret}}(\omega, \mathbf{k})] = \frac{\pi \text{sgn}(\omega)}{2E_k} (\omega + \mathcal{H}_0(\mathbf{k})) (\delta(\omega - E_k) + \delta(\omega + E_k)), \quad (\text{C.78})$$

$$\begin{aligned} S_F(\omega) &= -\frac{1}{\pi} \text{Tr}[G_0^{\text{ret}}(\omega, \mathbf{k})] \\ &= \delta(\omega + E_k) + \delta(\omega - E_k). \end{aligned} \quad (\text{C.79})$$

The density of states is given by

$$\begin{aligned} \rho(\omega) &= \int \frac{d^3k}{(2\pi)^3} S_F(\omega, \mathbf{k}) \\ &= \frac{|\omega|}{\pi^2} \int_0^\infty dk_\perp \int_0^\infty dk_z k_\perp \delta(\omega^2 - (t_\perp^2 k_\perp^4 + t_z^2 k_z^4)) \\ &= \frac{\Gamma(5/4)}{4\pi^{3/2}\Gamma(3/4)} \frac{|\omega|^{1/2}}{t_\perp t_z^{1/2}}, \end{aligned} \quad (\text{C.80})$$

where $\Gamma(x)$ is the gamma function and we use the identity,

$$\int_0^1 dR \frac{R}{(1 - R^4)^{3/4}} = \frac{\sqrt{\pi}\Gamma(5/4)}{\Gamma(3/4)}. \quad (\text{C.81})$$

C.4.2 Free energy

In this section, we will calculate the free energy at the TQPT in the non-interacting limit from which the specific heat and the compressibility are derived. The finite-temperature propagator of fermion is

$$G_0(i\omega_n, \mathbf{k})^{-1} = (-i\omega_n - \mu) + \mathcal{H}_0(\mathbf{k}), \quad (\text{C.82})$$

where we introduce the chemical potential μ for deriving the compressibility. The partition function and its logarithmic form are given by

$$\begin{aligned}\mathcal{Z} &= \text{Det}[\beta G_0^{-1}] \\ &= \prod_{i\omega_n} \prod_{\mathbf{k}} [\beta^2((\omega_n - i\mu)^2 + E(\mathbf{k})^2)],\end{aligned}\tag{C.83}$$

$$\begin{aligned}\ln \mathcal{Z} &= V \int \frac{d^3k}{(2\pi)^3} T \sum_{i\omega_n} \ln [\beta^2((\omega_n - i\mu)^2 + E(\mathbf{k})^2)] \\ &= \frac{V}{2} \int \frac{d^3k}{(2\pi)^3} T \sum_{i\omega_n} [\ln \{\beta^2(\omega_n^2 + (E(\mathbf{k}) - \mu)^2)\} + \ln \{\beta^2(\omega_n^2 + (E(\mathbf{k}) + \mu)^2)\}],\end{aligned}\tag{C.84}$$

where $\beta = T^{-1}$ and we use the relation

$$[(\omega_n - i\mu)^2 + E(\mathbf{k})^2] [(\omega_n + i\mu)^2 + E(\mathbf{k})^2] = [\omega_n^2 + (E(\mathbf{k}) - \mu)^2] [\omega_n^2 + (E(\mathbf{k}) + \mu)^2].\tag{C.85}$$

By using

$$\sum_{i\omega_n} \ln [\beta^2(\omega_n^2 + E(\mathbf{k})^2)] = E(\mathbf{k})/T + 2 \ln(1 + e^{-E(\mathbf{k})/T}) + \text{const.},\tag{C.86}$$

we obtain the free energy density as

$$\begin{aligned}\mathcal{F} &= -\frac{T}{V} \ln \mathcal{Z} \\ &= -T \int \frac{d^3k}{(2\pi)^3} \left[E(\mathbf{k})/T + \ln(1 + e^{-(E(\mathbf{k})-\mu)/T}) + \ln(1 + e^{-(E(\mathbf{k})+\mu)/T}) + \text{const.} \right].\end{aligned}\tag{C.87}$$

Subtracting $T = 0$ contribution, $\delta\mathcal{F}(T) := \mathcal{F}(T) - \mathcal{F}(0)$ is given by

$$\begin{aligned}\delta\mathcal{F}(T, \mu) &= -T \int \frac{d^3k}{(2\pi)^3} \left[\ln(1 + e^{-(E(\mathbf{k})-\mu)/T}) + \ln(1 + e^{-(E(\mathbf{k})+\mu)/T}) \right] \\ &= \frac{\Gamma(5/4)}{8\pi\Gamma(3/4)} \frac{T^{5/2}}{t_\perp t_z^{1/2}} \left[\text{Li}_{\frac{5}{2}}(-e^{\mu/T}) + \text{Li}_{\frac{5}{2}}(-e^{-\mu/T}) \right],\end{aligned}\tag{C.88}$$

where $\text{Li}_n(x)$ is the polylogarithm function.

C.4.2.1 Specific heat

For $\mu = 0$, using $\text{Li}_{\frac{5}{2}}(-1) = -\frac{(4-\sqrt{2})}{4}\zeta(5/2)$ with the zeta function $\zeta(x)$, we get the free energy $\delta\mathcal{F}(T, 0)$ as

$$\delta\mathcal{F}(T, 0) = -\frac{(4-\sqrt{2})\Gamma(5/4)\zeta(5/2)}{16\pi\Gamma(3/4)}\frac{T^{5/2}}{t_{\perp}t_z^{1/2}}. \quad (\text{C.89})$$

The specific heat at $\mu = 0$ is then given by

$$\begin{aligned} C_V &= -T\frac{\partial^2\delta\mathcal{F}(T, 0)}{\partial T^2} \\ &= \frac{15(4-\sqrt{2})\Gamma(5/4)\zeta(5/2)}{64\pi\Gamma(3/4)}\frac{T^{3/2}}{t_{\perp}t_z^{1/2}}. \end{aligned} \quad (\text{C.90})$$

C.4.2.2 Compressibility

The compressibility is given by

$$\begin{aligned} \kappa &= -\frac{\partial^2\delta\mathcal{F}(T, \mu)}{\partial\mu^2} \\ &= -\frac{\Gamma(5/4)}{8\pi\Gamma(3/4)}\frac{T^{1/2}}{t_{\perp}t_z^{1/2}}\left[\text{Li}_{\frac{1}{2}}(-e^{\mu/T}) + \text{Li}_{\frac{1}{2}}(-e^{-\mu/T})\right]. \end{aligned} \quad (\text{C.91})$$

At $\mu = 0$, we have

$$\kappa = -\frac{(\sqrt{2}-1)\Gamma(5/4)\zeta(1/2)}{4\pi\Gamma(3/4)}\frac{T^{1/2}}{t_{\perp}t_z^{1/2}}, \quad (\text{C.92})$$

where $\text{Li}_{1/2}(-1) = (\sqrt{2}-1)\zeta(1/2)$ is used. Note that $\zeta(1/2) < 0$, hence, $\kappa > 0$.

$$(\text{C.93})$$

C.4.3 Diamagnetic susceptibility

Using the Fukuyama formula [88], the diamagnetic susceptibility is given by

$$\chi_{D,x} = e_0^2 T \sum_{i\omega_n} \int \frac{d^3k}{(2\pi)^3} \text{Tr}[J_j G(i\omega_n, \mathbf{k}) J_k G(i\omega_n, \mathbf{k}) J_j G(i\omega_n, \mathbf{k}) J_k G(i\omega_n, \mathbf{k})], \quad (\text{C.94})$$

where $J_i \equiv \frac{\partial \mathcal{H}_0}{\partial k_i}$ is the current operator,

$$J_x = 2t_{\perp} k_x \sigma_x + 2t_{\perp} k_y \sigma_y, \quad (\text{C.95})$$

$$J_y = -2t_{\perp} k_y \sigma_x + 2t_{\perp} k_x \sigma_y, \quad (\text{C.96})$$

$$J_z = 2t_z k_z \sigma_z. \quad (\text{C.97})$$

Note that because of the C_4 symmetry of the Hamiltonian, $\chi_{D,x} = \chi_{D,y} = \chi_{D,\perp}$. Subtracting the zero temperature contribution to obtain a finite result, we have

$$\begin{aligned} \chi_{D,\perp} &= e_0^2 T \sum_{i\omega_n} \int \frac{d^3 k}{(2\pi)^3} \text{Tr}[J_y G(i\omega_n, \mathbf{k}) J_z G(i\omega_n, \mathbf{k}) J_y G(i\omega_n, \mathbf{k}) J_z G(i\omega_n, \mathbf{k})] \\ &\quad - e_0^2 \int \frac{d\omega d^3 k}{(2\pi)^4} \text{Tr}[J_y G(i\omega, \mathbf{k}) J_z G(i\omega, \mathbf{k}) J_y G(i\omega, \mathbf{k}) J_z G(i\omega, \mathbf{k})], \\ &= e_0^2 t_{\perp}^2 t_z^2 \int \frac{d^3 k}{(2\pi)^3} [-32(k_x^2 + k_y^2)k_z^2 M_2 + 128t_{\perp}^2 t_z^2 (k_x^2 + k_y^2)^3 k_z^6 M_4] \\ &= e_0^2 t_z^{1/2} T^{1/2} c_{\chi,\perp}, \end{aligned} \quad (\text{C.98})$$

where $c_{\chi,\perp} = 0.054$. Here, we use

$$\int_0^{\pi/2} \cos \theta_R \sin^{1/2} \theta_R d\theta_R = \frac{2}{3}, \quad (\text{C.99})$$

$$\int_0^{\pi/2} \cos^3 \theta_R \sin^{5/2} \theta_R d\theta_R = \frac{8}{77}, \quad (\text{C.100})$$

and the following Matsubara frequency summations (where the zero-temperature contribution has been subtracted)

$$\begin{aligned} M_1(\xi/T) &= T \sum_{i\omega_n} \frac{1}{(\omega_n^2 + \xi^2)} - \int_{-\infty}^{\infty} \frac{d\omega}{2\pi} \frac{1}{(\omega^2 + \xi^2)} \\ &= \frac{1}{2\xi} \left[\tanh\left(\frac{\xi}{2T}\right) - 1 \right], \end{aligned} \quad (\text{C.101})$$

$$\begin{aligned} M_2(\xi/T) &= T \sum_{i\omega_n} \frac{1}{(\omega_n^2 + \xi^2)^2} - \int_{-\infty}^{\infty} \frac{d\omega}{2\pi} \frac{1}{(\omega^2 + \xi^2)^2} \\ &= \frac{1}{4\xi^3} \left[\tanh\left(\frac{\xi}{2T}\right) - 1 \right] - \frac{1}{8\xi^2 T} \frac{1}{\cosh^2\left(\frac{\xi}{2T}\right)}, \end{aligned} \quad (\text{C.102})$$

$$\begin{aligned}
M_3(\xi/T) &= T \sum_{i\omega_n} \frac{1}{(\omega_n^2 + \xi^2)^3} - \int_{-\infty}^{\infty} \frac{d\omega}{2\pi} \frac{1}{(\omega^2 + \xi^2)^3} \\
&= \frac{3}{16\xi^5} \left[\tanh\left(\frac{\xi}{2T}\right) - 1 \right] - \frac{3}{32\xi^4 T} \frac{1}{\cosh^2\left(\frac{\xi}{2T}\right)} - \frac{1}{32\xi^3 T^2} \frac{\tanh\left(\frac{\xi}{2T}\right)}{\cosh^2\left(\frac{\xi}{2T}\right)},
\end{aligned} \tag{C.103}$$

$$\begin{aligned}
M_4(\xi/T) &= T \sum_{i\omega_n} \frac{1}{(\omega_n^2 + \xi^2)^4} - \int_{-\infty}^{\infty} \frac{d\omega}{2\pi} \frac{1}{(\omega^2 + \xi^2)^4} \\
&= \frac{5}{32\xi^7} \left[\tanh\left(\frac{\xi}{2T}\right) - 1 \right] - \frac{5}{64\xi^6 T} \frac{1}{\cosh^2\left(\frac{\xi}{2T}\right)} - \frac{1}{32\xi^5 T^2} \frac{\tanh\left(\frac{\xi}{2T}\right)}{\cosh^2\left(\frac{\xi}{2T}\right)} \\
&\quad + \frac{1}{384\xi^4 T^3} \frac{1}{\cosh^4\left(\frac{\xi}{2T}\right)} \left[2 - \cosh\left(\frac{\xi}{T}\right) \right].
\end{aligned} \tag{C.104}$$

Similarly, $\chi_{D,z}$ is given by

$$\begin{aligned}
\chi_{D,z} &= e_0^2 T \sum_{i\omega_n} \int \frac{d^3 k}{(2\pi)^3} \text{Tr}[J_x G(i\omega_n, \mathbf{k}) J_z G(i\omega_n, \mathbf{k}) J_x G(i\omega_n, \mathbf{k}) J_z G(i\omega_n, \mathbf{k})] \\
&\quad - e_0^2 \int \frac{d\omega d^3 k}{(2\pi)^4} \text{Tr}[J_x G(i\omega, \mathbf{k}) J_z G(i\omega, \mathbf{k}) J_x G(i\omega, \mathbf{k}) J_z G(i\omega, \mathbf{k})] \\
&= e_0^2 t_{\perp}^4 \int \frac{d^3 k}{(2\pi)^3} \left[-32(k_x^2 + k_y^2)^2 M_2 + 256 t_{\perp}^4 (k_x^2 + k_y^2)^4 k_x^2 k_y^2 M_4 \right], \\
&= \frac{e_0^2 t_{\perp}}{t_z^{1/2}} T^{1/2} c_{\chi,z},
\end{aligned} \tag{C.105}$$

where $c_{\chi,z} = 0.107$. Here, we used

$$\int_0^{\pi/2} d\theta \frac{\cos^2 \theta}{\sqrt{\sin \theta}} = \frac{4\pi^{1/2} \Gamma(5/4)}{3\Gamma(3/4)}, \tag{C.106}$$

$$\int_0^{\pi/2} d\theta \frac{\cos^6 \theta}{\sqrt{\sin \theta}} = \frac{80\pi^{1/2} \Gamma(5/4)}{77\Gamma(3/4)}. \tag{C.107}$$

In summary,

$$\chi_{D,\perp} = c_{\chi,\perp} e_0^2 t_z^{1/2} T^{1/2}, \quad \chi_{D,z} = c_{\chi,z} \frac{e_0^2 t_{\perp}}{t_z^{1/2}} T^{1/2}. \tag{C.108}$$

C.4.4 Optical conductivity

The optical conductivity is given by

$$\begin{aligned} \sigma_{ij}(\Omega, T) = & e_0^2 \int_{-\infty}^{\infty} \frac{d\omega}{\pi} \frac{n_F(\omega) - n_F(\omega + \Omega)}{\Omega} \\ & \times \int \frac{d^3k}{(2\pi)^3} \text{Tr} [J_i \text{Im}[G_0^{\text{ret}}(\omega, \mathbf{k})] J_j \text{Im}[G_0(\omega + \Omega, \mathbf{k})]], \end{aligned} \quad (\text{C.109})$$

where $n_F(x) = \frac{1}{1+e^{x/T}}$. Because of the C_4 symmetry of the Hamiltonian, $\sigma_{xx} = \sigma_{yy}$. Hence, we only need to consider σ_{xx} and σ_{zz} .

$$\begin{aligned} \sigma_{xx}(\Omega, T) = & e_0^2 \int_{-\infty}^{\infty} \frac{d\omega}{\pi} \frac{n_F(\omega) - n_F(\omega + \Omega)}{\Omega} \\ & \times \int \frac{d^3k}{(2\pi)^3} \text{Tr} [J_x \text{Im}[G_0^{\text{ret}}(\omega, \mathbf{k})] J_x \text{Im}[G_0^{\text{ret}}(\omega + \Omega, \mathbf{k})]] \\ = & \frac{e_0^2 T^{3/2}}{5t_z^{1/2}} \delta(\Omega) \int_0^{\infty} dR \frac{R^{3/2}}{\cosh^2\left(\frac{R}{2}\right)} + \frac{3}{20\sqrt{2}\pi} \frac{e_0^2}{t_z^{1/2}} |\Omega|^{1/2} \tanh\left(\frac{|\Omega|}{4T}\right), \end{aligned} \quad (\text{C.110})$$

$$\begin{aligned} \sigma_{zz}(\Omega, T) = & e_0^2 \int_{-\infty}^{\infty} \frac{d\omega}{\pi} \frac{n_F(\omega) - n_F(\omega + \Omega)}{\Omega} \\ & \times \int \frac{d^3k}{(2\pi)^3} \text{Tr} [J_z \text{Im}[G_0^{\text{ret}}(\omega, \mathbf{k})] J_z \text{Im}[G_0(\omega + \Omega, \mathbf{k})]] \\ = & \frac{e_0^2 T^{3/2}}{t_{\perp} t_z^{-1/2}} \frac{3\Gamma(-1/4)^2}{160\sqrt{2}\pi^{5/2}} \delta(\Omega) \end{aligned} \quad (\text{C.111})$$

$$\times \int_0^{\infty} dR \frac{R^{3/2}}{\cosh^2\left(\frac{R}{2}\right)} + \frac{\sqrt{\pi}\Gamma(3/4)}{40\sqrt{2}\Gamma(5/4)} \frac{e_0^2}{t_{\perp} t_z^{-1/2}} |\Omega|^{1/2} \tanh\left(\frac{|\Omega|}{4T}\right). \quad (\text{C.112})$$

Here, we used the following identities,

$$\int_0^\infty dR \frac{R^{3/2}}{\cosh^2\left(\frac{R}{2}\right)} = 4.06856, \quad (\text{C.113})$$

$$\int_0^{\pi/2} \frac{\cos^{7/2} \theta}{\sqrt{\cos \theta \sin \theta}} d\theta = \frac{8}{5}, \quad (\text{C.114})$$

$$\int_0^{\pi/2} \sin^{5/2} \theta d\theta = \frac{3\Gamma(-1/4)^2}{40\sqrt{2\pi}}, \quad (\text{C.115})$$

$$\int_0^1 dR \frac{R^3(R^4 - 2)}{(1 - R^4)^{3/4}} = -\frac{6}{5}, \quad (\text{C.116})$$

$$\int_0^1 dR \frac{R^5}{\sqrt{1 - R^4}} = \frac{\sqrt{\pi}\Gamma(3/4)}{10\Gamma(5/4)}, \quad (\text{C.117})$$

$$\lim_{\Omega \rightarrow 0} \frac{n_F(A) - n_F(A \pm \Omega)}{\Omega} = \pm \frac{1}{4T} \frac{1}{\cosh^2(A/2T)}. \quad (\text{C.118})$$

For $T = 0$,

$$\sigma_{xx}(\Omega) = \frac{3}{20\sqrt{2\pi}} \frac{e_0^2}{t_z^{1/2}} |\Omega|^{1/2}, \quad (\text{C.119})$$

$$\sigma_{zz}(\Omega) = \frac{\sqrt{\pi}\Gamma(3/4)}{40\sqrt{2}\Gamma(5/4)} \frac{e_0^2}{t_\perp t_z^{-1/2}} |\Omega|^{1/2}. \quad (\text{C.120})$$

C.5 Effect of extra relevant perturbations

In the presence of extra perturbations such as doping and disorder, a new parameter is introduced to characterize the extra perturbation in addition to the intrinsic length scale, correlation length ξ set by temperature. For example, for doping, the Fermi wave vector k_F is well defined. With the two parameters, the two regimes naturally appear. For a large doping $k_F \xi \gg 1$, our fixed point cannot be a good starting point, and it would be better to start from the Fermi liquid. On the other hand, $k_F \xi \ll 1$, our description is certainly a good starting point and one can investigate the doping effect as a perturbation even though a little more additional cautions are necessary as in one of the standard critical phenomena.

C.6 Sanity check of the power-law correction

In the main text, we included all the renormalization effects in the system parameters. Here, for a sanity check, equivalently we will include all the renormalization effects in the coordinates and obtain the associated anomalous dimensions.

Recall that the RG equations for t_\perp and t_z are given by

$$\frac{1}{t_\perp} \frac{dt_\perp}{d\ell} = z - 2z_\perp + \alpha F_\perp(\gamma), \quad (\text{C.121})$$

$$\frac{1}{t_z} \frac{dt_z}{d\ell} = z - 2 + \alpha F_z(\gamma). \quad (\text{C.122})$$

Imposing t_\perp and t_z as constants, then we have

$$z = 2 - \alpha F_z(\gamma), \quad (\text{C.123})$$

$$z_\perp = 1 + \frac{\alpha}{2} [F_\perp(\gamma) - F_z(\gamma)]. \quad (\text{C.124})$$

At the fixed point $(\alpha, \gamma) = (\alpha^*, \gamma^*)$,

$$z^* = 2 - \alpha^* F_z(\gamma^*), \quad (\text{C.125})$$

$$z_\perp^* = 1 + \frac{\alpha^*}{2} [F_\perp(\gamma^*) - F_z(\gamma^*)]. \quad (\text{C.126})$$

Now, let us find the power-law corrections of the physical observables by using scaling hypothesis with the renormalized quantity \mathcal{O}_R and the scaling dimension $d_{\mathcal{O}}$ for an observable \mathcal{O} . For the density of states, we have

$$\rho = b^{z-(2z_\perp+1)} \rho_R, \quad (\text{C.127})$$

whereas for the free energy,

$$\mathcal{F} = b^{-(z+2z_\perp+1)} \mathcal{F}_R. \quad (\text{C.128})$$

From Eq. (C.128), we obtain the specific heat and the compressibility, respectively, as

$$C_V = -T \frac{\partial^2 \mathcal{F}}{\partial T^2} = b^{-(2z_\perp+1)} C_{V,R}, \quad (\text{C.129})$$

$$\kappa = -\frac{\partial^2 \mathcal{F}}{\partial \mu^2} = b^{z-(2z_\perp+1)} \kappa_R. \quad (\text{C.130})$$

To determine the scaling relation of the optical conductivities and the diamagnetic susceptibilities, we use the minimal coupling $-i\partial_i \rightarrow -i\partial_i + e_0 A_i(\tau, \mathbf{x})$, where $A_i(\tau, \mathbf{x})$ is a gauge-field. Since e_0 receives no renormalization at all, the scaling dimension of A_i is the same as that of ∂_i . The optical conductivities and the diamagnetic susceptibilities can be obtained from the current-current response function $K_{ij}(i\omega, \mathbf{q}) = \frac{1}{(2\pi)^{d+1} \delta(\omega+\Omega) \delta^d(\mathbf{q}+\mathbf{p})} \langle \mathcal{J}_i(i\omega, \mathbf{q}) \mathcal{J}_j(i\Omega, \mathbf{p}) \rangle$ with $\mathcal{J}_i(i\omega, \mathbf{q}) = e_0 \int_{\mathbf{k}} \psi^\dagger(i\omega, \mathbf{k} + \mathbf{q}) \frac{\partial \mathcal{H}_0(\mathbf{k})}{\partial k_i} \psi(i\omega, \mathbf{k})$ by the following relations [88, 85]:

$$\sigma_{ij}(\omega) = \frac{1}{2\omega} \text{Im} K_{ij}^{\text{ret}}(\omega, \mathbf{q} = \mathbf{0}), \quad (\text{C.131})$$

$$\chi_{D,i}(\omega) = -\lim_{\mathbf{q} \rightarrow \mathbf{0}} \frac{\epsilon_{ijk}}{2q_j q_k} K_{jk}(0, \mathbf{q}). \quad (\text{C.132})$$

Here, the repeated indices are not summed. Because $\langle \mathcal{J}_i(i\omega, \mathbf{q}) \mathcal{J}_j(i\Omega, \mathbf{p}) \rangle$ is obtained by differentiating the logarithm of the partition function $Z[\mathbf{A}]$ with respect to $A_i(i\omega, \mathbf{q})$ and $A_j(i\omega, \mathbf{p})$, the scaling dimension of $K_{ij}(i\omega, \mathbf{q})$, namely $[K_{ij}]$, is given by

$$\begin{aligned} [K_{ij}] &= \left[\frac{\delta}{\delta A_i(i\omega, \mathbf{q})} \right] + \left[\frac{\delta}{\delta A_j(i\omega, \mathbf{q})} \right] - [d\tau] - [d^d \mathbf{x}] \\ &= -[\partial_i] - [\partial_j] + (z + 2z_\perp + d - 2). \end{aligned} \quad (\text{C.133})$$

Equipped with this scaling relation of K_{ij} , we can derive the following relations:

$$\sigma_{\perp\perp} = b^{d-2} \sigma_{\perp\perp,R}, \quad (\text{C.134})$$

$$\sigma_{zz} = b^{2z_\perp - d + 2} \sigma_{zz,R}, \quad (\text{C.135})$$

$$\chi_{D,\perp} = b^{-z+d-2} \chi_{D,\perp,R}, \quad (\text{C.136})$$

$$\chi_{D,z} = b^{-z+2z_\perp-d+2} \chi_{D,z,R}. \quad (\text{C.137})$$

The RG equation of the temperature and frequency is

$$\frac{d\mathcal{O}}{d \ln b} = z\mathcal{O}, \quad (\text{C.138})$$

where $\mathcal{O} = T, \Omega$. Let $z = z^*$ and $z_{\perp} = z_{\perp}^*$. Solving this, we obtain $\mathcal{O}(b) = b^{z^*} \mathcal{O}$. Let b^* be the cutoff value, so that $\mathcal{O}(b^*) = (b^*)^{z^*} \mathcal{O} = \Lambda$, then $b^* = (\Lambda/\mathcal{O})^{1/z^*} \propto \mathcal{O}^{-1/z^*}$. Using this, we can obtain the power-law corrections of the observables in terms of the temperature and frequency.

For the density of states, we have

$$\rho \propto |\Omega|^{(2z_{\perp}^*+1-z^*)/z^*} \propto |\Omega|^{1/2+c_{\perp}+\frac{1}{2}c_z}. \quad (\text{C.139})$$

For the specific heat and compressibility,

$$C_V \propto T^{(2z_{\perp}^*+1)/z^*} \approx T^{3/2+c_{\perp}+\frac{1}{2}c_z}, \quad (\text{C.140})$$

$$\kappa \propto T^{(2z_{\perp}^*+1-z^*)/z^*} \approx T^{1/2+c_{\perp}+\frac{1}{2}c_z}. \quad (\text{C.141})$$

For the diamagnetic susceptibility,

$$\chi_{D,\perp} \propto T^{(z^*-1)/z^*} \approx T^{1/2-\frac{1}{2}c_z}, \quad (\text{C.142})$$

$$\chi_{D,z} \propto T^{(z^*-2z_{\perp}^*+1)/z^*} \approx T^{1/2-c_{\perp}+\frac{1}{2}c_z}. \quad (\text{C.143})$$

For the optical conductivity,

$$\sigma_{xx} \propto \Omega^{1/z^*} \approx \Omega^{1/2+c_z}, \quad (\text{C.144})$$

$$\sigma_{zz} \propto \Omega^{(2z_{\perp}^*-1)/z^*} \approx \Omega^{1/2+c_{\perp}-\frac{1}{2}c_z}. \quad (\text{C.145})$$

Here, $c_{\perp} \approx 0.402/N_f$ and $c_z \approx 0.044/N_f$ in the large N_f approximation. Thus, we obtain the same results as in the main text. If the symmetry-allowed parabolic term is included, we have $c_{\perp} \approx 0.145/N_f$ and $c_z \approx 0.050/N_f$.

For the candidate materials of DWSM, HgCr_2Se_4 and SrSi_2 , HgCr_2Se_4 has one pair ($N_f = 1$) of double-Weyl points, whereas SrSi_2 has six pairs ($N_f = 6$) of double-Weyl points. In particular, for SrSi_2 , it has cubic symmetry, therefore,

to see the anisotropic behaviors, we need to maintain only one C_4 symmetry. For example, if we apply a uniaxial pressure along \hat{z} , then the C_4 symmetry along \hat{x} and \hat{y} is broken, so we only have two pairs of double-Weyl points on the \hat{z} axis [82]. Therefore, under this situation, the effective number of pairs of double-Weyl points of SrSi₂ is two ($N_f = 2$). Then, for $\eta_2 \equiv c_z/2$ and $\eta_3 \equiv c_\perp - c_z/2$ we find that $\eta_2 - \eta_3$ values for HgCr₂Se₄ and SrSi₂ are -0.198 and -0.132 , respectively. We expect that the anisotropic scaling will be manifested at low temperatures or low frequencies.

국문초록

많은 수의 물질과 물질의 상(phase)을 연구함에 있어서 이들을 일관되고 유용한 방식으로 구분하는 것은 본질적으로 그 물질에 대한 이해를 필요로 하고 더 깊은 연구를 위한 도움이 된다. 물질의 상(phase)을 구분하는 대표적인 방법은 Landau의 상전이에 대한 연구를 기반으로 발전하였는데, 물질이 상전이를 거치면서 깨진 대칭성(broken symmetry)을 이용한다.

그러나 2000년대 중반에 이런 대칭성에 기반한 방식으로는 구분 할 수 없는 새로운 상과 전자 구조의 위상학적 성질과 연관되어 있다는 것이 밝혀지면서 이 새로운 '위상학적 상'(topological phase)에 대한 탐구가 응집물질물리계 전반에 걸쳐서 활발히 진행되었다. 본 논문에서는 이러한 학계 흐름의 연장선에서 위상적 성질이 특별한 새로운 물질들에 대해서 전자간 원거리 상호작용에 의한 효과를 연구하였다.

첫째로 단층 전이금속 칼코겐 화합물(transition metal dichalcogenides)를 이용한 광학 공동에서 엑시톤-폴라리톤에 대한 연구를 하였다. 엑시톤은 반도체 물질의 최외곽 띠에 있는 전자가 들뜨면서 생기는 정공(hole)와 함께 전자-정공 원거리 상호작용을 통해 서로 속박 된 상태이다. 양전하의 정공과 음전하의 전자가 서로를 속박하고 있으므로 수소에 대응하는 준입자로 이해할 수 있다. 전자와 정공의 결합체로서 극성을 강하게 띠는 엑시톤은 빛과 강하게 상호 작용 하는데, 이 때 엑시톤과 엑시톤이 흡수하고 내뿜는 광자가 모두 걸맞은 상태가 되는 경우, 이 새로운 상태를 엑시톤-폴라리톤이라고 한다.

엑시톤-폴라리톤은 질량이 없는 광자의 성질을 닮아서 질량이 매우 작은 준입자로 해석 할 수 있다. 질량이 작은 입자의 경우 보즈-아인슈타인 응축이

발현하는 온도가 높다. 엑시톤-폴라리톤의 경우 상온에서 보즈-아인슈타인 응축이 발현 할 수도 있을 정도로 질량이 작기에, 상온 보즈-아인슈타인 응축 물질의 후보로 각광 받았다. 본 논문에서는 단층 전이금속 칼코겐 화합물의 경우 최외곽 전자띠와 전도띠의 위상적으로 평범하지 않은 '질량을 지닌 이차원 디랙 페르미온'의 구조를 고려하여 연구를 진행하였다. 연구를 통해서 평범한 전자 기체 모델에서 등장하는 연속적인 BEC-BCS 교차(BEC-BCS crossover) 대신 위상적 일차 상전이(1st order phase transition)가 나타나는 결과를 얻었다. 이 결과를 바탕으로 단층 전이금속 칼코겐 화합물을 바탕으로 하는 엑시톤-폴라리톤계가 보일 수 있는 다양한 위상적 상들을 제시하였다.

둘째로 이중-바일 마디(double-Weyl node)가 있는 위상 준금속의 위상학적 상전이점에서 전자-전자 상호작용의 영향을 연구하였다. 이중-바일 마디는 바일 마디의 확장된 형태이다. 바일 마디가 물질의 브릴루앙 영역 내부 임의의 지점에서 생길 수 있고, ± 1 의 위상학적 전하(topological charge)을 지니고 있는데 반해, 이중-바일 마디는 C_4 혹은 C_6 회전 대칭이 있는 물질에서 이 회전의 축 상에서만 나타날 수 있다. 그리고 ± 2 의 위상학적 전하를 지닌다. 특히 에너지 분산식 관점에서 바일-마디의 에너지 분산식이 운동량에 모든 방향으로 선형적(linear)인 의존성을 보여 주는 것에 반해, 이중-바일 마디의 경우 회전축과 나란한 방향의 운동량에 대해선 에너지 분산식이 선형으로 의존하지만, 회전축과 수직인 방향으로는 이차(quadratic) 의존성을 보여준다.

이중-바일 마디가 있는 위상 준금속에 물리적 혹은 화학적 압력을 가하는 방식으로 위상적 전하의 부호가 다른 두 이중-바일 페르미온을 쌍소멸시킬 수 있다. 이중-바일 페르미온의 쌍소멸이 일어난 후에는 물질이 준금속이 아닌 부도체가 되는데, 준금속과 부도체 상의 경계면에서 위상적 상전이(topological phase transition)가 일어나게 된다. 이런 상전이 점에서는 전자 구조의 낮은 에너지 영역이 눈금 바꿈(scaling)에 대해 불변인 특성을 보인다. 이런 눈금 바꿈에 대해 불변인 계는 재규격화군(renormalization group)을 이용해 연구하는데, 본 논문에서는 재규격화군의 표준적인 두 가지 방식(large- N_f method, $\epsilon = 4 - d$ expansion)을 이용하여 이중-바일 준금속의 위상적 상전이점에서

전자간 쿨롱 상호작용의 영향을 연구하였다. 이중-바일 준금속의 위상적 상전이점에서 상호작용으로 인해 비등방성(anisotropy)이 발생되고 고체 내 전자에 대한 준입자(quasiparticle) 기술이 한계에 봉착하는 비-페르미 액체(non-Fermi liquid)가 구현됨을 보였으며, 이에 대한 실험적 신호들을 제시하였다. 기존에 이론적으로 제안된 비등방성 비-페르미 액체 상들은 질서 변수(order parameter)의 대칭성 깨짐(symmetry breaking)을 수반하는 것에 반해, 본 연구에서 제안된 비등방성 비-페르미 액체는 대칭성 깨짐과 무관한 위상적 상전이를 통해 나타난다는 점에서 비등방성 비-페르미 액체를 구현하는 새로운 보편성 부류(universality class)를 제안하였다는 의미가 있다.

주요어: 엑시톤, 엑시톤-플라리톤, 위상적 상전이, 이중-바일 준금속, 원거리 쿨롱 상호작용

학번: 2013-22992

Acknowledgement

First of all, I would like to express my sincere gratitude to my advisor Professor Hongki Min. He has provided immense support and guidance during the 6 years I spent in research for my Ph. D study, not only as my academic advisor but also as my mentor. I thank him especially for allowing me to fulfil my research in the areas of my own interest, and also granting me the opportunity to work with professors from the relevant field.

My gratitude extends to the assessors Prof. Jaejun Yu, Prof. Keehoon Kim, Prof. Bohmjung Yang, and Prof. Sukbum Cheong from Seoul university, for their profound questions and encouragement.

I am also grateful to my parents. I have been at Seoul national university for more than ten years, and without their financial and emotional support, I would not have been able to achieve this Ph. D. Thank you my parents, for believing in me and supporting me.

And to those who shared the research office with me, Yunsu Jang, Seongjin Ahn, Seungchan Woo, Sanghyun Park, Chiho Yoon, Jiho Jang, Sunghoon Kim, I also express my gratitude. Yunsu Jang, Seongjin Ahn, Seungchan Woo helped me settle in when I first joined this group. Seongjin Ahn and Chiho Yoon, thank you for putting up with my mischief. I wish you all the best.

Lastly, I thank Sunwouk Yi who helped me through the stressful times while I was deciding my career path. I was able to attain a healthy body and a healthy hobby of exercising because of him. The members of the gym Eugene Jung,

Sang-moo Lee, Jinwook Kim, Woocheon Chung, Hosun Ryu, and Yongwook Kim, and the tutors Younghoon Eom, Hwanseok Cho, and Seungkyu Lee who I spent three years exercising together, I also thank you